



# Lawrence Berkeley Laboratory

UNIVERSITY OF CALIFORNIA

## Materials & Molecular Research Division

BUBBLE DYNAMICS AT GAS-EVOLVING ELECTRODES

Paul J. Sides  
(Ph.D. thesis)

December 1980

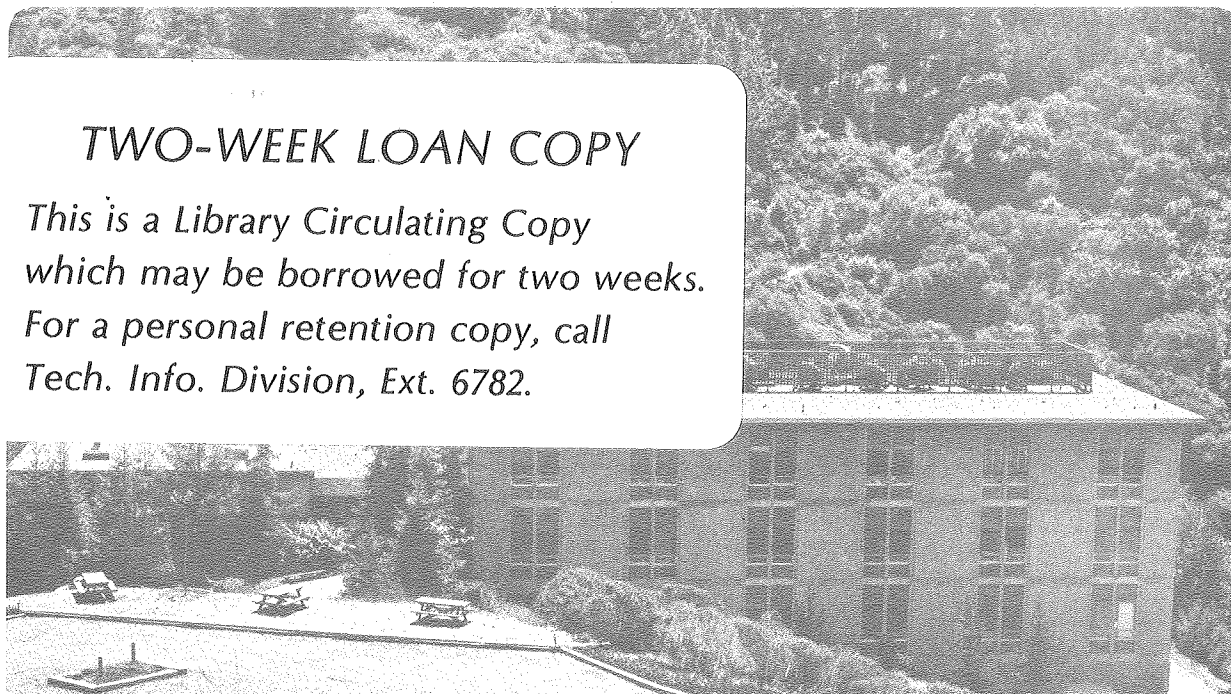
LAWRENCE  
BERKELEY LABORATORY

MAR 2 1981

LIBRARY AND  
DOCUMENTS

### TWO-WEEK LOAN COPY

*This is a Library Circulating Copy  
which may be borrowed for two weeks.  
For a personal retention copy, call  
Tech. Info. Division, Ext. 6782.*



LBL-11849 c.2

## DISCLAIMER

This document was prepared as an account of work sponsored by the United States Government. While this document is believed to contain correct information, neither the United States Government nor any agency thereof, nor the Regents of the University of California, nor any of their employees, makes any warranty, express or implied, or assumes any legal responsibility for the accuracy, completeness, or usefulness of any information, apparatus, product, or process disclosed, or represents that its use would not infringe privately owned rights. Reference herein to any specific commercial product, process, or service by its trade name, trademark, manufacturer, or otherwise, does not necessarily constitute or imply its endorsement, recommendation, or favoring by the United States Government or any agency thereof, or the Regents of the University of California. The views and opinions of authors expressed herein do not necessarily state or reflect those of the United States Government or any agency thereof or the Regents of the University of California.

## BUBBLE DYNAMICS AT GAS-EVOLVING ELECTRODES

Contents

Abstract . . . . .	v
Acknowledgements . . . . .	ix
I. Introduction . . . . .	1
II. Review of the Effective Conductivity of Electrolytes Containing Dispersions of Dielectric Spheres . . . . .	4
1. Introduction to the Literature Survey . . . . .	4
2. Random Arrangements of Monosized Spheres . . . . .	5
3. Ordered Arrangements of Uniform Spheres . . . . .	26
4. Random Arrangements of Multisized Spheres . . . . .	31
5. Conclusion: The Best Equation Over the Whole Range . . . . .	33
III. The Tangent Sphere and Other Calculations Appropriate to the Conductivity of Bubble Layers . . . . .	42
1. Literature of the Bubble Layer . . . . .	42
2. Introduction to the Calculations . . . . .	44
3. The Tangent-Sphere Calculation . . . . .	45
4. Maxwell's Equation, the Single Bubble Calculation, the Tangent Sphere Result . . . . .	58
5. Effect of Orientation of Two-sphere Combinations on the Resistance They Present . . . . .	62
6. The Constriction Calculation . . . . .	73
7. Conclusions . . . . .	77

IV. Experiments on a Model of A Bubble Layer . . . . .	80
1. The Hexagonal Cell Experiments . . . . .	80
2. Results of the Hexagonal Cell Experiments . . . . .	89
3. Conclusions . . . . .	95
V. A Close View of Gas Evolution from the Backside . . . . .	98
1. A Review of Literature on the Observation of Bubble Behavior . . . . .	98
2. The Transparent Electrode Experiment . . . . .	108
3. Conclusions . . . . .	132
Nomenclature . . . . .	135
Appendices . . . . .	138
References . . . . .	150

## BUBBLE DYNAMICS AT GAS-EVOLVING ELECTRODES

Paul J. Sides

Materials and Molecular Research Division  
Lawrence Berkeley Laboratory  
and Department of Chemical Engineering  
University of California  
Berkeley, CA 94720

## ABSTRACT

Nucleation of bubbles, their growth by diffusion of dissolved gas to the bubble surface and by coalescence, and their detachment from the electrode are all very fast phenomena; furthermore, electrolytically generated bubbles range in size from ten to a few hundred microns; therefore, magnification and high speed cinematography are required to observe bubbles and the phenomena of their growth on the electrode surface. Viewing the action from the front side (the surface on which the bubbles form) is complicated because the most important events occur close to the surface and are obscured by other bubbles passing between the camera and the electrode; therefore, oxygen was evolved on a transparent tin oxide "window" electrode and the events were viewed from the backside. The movies showed that coalescence of bubbles is very important for determining the size of bubbles and in the chain of transport processes; growth by diffusion and by coalescence proceeds in series and parallel; coalescing bubbles cause significant fluid motion close to the electrode; bubbles can leave and reattach; and bubbles evolve in a cycle of growth by diffusion and different modes of coalescence.

An analytical solution for the primary potential and current distribution around a spherical bubble in contact with a plane electrode is presented. Zero at the contact point, the current density reaches only one percent of its undisturbed value at 30 percent of the radius from that point and goes through a shallow maximum two radii away. The solution obtained for spherical bubbles is shown to apply for the small bubbles of electrolytic processes. The incremental resistance in ohms caused by sparse arrays of bubbles is given by

$$\Delta R = 1.352 af/kS$$

where  $f$  is the void fraction of gas in the bubble layer,  $a$  is the bubble layer thickness,  $k$  is the conductivity of gas free electrolyte, and  $S$  is the electrode area.

A densely populated gas bubble layer on an electrode was modeled as a hexagonal array of dielectric spheres. Accurately machined lucite spheres were placed one at a time in one end of a hexagonal cell which simulated the unit cell of such an array. The resistance as a function of gas bubble layer packing density sharply increased as close packing was approached. Because the interaction of the fields around bubbles closely spaced in the direction perpendicular to the current dominates the added resistance, and because there is a tri-modal distribution of

bubble sizes in a bubble layer, the Distribution Model of Meredith and Tobias (16), derived for three dimensional gas dispersions, approximately predicted the conductivity of a bubble layer at void fractions greater than 0.3. At moderate-to-high current densities, the bubble layer in a cell having an interelectrode gap of half a centimeter could increase the ohmic resistance by as much as 20 percent.



## ACKNOWLEDGEMENTS

I wish most of all to thank Charles W. Tobias for his faith, support and humor during my work at Berkeley. Being under his guidance has been an unforgettable privilege.

I also wish to thank Catherine Sides who suffered more at the hands of this thesis than anyone else. I further wish to recognize the special friendship of Geoffrey Prentice and Karrie Hanson without whom my stay at Berkeley, while undoubtedly shorter, would have been far less agreeable.

This work was supported by the U. S. Department of Energy under contract No. W-7405-ENG-48. Work also supported by a Department of Energy Domestic Mining and Mineral Fellowship.



## I. INTRODUCTION

Gas evolution is an important phenomenon in nearly all industrial electrolytic processes, including production of chlorine and aluminum, which together consume 6 percent of all the electricity generated in the United States. Gas producing side reactions are also a concern in charging of conventional and advanced batteries, which might be important to electric vehicles in the future. Conserving energy in both of these applications must in part follow from fundamental understanding of the physics of gas evolution; that is, both its phenomena and effects.

Electrolytically evolved gases affect electrochemical processes in several ways. First, they increase the effective resistivity of the electrolyte by forcing current to take longer paths through the solution than it would in their absence. Also, bubbles attached to the electrode surface force the current through smaller areas of the electrode than would otherwise be available; since the driving force for reaction is a function of current density, there must be a net addition to the surface overpotential caused by the shifting of the current. Furthermore, bubbles not only affect the processes' gross hydrodynamics through gas lift, but also disturb the electrolyte close to an electrode surface and thereby enhance mass transport of any diffusion-controlled species to the electrode surface. Finally, in a plating operation, the nonuniform current distribution around a bubble on a surface may cause defects in the finish if the bubble adheres over a significant time interval.

Past work on the effect of dispersed gas on the conductivity of an electrolyte is reviewed in detail in Chapter I. The effect of the bubbles attached to the electrode surface, however, must differ from that of bubbles dispersed in the bulk because the environment of a bubble at the interface is asymmetric; that is, the bubble adheres to an equipotential surface but is everywhere else submerged in electrolyte. In Chapter II, the primary potential and current distribution around a spherical bubble tangent to a planar electrode, an idealized model of a bubble layer, are presented.

Although the ideal non-interacting bubbles of the analytical solution in Chapter III shield the electrode, they do not severely constrict the current to the electrode and hence do not present significant resistance. The analysis is only accurate for bubbles on an electrode which have neighbors no closer than approximately  $1\frac{1}{2}$  diameters away. The interactions between the fields around bubbles which sit closer on the electrode are too complicated for convenient theoretical analysis; hence, conductivity measurements were performed on a large scale model of a planar hexagonal array of bubbles tangent to an electrode. The results of these experiments are presented in Chapter III.

After ions are discharged and form molecules at an electrode, the molecules are dissolved in the electrolyte and diffuse away toward the bulk solution. Because gases such as  $H_2$ ,  $O_2$ , and  $Cl_2$  are only sparingly soluble in electrolytes, dissolved gases cannot be transported away from the electrode fast enough, even at low current

densities, to prevent significant supersaturation of gas at the interface and subsequent nucleation of gas bubbles. Once a nucleus exists, it grows only as rapidly as additional molecules can diffuse to the gas-liquid interface. Thus growth is mass-transfer limited. This mechanism has been extensively studied mathematically and verified experimentally. As the bubble grows, it may coalesce with other bubbles close to it or it may depart never having coalesced. When the stress on a bubble overcomes the surface forces which attach it to the electrode, it departs.

All of the above processes, nucleation, growth by diffusion, growth by coalescence, and departure from the electrode, occur rapidly and on a small scale. Microscopy and high speed cinematography are required to reveal details of these processes at the electrode surface. Viewing the action from the front side is complicated because the most important events occur close to the surface and these are obscured by other bubbles passing between the camera and the electrode; therefore, we evolved oxygen on a transparent electrode and viewed the events from the backside. A discussion of the experiments which includes some frame sequences from the motion pictures compose the last part of this dissertation.

## II. REVIEW OF THE EFFECTIVE CONDUCTIVITY OF ELECTROLYTES CONTAINING DISPERSIONS OF DIELECTRIC SPHERES

### 1. Introduction to the Literature Survey

Many investigators have discussed the conductivity of heterogeneous media; there is at least one extensive review of the subject in the electrochemical literature (1). One should consult this article for information on the effect of dispersed phase shape and non-zero conductivity; I shall not duplicate its broad aspects but will concentrate on the results suitable for small gas bubbles, that is, on the results for dielectric spheres.

The experimental and theoretical results predict the conductivity for three types of arrangements of spheres.

1. Random arrangements of uniform spheres.
2. Ordered arrangements of uniform spheres.
3. Random arrangements of broad ranges of sphere sizes.

In the discussion to follow, the equations appropriate to each of these categories are presented and compared to experimental data in both dilute and concentrated ranges of gas void fraction. (The data, compiled from the literature, are presented numerically with short discussions of their origins in Appendix A.) Then the most accurate equations are selected and compared over the whole range of void fraction with all of the experimental data.

These equations and data are suitable for use in the bulk electrolyte but may not be appropriate for the layer of gas bubbles on the electrode surface because the bubbles there may be more densely

packed, they are not perfect spheres, and their environment is not isotropic on the average since there is an electrode on one side and bulk electrolyte on the other. After the discussion of the bulk conductivities, some empirical results for the resistance of bubble layers are reviewed with the conclusion that theoretical work on the subject is justified.

## 2. Random Arrangements of Monosized Spheres

The classical result of Maxwell (2) plus several other theoretically derived equations can be grouped into the category of equations which predict the conductivity of random arrangements of monosized spheres. Each of the equations in this section is compared to the appropriate data in both dilute and concentrated regions. Because Maxwell's result is fundamental to the theory of heterogeneous conductivity, because many authors have rederived the same result, and because their derivations reveal important concepts in the theoretical approaches to this subject, I begin the survey of this category with four different derivations of the Maxwell equation.

Maxwell considered a spherical surface of radius "a" which has resistivity  $\rho_d$  inside and  $\rho_d$  outside. He expanded the potential inside the surface and outside in spherical harmonics. (For simplicity, I use only the first harmonic.)

$$V_d = (A_d r + B_d / r^2) S_1 \quad (1)$$

$A_d$  is related to the field driving the current and  $B_d$  is the amount of disturbance caused by the sphere.  $S_1$  is the first harmonic,  $\cos \theta$ . Likewise outside the sphere

$$V_c = (A_c r + B_c / r^2) S_1 \quad (2)$$

At the surface,  $r = a$ , Maxwell required equivalence of currents and equivalence of potentials from both regions.

$$V_d = V_c \quad (3)$$

$$\frac{1}{\rho_d} \frac{dV_d}{dr} = \frac{1}{\rho_c} \frac{dV_c}{dr} \Big|_{r=a} \quad (4)$$

Applying these conditions and solving for  $B_c$  and  $A_c$ , Maxwell obtained

$$B_c = \frac{A_d a^3}{3\rho_d} (\rho_d - \rho_c) + \frac{B_d}{3\rho_d} (\rho_d + 2\rho_c) \quad (5)$$

$$A_c = \frac{A_d}{3\rho_d} (2\rho_d + \rho_c) + \frac{2B_d}{3\rho_d a^3} (\rho_d - \rho_c) \quad (6)$$

If there are no sources or sinks within the sphere, the potential cannot be infinite anywhere inside; hence  $B_d$  is zero. Maxwell solved for  $B_c$ , the disturbance coefficient outside the sphere, in

terms of  $A_c$ , the slope of the impressed linear potential which drives the flow of electricity.

$$B_c = \frac{a^3(\rho_d - \rho_c)}{2\rho_d + \rho_c} A_c \quad (7)$$

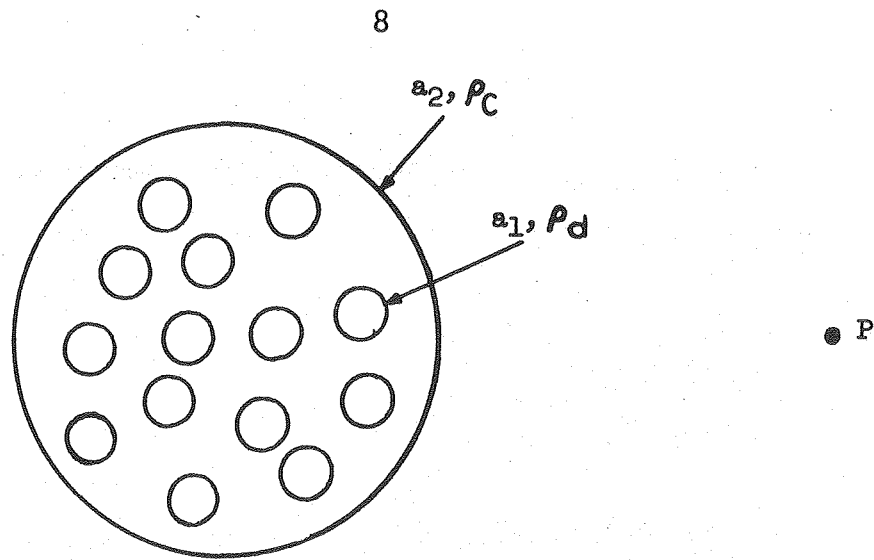
He then considered two cases. First, he drew an imaginary sphere of radius  $a_2$  around a dispersion of small spheres each of radius  $a_1$ . The resistivity inside the inner spheres is  $\rho_d$  while the resistivity in the continuous medium inside and outside of  $a_2$  is  $\rho_c$ . The system appears in Fig. 1. At point P he wrote the potential as

$$V = \left[ A_c r + \frac{na_1^3(\rho_d - \rho_c)}{2\rho_d + \rho_c} \frac{A_c}{r^2} \right] \cos \theta \quad (8)$$

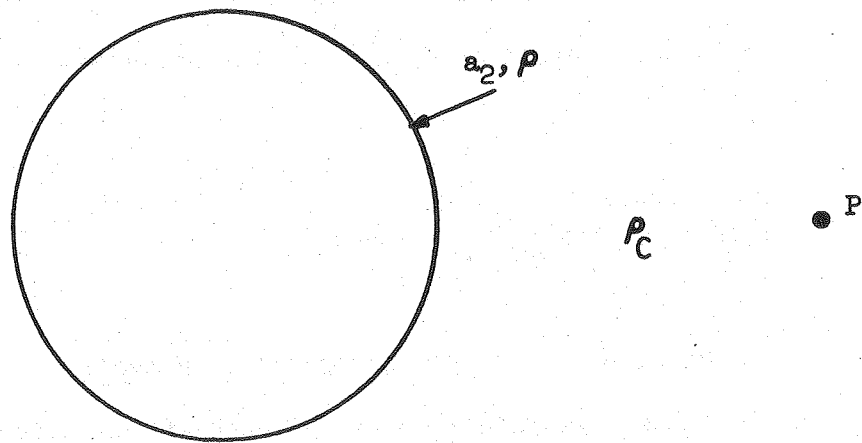
where  $n$  is the number of dispersed spheres. Maxwell assumed in this equation that the disturbance caused by each of the small spheres can be expressed by Eq. (7), derived for a concentric sphere, and that these disturbances can be summed to give the disturbance of  $n$  spheres.

For the second case, he considered a sphere having resistivity  $\rho$ , radius  $a_2$ , and immersed in a medium of resistivity  $\rho_c$ . This system appears in Fig. 1(b). He again wrote the potential at a point P outside the sphere.

$$V = \left[ A_c r + \frac{a_2^3(\rho - \rho_c)}{2\rho + \rho_c} \frac{A_c}{r^2} \right] \cos \theta \quad (9)$$



(a)



(b)

XBL 8011-7575

Fig. 1. The two cases of Maxwell's derivation (a)  $n$  small spheres disseminated in a large sphere (b) homogeneous sphere embedded in a continuous medium.

where  $\rho$  is a heterogeneous resistivity which accounts for both the dispersed and continuous media inside radius  $a_2$ . Equating the disturbance coefficients in the two equations, Maxwell obtained his expression for the resistivity of heterogeneous media.

$$\rho = \frac{2\rho_d + \rho_c + f(\rho_d - \rho_c)}{2\rho_d + \rho_c - 2f(\rho_d - \rho_c)} \quad (10)$$

where  $f$  is the void fraction of the dispersed medium. For infinite dispersed phase resistivity, such as for gas bubbles, the equation reduces to

$$\frac{\rho}{\rho_c} = \frac{1 + \frac{f}{2}}{1 - f} \quad (11)$$

$$K_m = \frac{1 - f}{1 + \frac{f}{2}} \quad (12)$$

where  $K_m$ , as in all subsequent equations, is the ratio of the gas-present bulk conductivity to the gas-absent conductivity of the continuous medium. One would derive the same result if one considered a single concentric sphere of volume  $\pi a_1^3$  surrounded by an imaginary spherical shell of radius  $a_2$  and resistivity the same as that of the surroundings; therefore, Maxwell's solution is not determined by the arrangement of gas within the system. It is accurate in the dilute range of void fractions in heterogeneous media because, as he noted,

". . . whether the spherical shell (i.e., the continuous medium), conducts better or worse than the rest of the medium, the electrical action in the space occupied by the shell is less than it would otherwise be. If the shell is a better conductor than the rest of the medium it tends to equalize the potential all around the inner sphere. If it is a worse conductor, it tends to prevent the electrical currents from reaching the inner sphere at all."

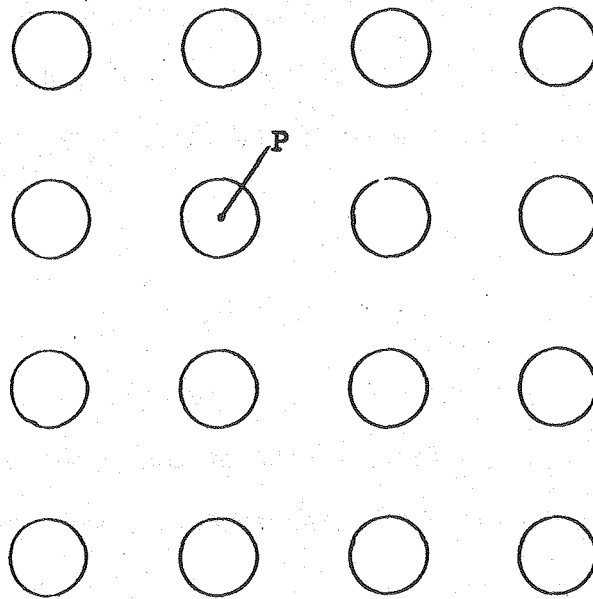
When the concentration of spheres reaches approximately 20 percent, the interactions of fields around bubbles become significant and the electrical activity in the shells surrounding bubbles is no longer reduced; hence Eq. (12) cannot give very accurate answers past this point.

While calculating the conductivity parallel to the principal planes of a cubic array of spheres, Rayleigh (6) produced an alternate derivation of Maxwell's result for randomly disseminated spheres. Rayleigh's complete answer is an infinite series which gives a better approximation as more terms are included. I present his derivation in an abbreviated form which includes only the lower order terms to compare it to Maxwell's derivation.

A cubic array schematic appears in Fig. 2. Rayleigh expanded the potential in the continuous and dispersed media in spherical harmonics around the sphere at point P.

$$V_c = D_o + (A_c r + B_c / r^2) \cos \theta \quad (13)$$

$$V_d = C_o + C_d r \cos \theta \quad (14)$$



XBL 8011-7577

Fig. 2. Section through a cubic array of spheres.

$V_c$  is the potential in the continuous medium while  $V_d$  is that in the dispersed medium.  $D_0$  and  $C_0$  are constants which vary from sphere to sphere (but not in between). Applying equivalence of potential and current at the spherical surface, Rayleigh found a relation between the constants of the first equation.

$$B_c = \frac{1}{2} a^3 A_c \quad (15)$$

He then derived the conductivity as a function of the first coefficient of disturbance,  $B_c$ , and the strength of the impressed field,  $E_0$ , by applying Green's theorem to the spherical and rectangular boundary of a unit cell in the array.

$$K_m = 1 - \frac{4\pi B_c}{\alpha^3 E_0} \quad (16)$$

where  $K_m$  is the conductivity ratio and  $\alpha$  is the length of a side.

Needing to relate  $B_c$  to  $E_0$ , Rayleigh equated an expansion for the potential around point P to the sum of the driving potential,  $E_0 \cos \theta$ , and potential due to sources located at the center of the other spheres of the array.

$$D_0 + A_c x = E_0 x + B_c \sum_{i=1}^{\infty} \frac{(x - \xi)}{((x - \xi)^2 + (y - \eta)^2 + (z - \rho)^2)^{3/2}} \quad (17)$$

$x, y, z$  are the Cartesian equivalents of  $r$ ,

$\xi, \eta, \zeta$  are the coordinates of the spheres in the cubic array referred to the sphere at point P.

$$\rho^2 = (\xi^2 + \eta^2 + \zeta^2).$$

After grouping the two terms in  $x$  on the left, Rayleigh expanded the right side in  $x$  around the point P at  $x, y, z = 0, 0, 0$ . He then equated the terms first order in  $x$  to find

$$(A_c - E_0) = -B_c \sum \frac{\rho^2 - 3\xi^2}{\rho^5} \quad (18)$$

Using Eqs. (15) and (18), Rayleigh obtained

$$E_0 a^3 / B_c = 2 + a^3 \sum \frac{\rho^2 - 3\xi^2}{\rho^5} \quad (19)$$

$$-\frac{1}{2} \sum \frac{d}{d\xi} \left( \frac{\xi}{\rho^3} \right) = \sum \frac{\rho^2 - 3\xi^2}{\rho^5} \quad (20)$$

Noting that the right hand term is a perfect differential, Eq. (20), he let it pass to an integral; that is, he evaluated the integral

$$\iiint \frac{d}{d\xi} \left( \frac{\xi}{\rho^3} \right) d\xi d\eta d\rho \quad (21)$$

This step implies that the points of potential are uniformly dispersed about the central sphere and thus echoes Maxwell's derivation for the

randomly disseminated spheres. Integrating and inserting the result in Eqs. (19) and (16), Rayleigh obtained Maxwell's result.

$$K_m = \frac{1 - f}{1 + \frac{f}{2}} \quad (22)$$

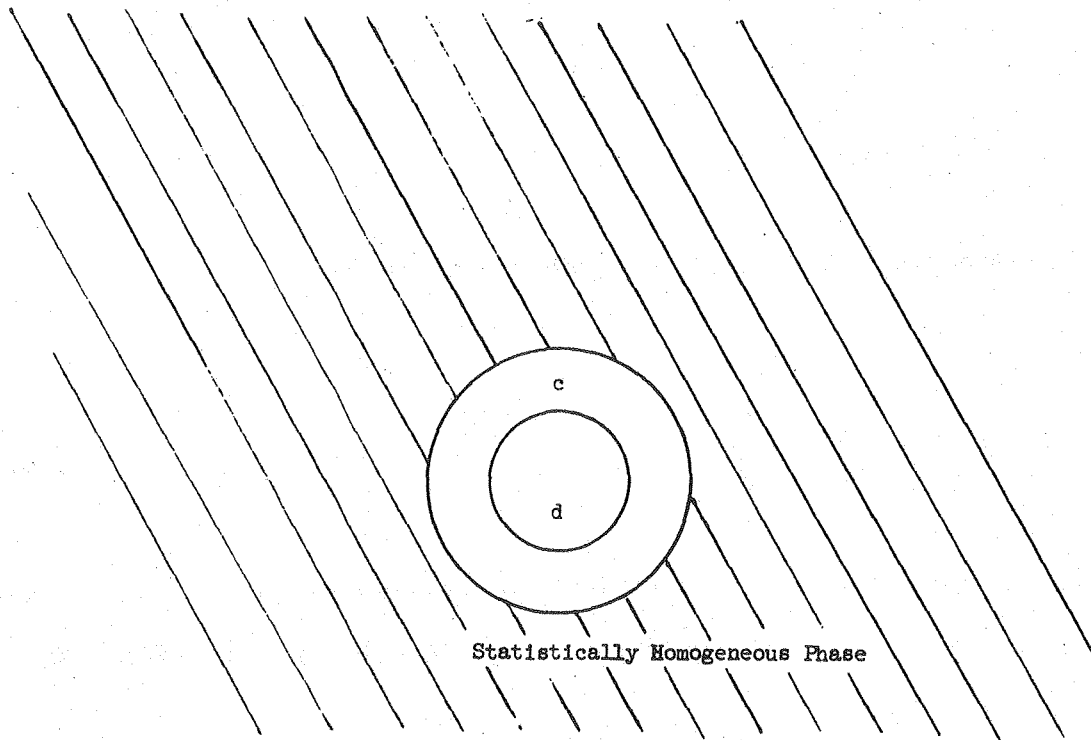
Z. Hashin (7) derived Maxwell's relation by considering a sphere (representing the dispersed phase) embedded concentrically in another sphere (representing the continuous phase) which is in turn embedded in a third statistically homogeneous phase consisting of dispersed and continuous phases. A schematic of this model appears in Fig. 3. He first defined volume averages of the fluxes in the three phases,

$$\bar{T}_c = k_c \bar{E}_c$$

$$\bar{T}_d = k_d \bar{E}_d \quad (23)$$

$$\bar{T} = k \bar{E}$$

where  $\bar{i}$  is the average current density,  $k$  is the effective conductivity and  $\bar{E}$  is the volume averaged electric field. The letters  $c$ ,  $d$  and no subscript represent the continuous, dispersed, and outer homogeneous phases, respectively. Since the total current in the concentric spheres is the sum of the two partial currents and the average current density in the spheres is the same as that in the outer medium, Hashin wrote



XBL 8011-7576

Fig. 3. The self-consistent volume averaged model of Hashin  
d: dispersed phase  
c: continuous phase

$$k\bar{E} = k_c(1 - f)\bar{E}_c + k_d f\bar{E}_d \quad (24)$$

Combining Eq. (24) with

$$\bar{E} = f\bar{E}_d + (1 - f)\bar{E}_c \quad (25)$$

and eliminating the continuous phase field, he found

$$k = k_c + (k_d - k_c) \frac{\bar{E}_d}{\bar{E}} f \quad (26)$$

and concluded that "it is sufficient to know the average of the intensity (field) over one phase only in order to calculate the effective conductivity."

In order to determine the ratio of the average electric field in the dispersed phase to the average electric field in the outer mixture, he developed expressions that one may also find in Maxwell's Electricity and Magnetism (2); Hashin expanded the potential in spherical harmonics and deduced the necessary relationships between the fields in three concentric phases by applying the usual conditions on current and potential at the phase boundaries. When  $k_d$  is zero, as for gas bubbles,

$$\frac{\bar{E}_d}{\bar{E}} = \frac{9/2 k}{2k + k_c + (k - k_c) f} \quad (27)$$

Inserting (27) into (26) and letting

$$K_m = k/k_c \quad (28)$$

he found

$$(2 + f) K_m^2 + \frac{5}{2} f - 1 + (f - 1) = 0 \quad (29)$$

from which by the quadratic formula he obtained

$$K_m = \frac{1 - f}{1 + \frac{f}{2}} \quad (30)$$

which is Maxwell's result.

Neale and Nader (8) used Hashin's (7) model as the basis for their derivation; however, they evaluated the disturbances in the concentric continuous phase instead of those in the dispersed phase. In the nomenclature of the previous derivation, they first expressed the potential in the concentric continuous phase as

$$V_c = A_c \bar{E} \left[ r + \frac{1}{2} \frac{a_c^3}{r^2} \right] \cos \theta \quad (31)$$

The coefficient  $A_c$ , the disturbance in the concentric (continuous) phase, can again be found from Maxwell's developments.

$$A_c = \frac{3k}{2k + kf + 1 - f} \quad (32)$$

Having an expression for the potential in the continuous phase, they used it to satisfy the requirement that all the current flowing in a tube of diameter equal to that of the outer concentric sphere must equal the current derived from Eq. (31) integrated from the inner sphere surface to the outer spherical surface, that is

$$\int_{a_c}^{a_d} -k_c \frac{1}{r} \left. \frac{\partial V_c}{\partial \theta} \right|_{\theta=\pi/2} 2\pi r dr = \pi a_c^2 K_m \bar{E} \quad (33)$$

Differentiating Eq. (31) and integrating according to Eq. (33), they found

$$\frac{3(a_c^3 - a_d^3)}{2K_m + K_m f + (1 - f)} = a_c^3 \quad (34)$$

from which they deduced

$$K_m = \frac{1 - f}{1 + \frac{f}{2}} \quad (35)$$

where

$$f = \frac{a_d^3}{a_c^3} \quad (36)$$

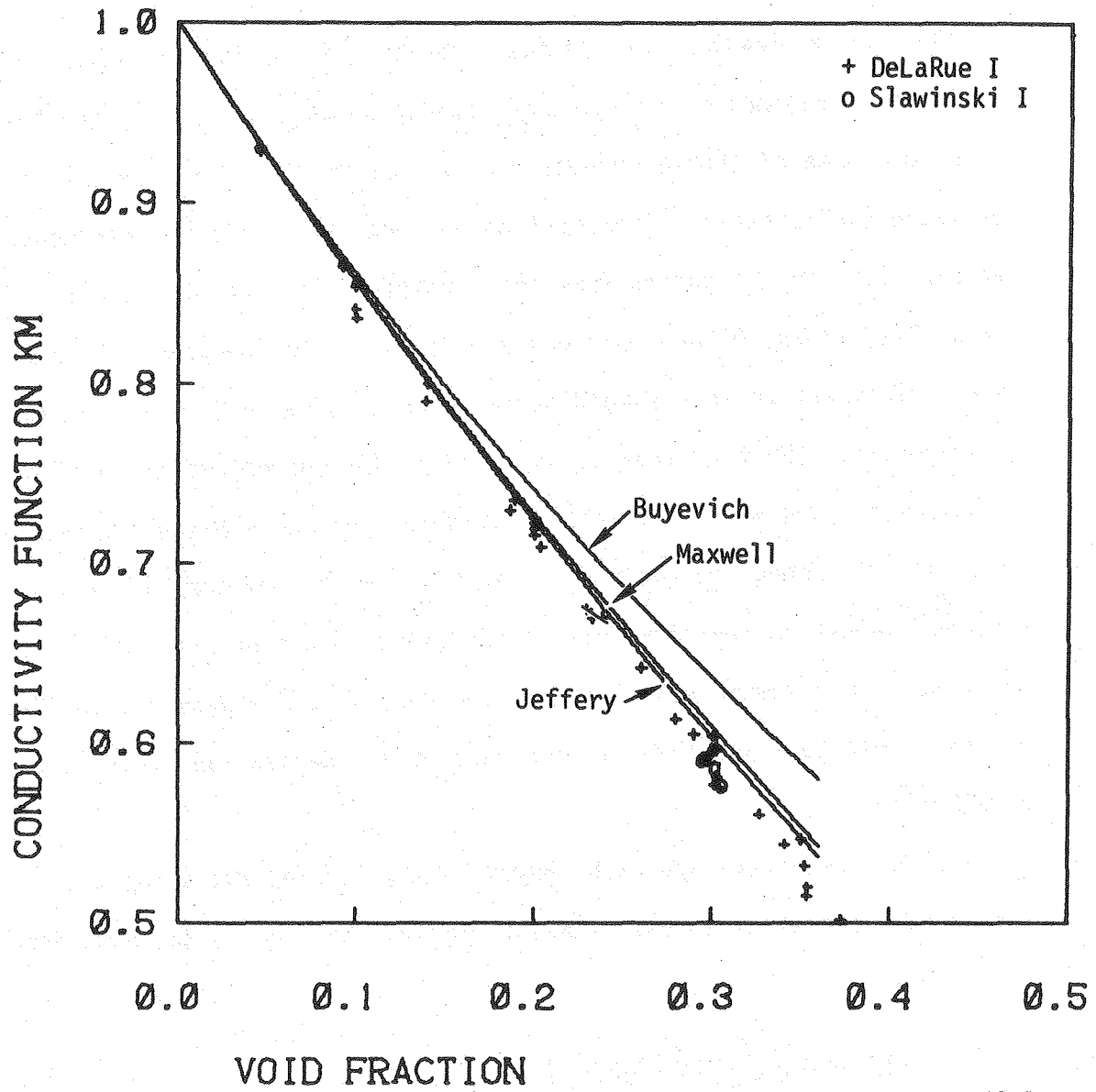
The four derivations of the same result indicate that Maxwell's result is a fundamental relation of heterogeneous conductivity and they illustrate some of the techniques one can use to theoretically investigate such systems. The equation has been popular for experimental verification; investigators from the turn of the century to recent years (8,13,17,19,20) have claimed and disputed its applicability even up to void fractions corresponding to touching spheres in some packing arrangements. The fact that it is valid at low concentrations and that it passes through zero at a void fraction of one makes Maxwell's result never grossly wrong, as one can see in Figs. 4 and 5 where Eq. (12) is plotted against appropriate data in the dilute and concentrated regions. The maximum deviation from the data is a few percent; in view of its simple form and the relative ease of its derivation, this is remarkable.

Trying a different approach, Buyevich (3) modeled the spheres surrounding a central sphere as point dipoles and deduced the equation

$$K_m = \frac{\beta(17\beta + 7)}{(1-f)(17\beta + 7) + 36f\beta} \quad (37)$$

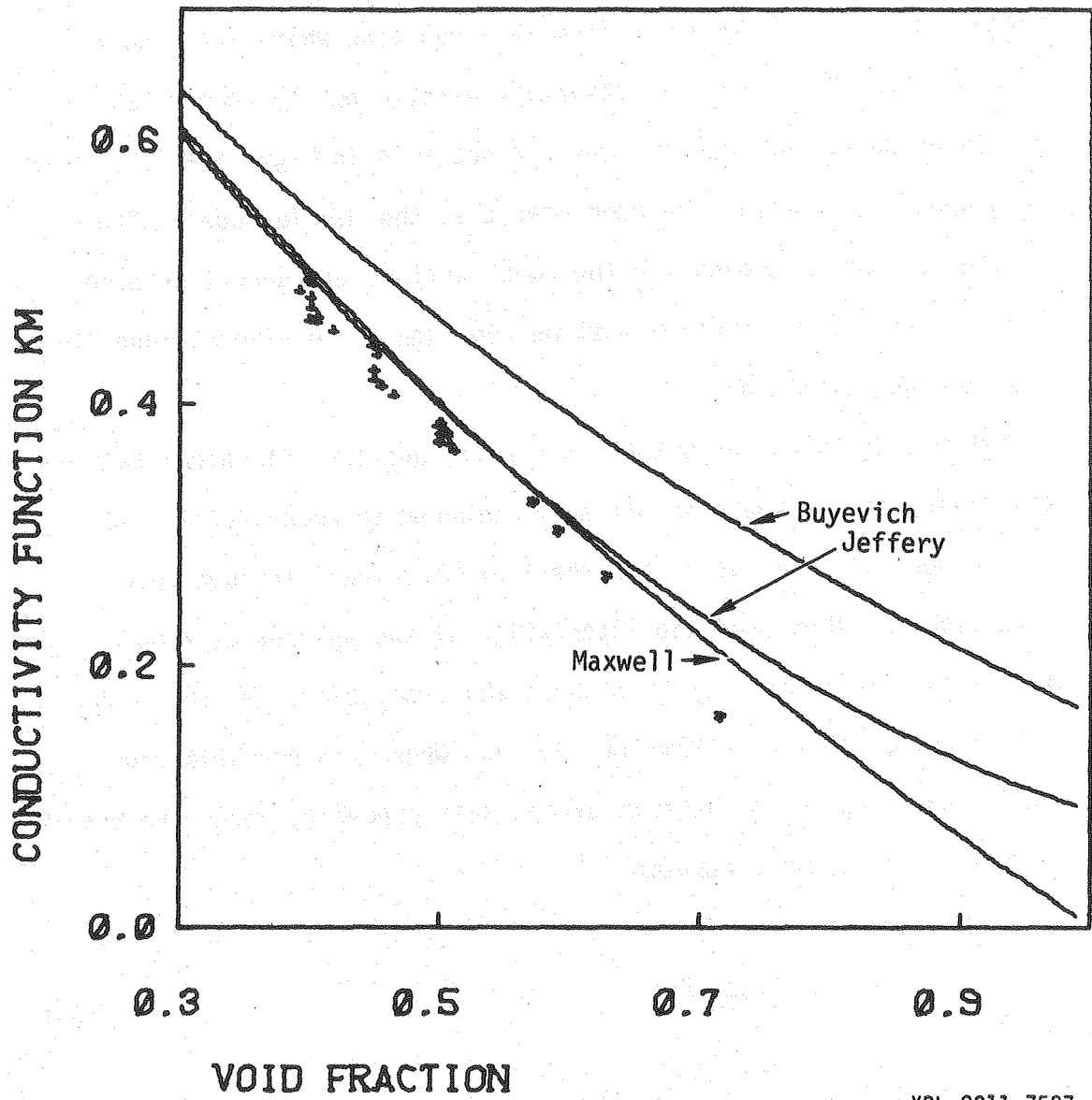
where

$$\beta = \frac{1}{34} \left\{ 10 - 17f + [(10-17f)^2 + (1-f)(476)]^{1/2} \right\}$$



XBL 8011-7586

Fig. 4. Equations for random arrangements of monosized spheres.



XBL 8011-7587

Fig. 5. Equations for random arrangements of monosized spheres (concentrated region).

One calculates conductivities from this equation which are higher than those of Maxwell, a physical absurdity pointed out by Turner (19) and noticed by Buyevich himself. One can see this in Figs. 4 and 5, which are graphs of Eq. (37). He concluded that the dipole model suffers because it cannot account for the constrictions of current between spheres; hence this solution must be regarded as an elegant model that is a poor approximation.

Attempting to extend Maxwell's result, Jeffery (4) calculated the resistivity of a suspension of random spheres to order  $O(f^2)$ . He wrote a general formulation for the flux of current through such a suspension and then used the interaction of two spheres as a model for the interactions occurring throughout the suspension. He found the coefficient of  $f^2$  explicitly for the case where all possible configurations of pairs of spheres are equally probable; hence the result is good for a random arrangement.

$$K_m = 1 - \frac{3}{2} f + 0.588 f^2 \quad (38)$$

The values of  $K_m$  calculated from this equation appear in Figs. 4 and 5. One can see that there is a slight improvement on Maxwell's solution at void fractions less than 0.5, but that Jeffery's result deviates severely at greater void fractions.

Higuchi (5) also tried to improve the classical result of Clausius and Mossotti for the dielectric constant analogous to Maxwell's result by deducing a correction to the average field which surrounds the

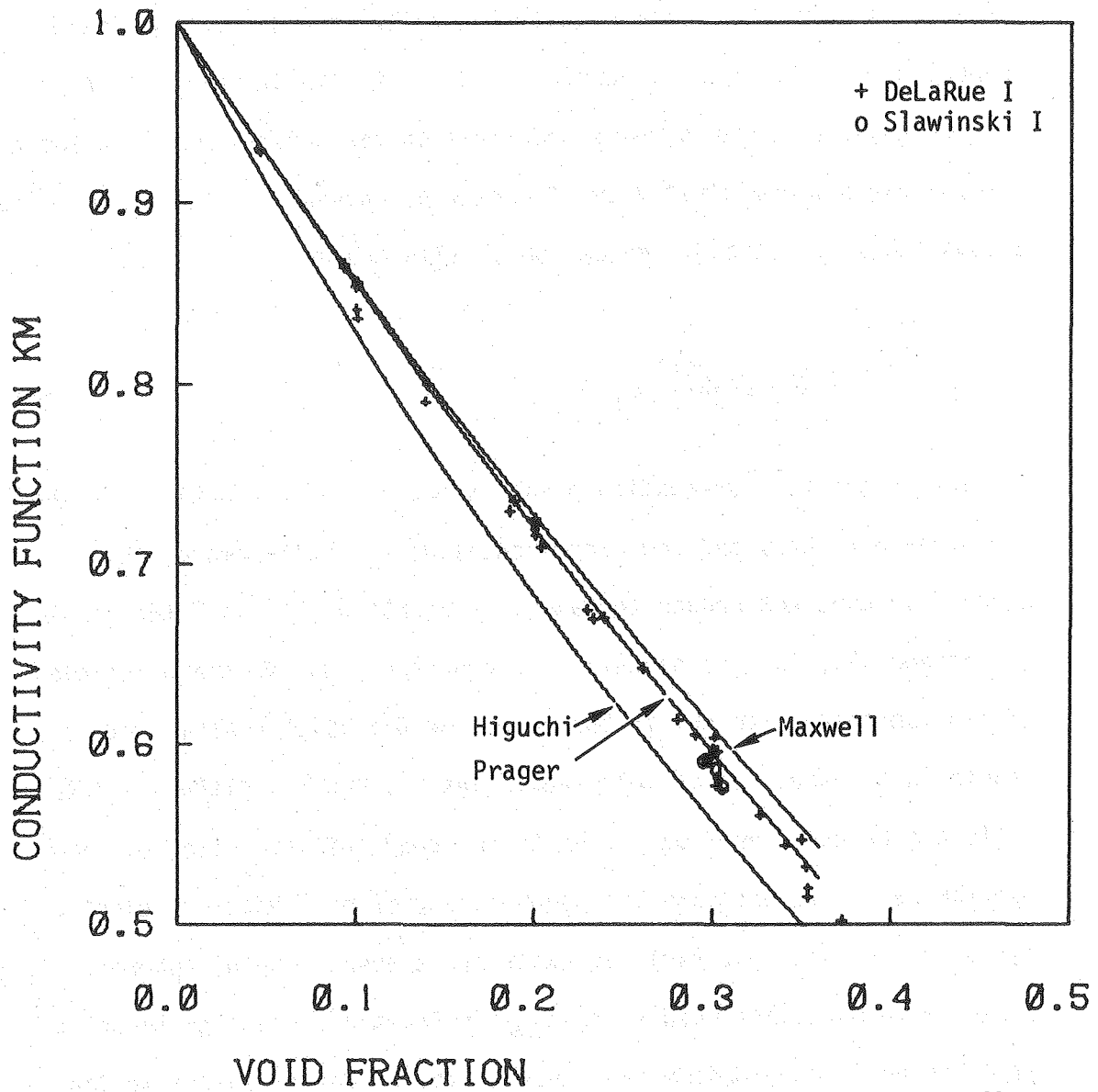
particle of interest. Specifically, he calculated a reaction field proportional to an unknown constant and due to dipole interactions between adjacent spheres; he summed this to the conventionally assumed average field and evaluated the constant by comparing his equation with a compilation of data by Pearce (30). Illustrated

$$K_m = \frac{2(1 - f) - 0.39(1 - f)}{2 + f - 0.39(1 - f)} \quad (39)$$

in Figs. 6 and 7, his equation predicts much lower conductivities than the other equations and the experimental data. Furthermore, the expression does not reduce to Maxwell's result at low void fractions.

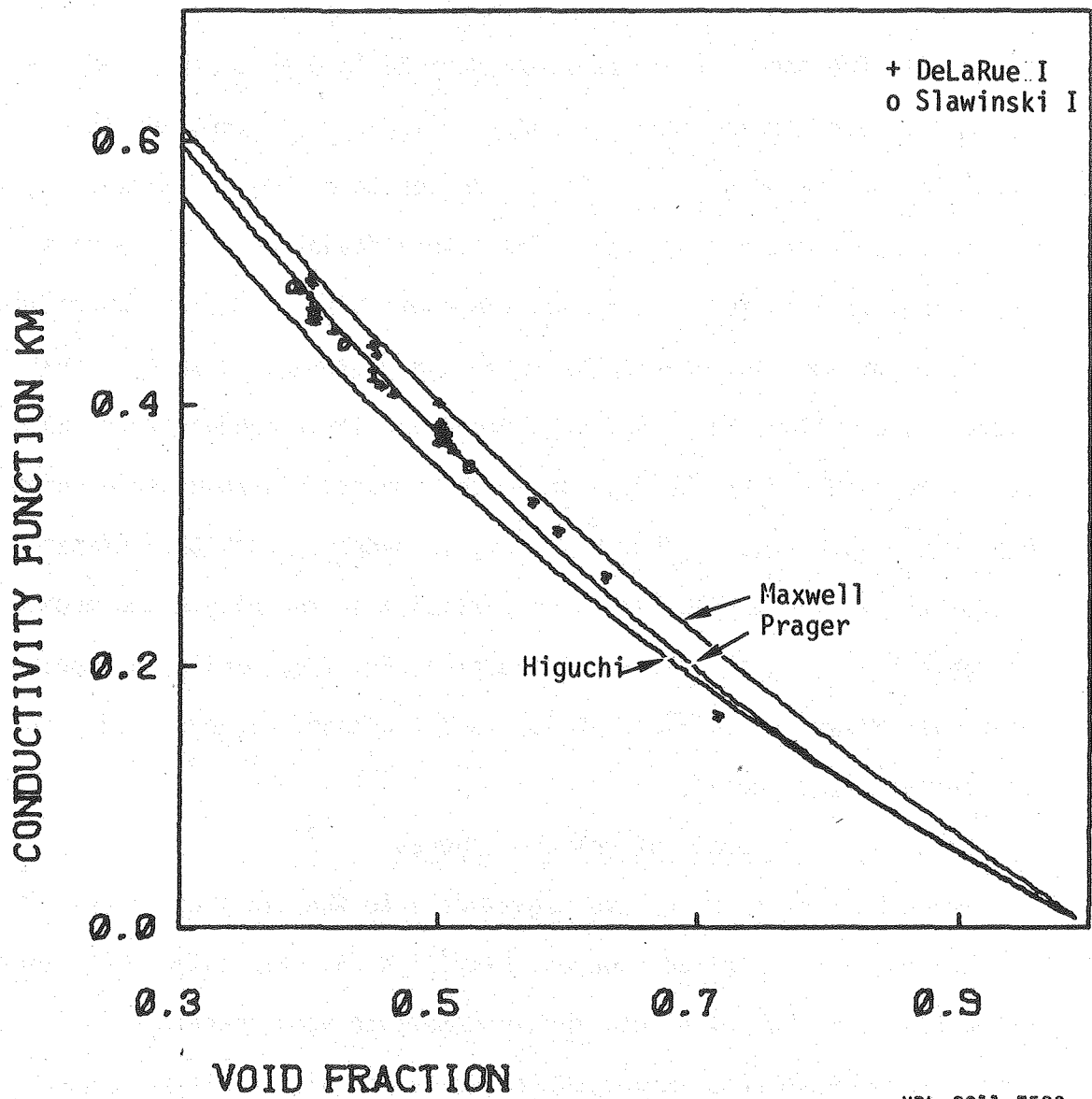
Prager (9), in an apparently new approach, applied the principle of minimum entropy to obtain bounds on the diffusion coefficient of a solute in a suspension of solid particles. Since the diffusion rate ratio can be considered analogous to the conductivity ratio, one may use the result to estimate the conductivity of heterogeneous electrolyte. His result, Eq. (40), is exact for a suspension of spheres. It agrees with Maxwell's result at low void fractions and significantly improves on it over medium and concentrated ranges of void fraction. Its predictions appear in Figs. 6 and 7 with appropriate data. Prager's equation agrees with the data of DeLaRue (10) and Slawinski (11), while Meredith's data (12) bracket the predictions of Prager's equation:

$$K_m = 1 - \frac{3}{2} f + 0.5 f^2 \quad (40)$$



XBL 8011-7588

Fig. 6. Equations for random arrays of monosized spheres (dilute region).



XBL 8011-7589

Fig. 7. Equations for random arrangements of monosized spheres (concentrated region).

Of all the theoretical equations derived to predict the conductivity ratio of random arrangements of monosized spheres, I conclude that Prager's fits the data significantly better than those of Maxwell, Jeffery, Buyevich, and Higuchi. The severe deviation of Buyevich's result Eq. (37) indicates the importance of using potential expressions derived from spherical harmonics to obtain reasonable results. That Higuchi's equation, Eq. (39), gives much too low a conductivity ratio must mean either that the data on which he based his adjustable parameter were inaccurate or that his analysis overestimates the interactions between the dipole fields of particles in the dilute and medium concentration ranges. Jeffery's equation, Eq. (38), while an improvement over Maxwell's equation at low void fraction, diverges badly in the concentrated region.

### 3. Ordered Arrangements of Uniform Spheres

There have been three investigations into the class of ordered arrangements of monosized spheres. Rayleigh (6) calculated theoretical conductivity ratios at dilute to intermediate void fractions in a cubic array of spheres, Meredith (13) extended his result to higher order terms and experimented with these arrays, while Mashovets (14) also experimented with ordered arrangements of monosized spheres and suggested an empirical equation to fit his data.

Rayleigh (6) extended the derivation presented earlier to include another term and obtained a formula which gave a better value for the conductivity of his cubic array. Not finding a convenient calculation for the second coefficient as he did for the first discussed earlier,

he summed the contributions of the spheres closest to the reference sphere to obtain its value.

$$K_m = \frac{2(1 - f) - 0.394 f^{10/3}}{2 + f - 0.394 f^{10/3}} \quad (41)$$

Meredith and Tobias (13) extended this solution to give better results for high gas concentrations.

$$K_m = \frac{(2 + f) + 0.614 f^{7/3} - 0.680 f^{10/3}}{2(1 - f) + 0.614 f^{7/3} - 1.60 f^{10/3}} \quad (42)$$

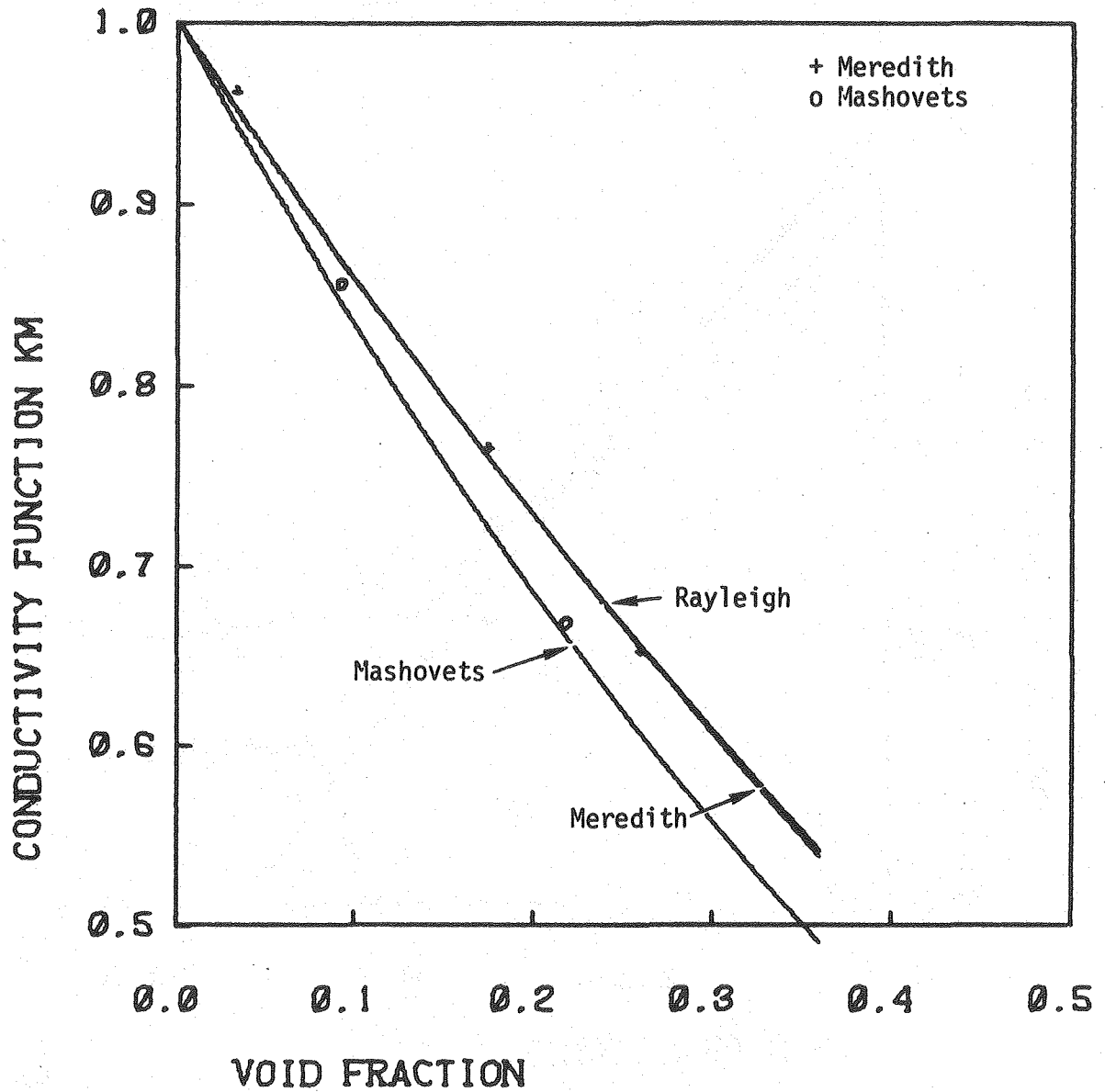
Graphs of Eqs. (41) and (42) appear in Fig. 8 for the dilute region and in Fig. 9 for the concentrated region. They are indistinguishable up to nearly 30 percent gas fraction. Improving on Rayleigh's result, Meredith's equation predicts the lower conductivity as void fraction increases. The small difference between his equation's prediction and his carefully measured data point at a void fraction of 0.52 reflects the accuracy obtained by including an additional term in the series solution to this problem. The equations cannot be physically meaningful past the void fraction corresponding to cubic close packing and in fact both Rayleigh's and Meredith's results diverge severely from the general boundary requirement that the conductivity be zero at a void fraction of one. I conclude that these two relations are unsuitable as candidates for best overall equation.

Mashovets (14) produced an equation which fit his data on ordered arrangements of spheres.

$$K_m = 1 - 1.78 f + f^2 \quad (43)$$

Equation (43) and his data appear in Figs. 8 and 9 with those of Rayleigh and Meredith. Mashovets' data (and equation) are significantly below those of Meredith in the dilute range but lie significantly above those of Meredith in the concentrated range. The three lowest void fractions correspond to dilute face-centered cubic arrangements. The point at  $f = 0.52$ , agreeing with Meredith's result, corresponds to a close packed cubic array (as also does Meredith's). The other points are for hexagonal and face-centered cubic packings where the spheres touch. Mashovets' results seem inconsistent with the fact that at low void fractions one expects agreement with Maxwell's result, even for ordered arrays, as Rayleigh showed. They also seem incorrect at high void fractions where they sharply diverge to higher conductivities. Curiously, his result for cubic close packing agrees with that of Meredith, but I conclude that Mashovets' equation is not generally accurate.

The equations of this section are not suitable for the entire range of void fractions. Meredith's equation is accurate to void fractions near where the spheres touch in a cubic array, but it diverges badly afterward. It might be worthwhile to reproduce Mashovets' work on other types of packings to show the differences between various types of arrangements.



XBL 8011-7583

Fig. 8. Equations for Ordered Arrangements of monosized spheres (dilute region).

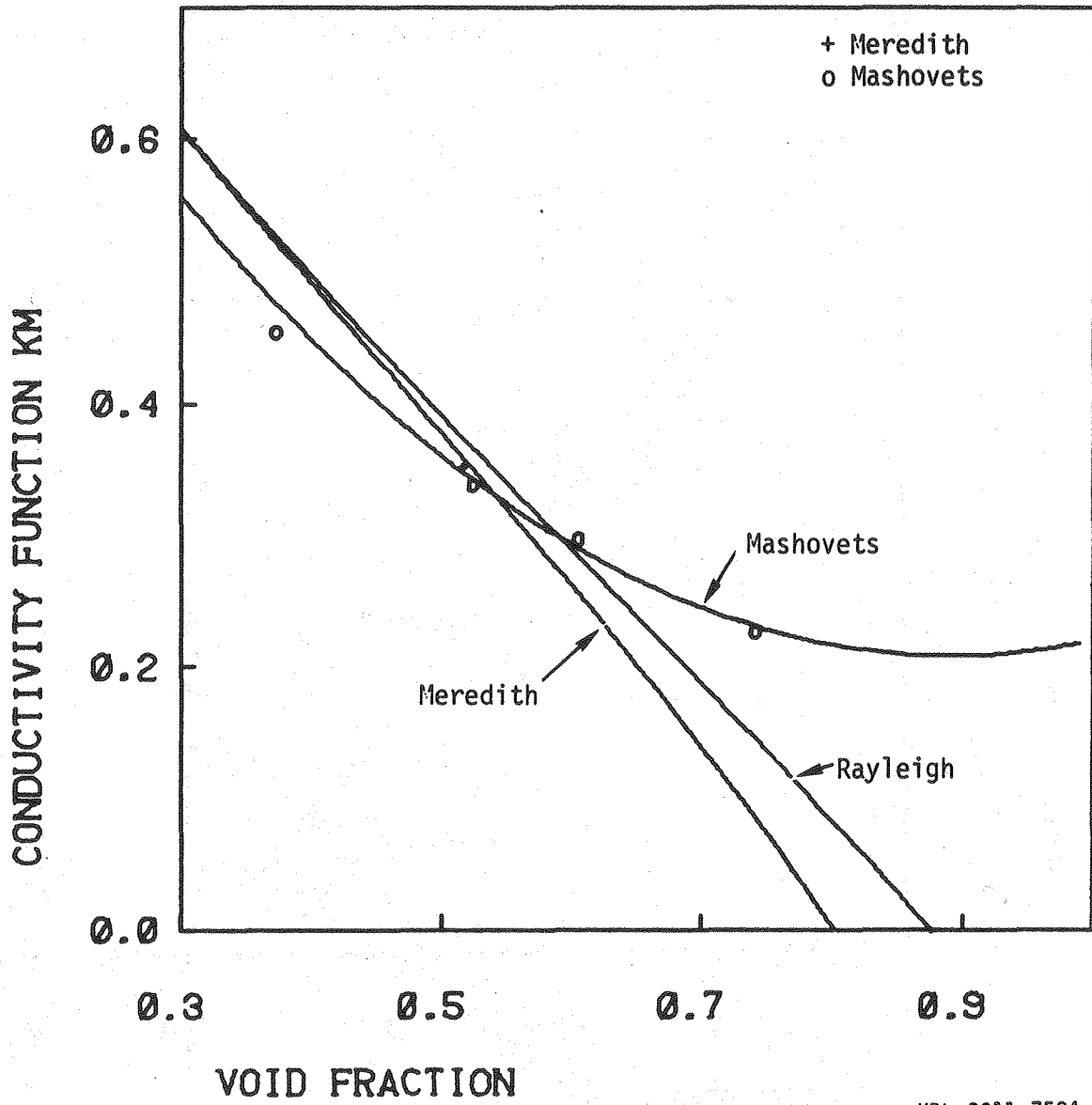


Fig. 9. Equations of ordered arrangements of monosized spheres (concentrated region).

XBL 8011-7584

#### 4. Random Arrangements of Multisized Spheres

There are two theoretical models based on size distributions of dielectric particles and one equation said to be applicable to multi-sized dispersions. Bruggeman (15) treated a "pseudo-continuous" distribution of sizes by accumulating the contributions of a range of bubble sizes. I call it a pseudo-continuous range because each size fraction of bubbles must be very different from each of the other sizes included in the integration. Adding infinitesimal size fractions, he treated the mixture already present as continuous with a bulk conductivity. One can write this process in differential form (10), from which integration gives

$$K_m = (1 - f)^{3/2} \quad (44)$$

Appearing in Figs. 10 and 11, Bruggeman's result agrees with Maxwell's at low void fractions; it also agrees well with DeLaRue's data in dilute and in intermediate ranges, but it underestimates the conductivity at high void fractions. It does not agree with Slawinski's data in the dilute region, but neither does this data agree with Maxwell's result and must therefore be suspect.

Meredith and Tobias (16) noted the tendency of Bruggeman's equation to overcorrect in the concentrated ranges and devised another approach called the Distribution Model by considering only two size fractions. As in the Bruggeman derivation, the smaller size fraction is added first and then is considered as part of a continuous medium having its

own bulk conductivity when the larger size fraction of bubbles is added. The Distribution Model result, Eq. (45), appears in Figs. 10 and 11.

$$K_m = \frac{8(2-f)(1-f)}{(4+f)(4-f)} \quad (45)$$

Intermediate between Maxwell's and Bruggeman's equations, Eq. (45), is as accurate as Bruggeman's at low void fractions, seems not quite as accurate in the intermediate range, but represents the data well in the concentrated range. As Meredith concluded in his 1962 review (1), the Distribution Model is a compromise between the fact that the conductivity of dispersions which are neither perfectly uniform nor which have the broad range of sizes necessary to justify using the Bruggeman relation falls between Maxwell's and Bruggeman's results.

Slawinski (11) did not use spherical potential theory but deduced average current path lengths which he loaded into simple algebraic expressions for the resistance of general systems. After analyzing various configurations of spheres, he deduced an equation which one must modify as a function of the range of gas fraction.

$$K_m = \frac{1}{1 + \frac{f}{p} \left\{ (1 + 0.321 p^2)^2 / (1 - p) - 1 \right\}} \quad (46)$$

$$p = 0.806 f^{2/3} \quad f < 0.15$$

$$p = (0.806 + 0.133 f) f^{2/3} \quad 0.15 < f < 0.6$$

$$p = 0.904 f^{2/3} \quad 0.6 < f$$

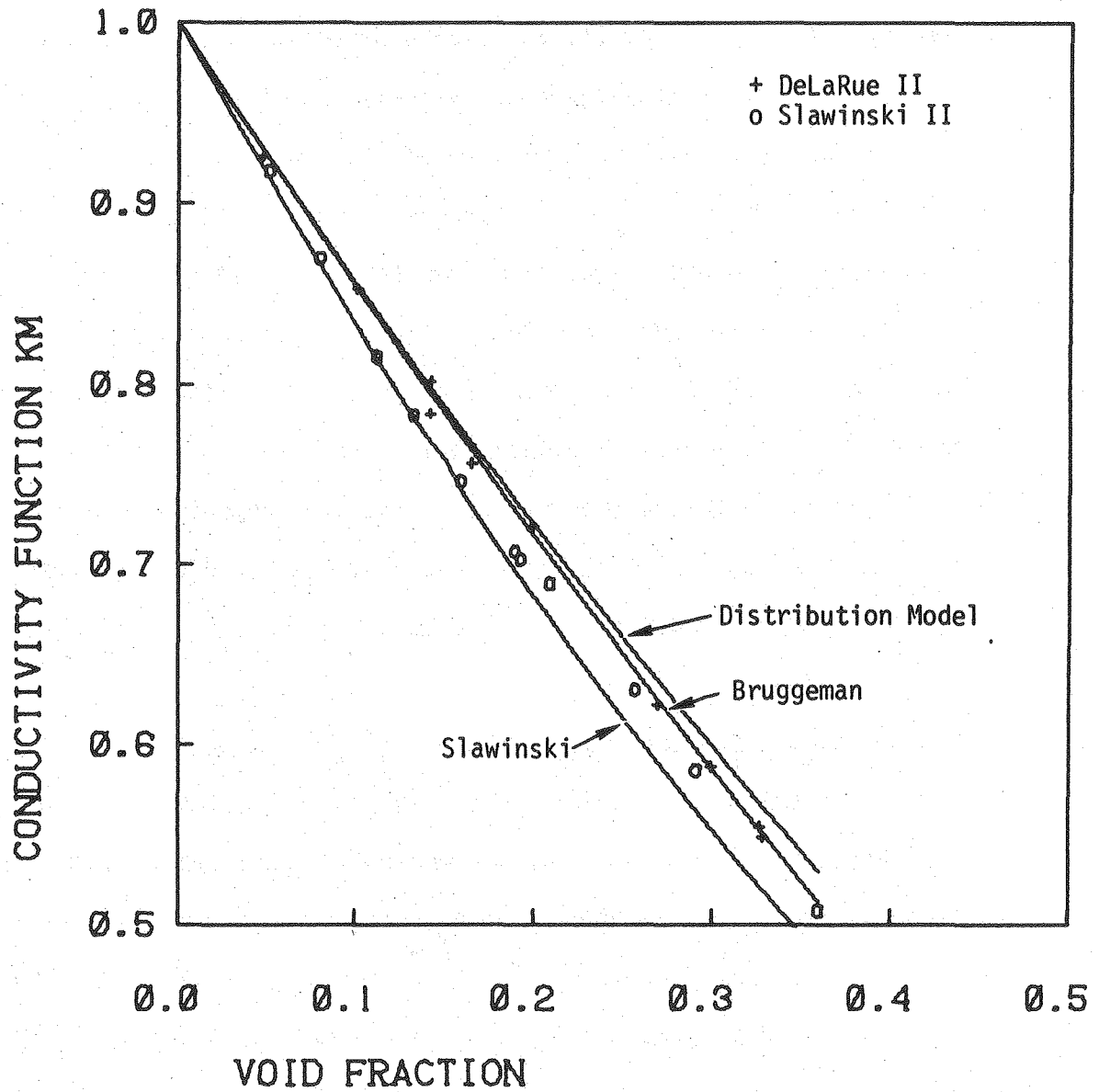
Appearing in Figs. 10 and 11, Eq. (46) apparently agrees with the writer's own data on heterogeneous systems; but neither the data nor the equations agree with Maxwell's result at low void fractions. Furthermore, Slawinski's result diverges from the data at high void fractions so it cannot be suitable over the whole range.

Two of the three equations in this section, Bruggeman's and the Distribution Model, are candidates for the best equation over the whole range of void fraction. They both agree with Maxwell's result at low void fraction. Although they differ in their agreement with data through the medium and concentrated regions, neither diverges badly as some of the others and they both give zero conductivity at a void fraction of one.

##### 5. Conclusion: The Best Equation Over the Whole Range

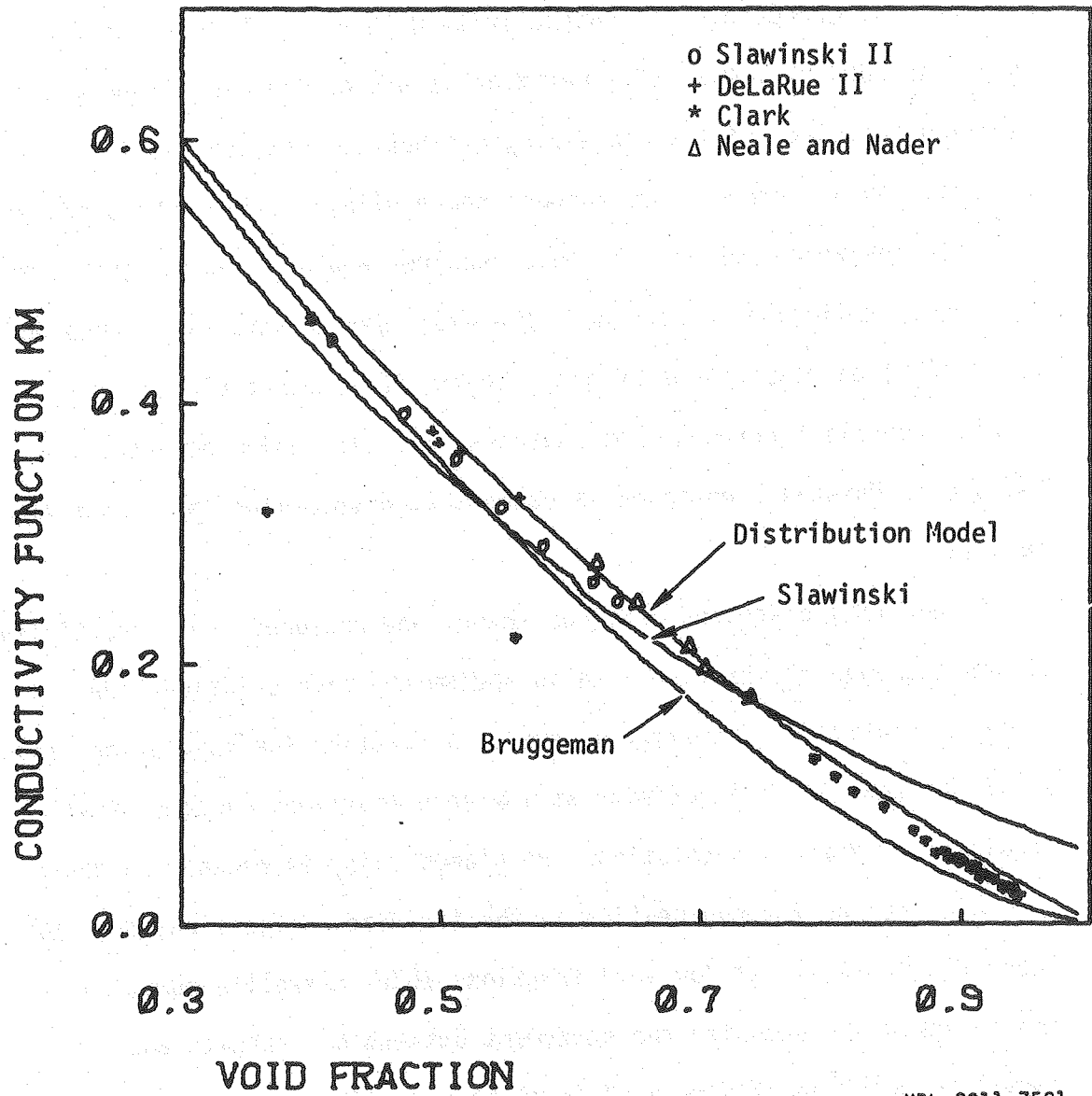
Many investigators, some of whose results were not included in this review because they were not given numerically, have experimented with heterogeneous systems and have claimed success for several of the equations discussed previously. Neale and Nader (8), whose experimental work is discussed in Appendix A, endorsed Maxwell's equation even at void fractions greater than those at which spheres touch in some packings. DeLaRue (10) advocated Bruggeman's equation for random dispersions of multisized spheres.

Sigrist, Dossenbach, and Ibl (17) measured the conductivity of electrolytes containing gas bubbles dispersed through a glass frit. They added 1 percent ethanol to a mixture of aqueous copper sulfate, sulfuric acid, and sodium nitrate; the alcohol favored a uniform size



XBL 8011-7582

Fig. 10. Equations for Random Arrangements of multisized spheres (dilute region).



XBL 8011-7581

Fig. 11. Equations for random arrays of multisized spheres (concentrated region).

of half a millimeter. They determined the void fraction by a static pressure difference and the conductivity with a conventional bridge. They concluded that Maxwell's relation is better than the Bruggeman relation for electrolytes containing gas bubbles because the size distribution is narrow. One wonders how a dilute system result can be accurate for void fractions at which spheres would be touching in some packings. While the authors note the experimental work of DeLaRue and Tobias (18) on dispersions of glass beads, they do not explain the apparent conflict between these authors' results, which depicted the failure of Maxwell's equation in concentrated solutions, and their own results.

Turner (19) discussed previous theory and measured the conductivity of ion exchange resins fluidized in sodium chloride solution. He plotted relative conductivity versus void fraction for insulating beads and found that the conductivity at low void fractions exceeded that predicted by Maxwell's solution. He blamed this discrepancy on experimental error or inhomogeneities in the fluidized dispersion; despite these discrepancies at low void fractions where Maxwell's equation should apply, he accepted the agreement between his results and Maxwell's relation at high void fraction where it should not be accurate.

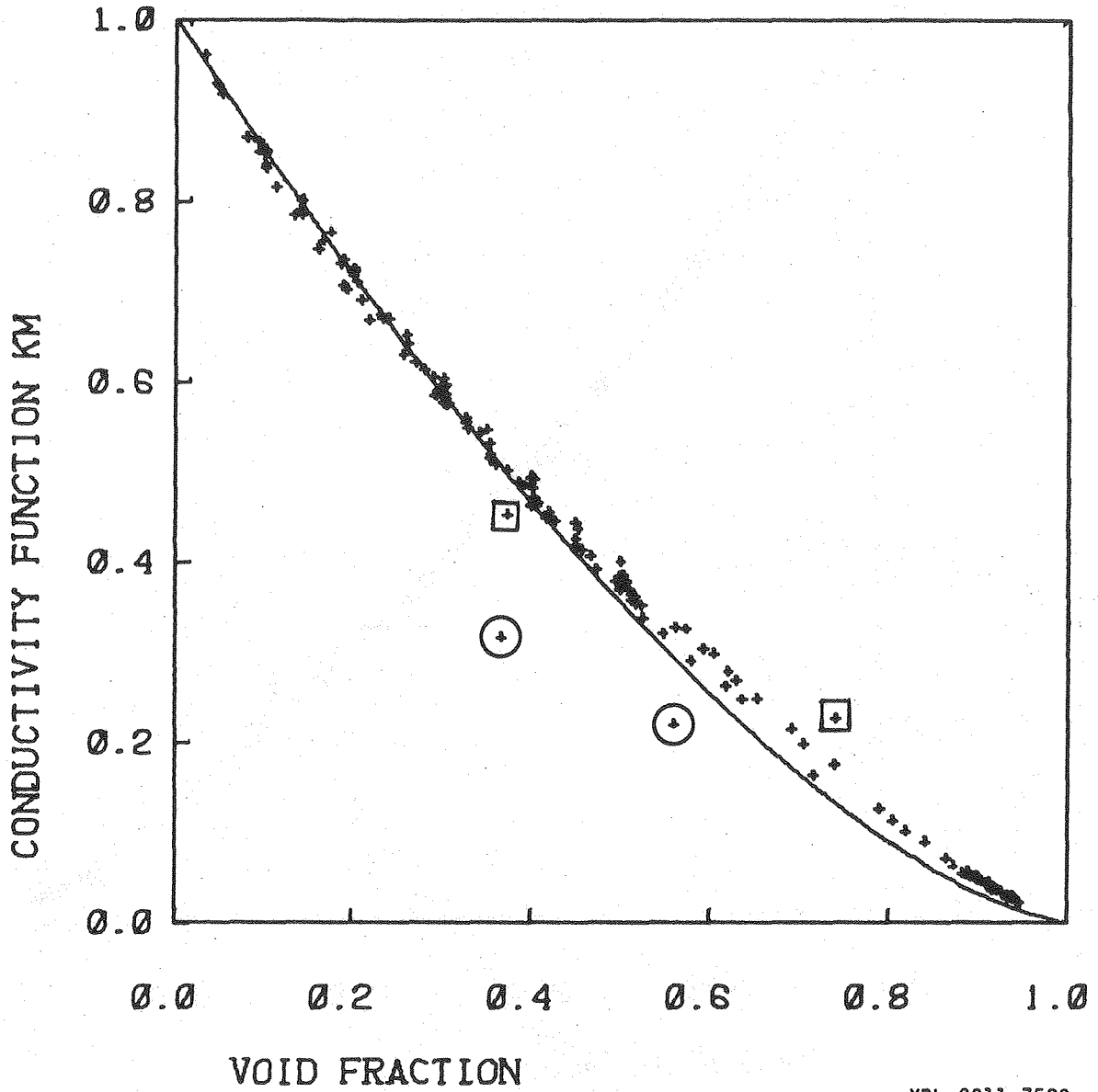
There is another puzzling detail of this paper. The author inserted a relatively high void fraction (0.6) into a Taylor expansion of  $K_m$  in  $f$  around zero carried out to only the  $f^2$  term. He then inexplicably attributed the result of this arithmetic, which gives a

grossly high conductivity ratio, to Rayleigh's original equation. Even after noting twice that his answer exceeded Maxwell's and that this is physically absurd, he concluded that Rayleigh's equation is not useful. In fact, Rayleigh's equation gives a conductivity ratio of 0.288 at a void fraction of 0.6 rather than the 0.370 Turner erroneously derived from the expansion and then attributed to the original.

Fricke and Morse (20) measured the resistance of cream with alternating current. They claim to have investigated void fractions from 0.08 to 0.62 but they list only two data points. After measuring the resistances of skimmed milk and a dilute cream and dividing the latter by the former they found a resistance ratio; then they calculated a void fraction from Maxwell's solution. They calculated subsequent void fractions from known amounts of dilution and compared them with the measured resistances. Because Maxwell's equation is not accurate for large void fractions, their fitting the equations at 0.225 void fraction may account for the continued good agreement with this expression up to void fractions greater than 0.6.

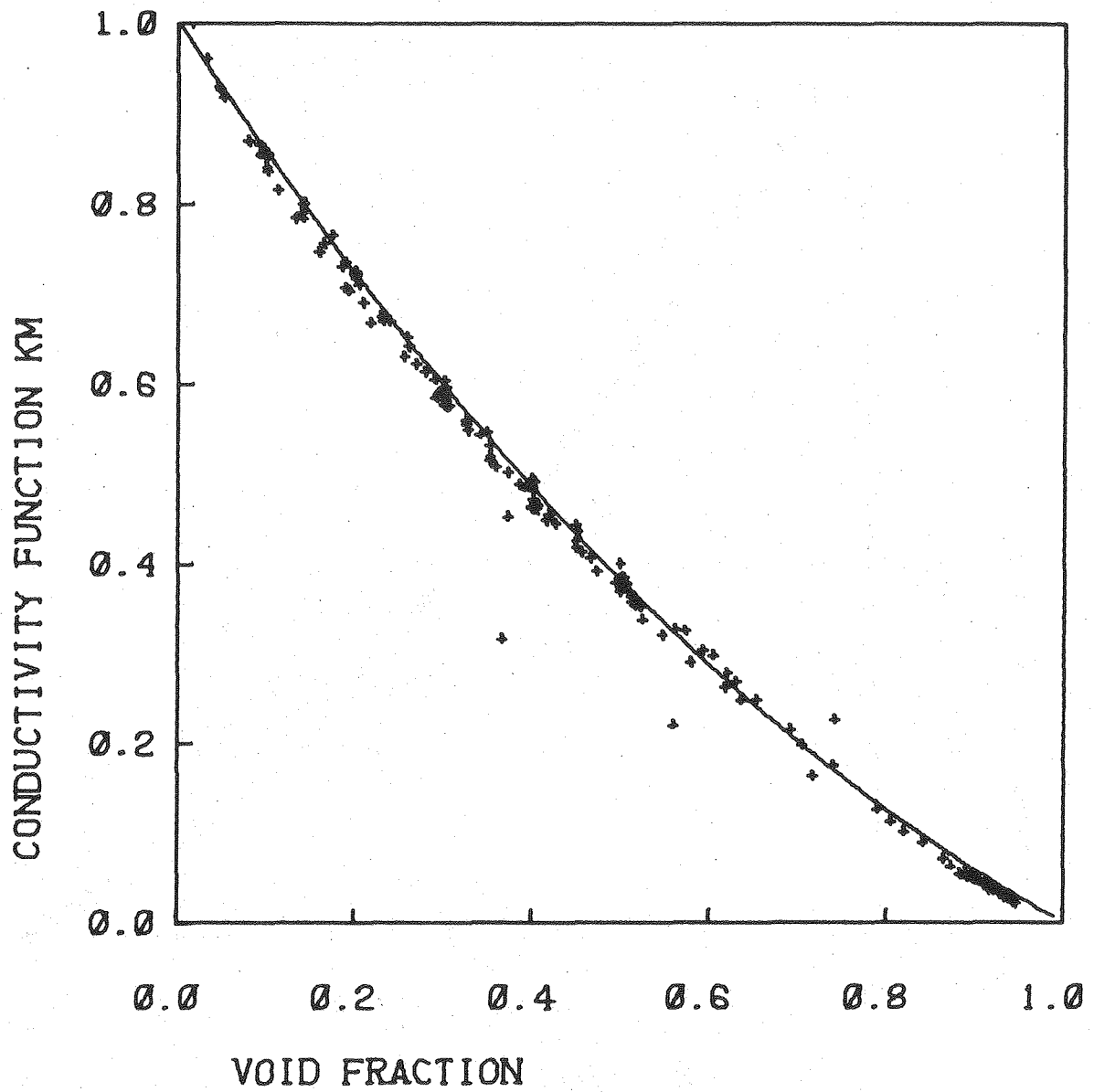
Wyllie and Gregory (21) measured the relative conductivity of unconsolidated packings of glass and plastic spheres. They used 0.1 N and 0.5 N KCl solution but did not discuss their electrical techniques. They experimented with random arrangements of multisized particles and compared their results to Slawinski's (11) equation at relatively high void fractions. They found that his equation agreed with their results at medium void fractions but overestimated the conductivity at void fractions greater than 80 percent.

These experiments notwithstanding, the three equations, Bruggeman's, the Distribution Model of Meredith and Tobias, and Prager's relation, which best represent the data plotted in the foregoing figures, are illustrated in Figs. 12-14 with all of the data included. All of the equations agree with Maxwell's result at low void fractions and all of the equations give a zero conductivity at a void fraction of zero. As noted before, Bruggeman's relation seems to be a lower limit in the medium and concentrated void fractions ranges. In a case where a broad range of particles sizes is present, Bruggeman's relation would fit the data better; however, Prager's result, Eq. (40), and the Distribution Model, Eq. (45), fit the data better than the other equation over the whole range and are almost indistinguishable from each other. I conclude that the two equations may be used interchangeably.



XBL 8011-7580

Fig. 12. The Bruggeman equation compared to all the data. The points with circles (from Clark) and squares (from Mashovets) are included for the sake of completeness even though they obviously deviate from the great body of the data. One must suspect significant experimental error in these points.



XBL 8011-7579

Fig. 13. The Distribution Model compared to all the data.

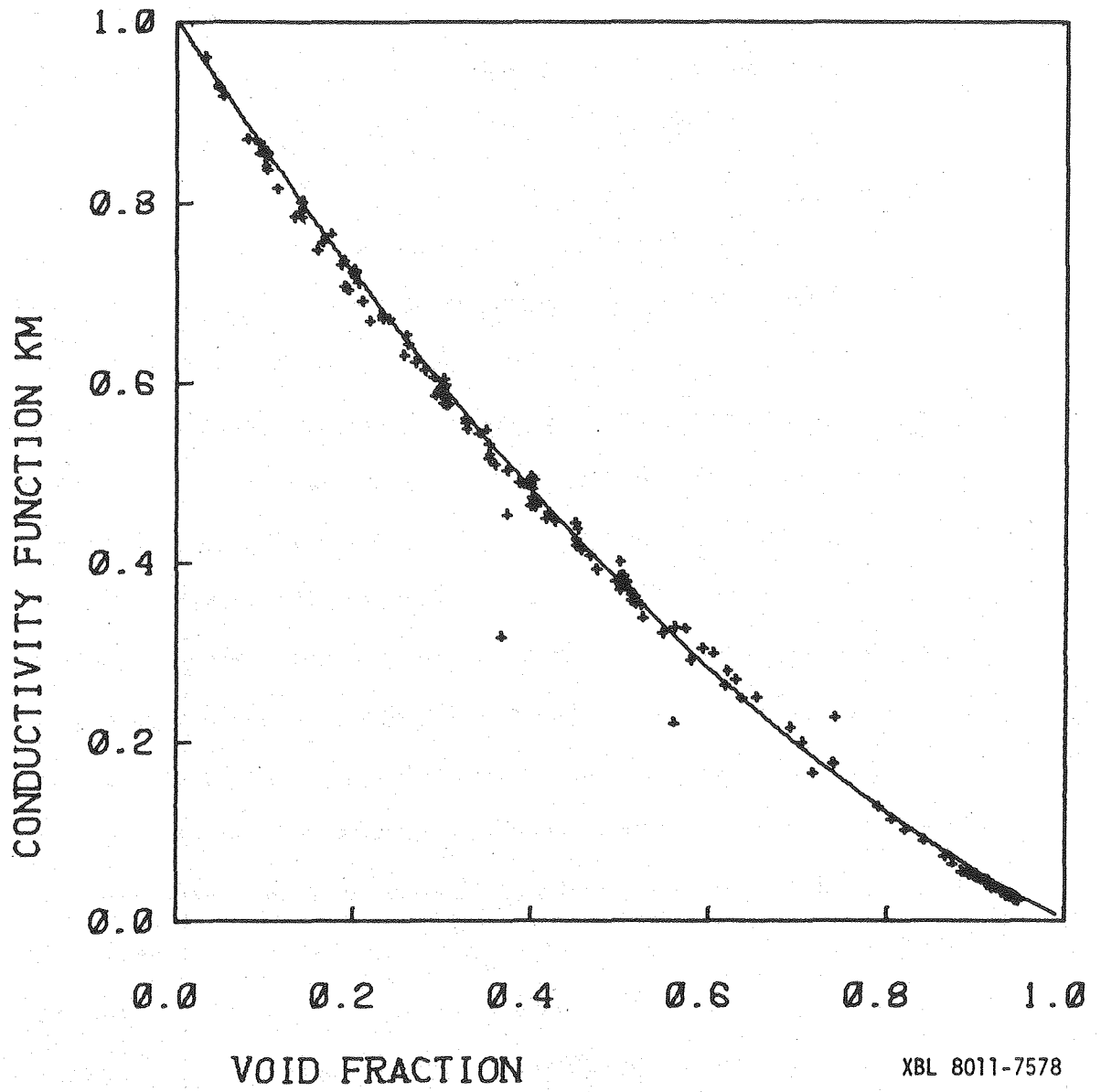


Fig. 14. Prager's equation compared to all the data.

### III. THE TANGENT SPHERE AND OTHER CALCULATIONS APPROPRIATE TO THE CONDUCTIVITY OF BUBBLE LAYERS

#### 1. Literature of the Bubble Layer

A few investigators have studied the gas layer on the electrode surface. Kubasov and Volkov investigated the voltage increase caused by a bubble layer on graphite anodes which face downward during chlorine evolution. Using a mercury pool as a counter electrode, they measured the cell voltage during electrolysis twice; once in otherwise quiescent solution and once with sufficient stirring to remove the gas from the electrode surface. After subtracting the latter from the former, they reported an increment of voltage which includes both ohmic and an anode shift potential caused by bubbles screening the electrode and changing the local current distribution. Measuring this voltage at various current densities, electrode widths and temperatures, the authors found bubble layer voltages as high as three volts when the solution was acidified 5M sodium chloride and the current density was greater than one ampere per square centimeter. The authors did not relate their data to any previous theoretical work on the conductivity of heterogeneous media; the article applies specifically to the chlorine/caustic mercury cell. Errors related to taking the difference between two large terms probably accounts for the data scatter they mention.

Takata, Morishita, and Kihara (33) experimentally investigated the resistance of chlorine gas bubble layers on electrodes by varying the distance between Luggin reference and platinum working electrodes for

horizontal, tilted, and vertical orientations. Plotting potential against distance between the electrodes, they noticed a sharp increase of electric field as the reference electrode approached the working electrode. They designated the point of field change as the outer boundary of the bubble layer and found layer thicknesses of 2, 1.8, and 1.4 mm for the horizontal, tilted, and vertical orientations, respectively. They devised an equation based on Maxwell's result to predict the additional potential required to push current through the bubble layer. One must know the amount of gas per square centimeter and the void fraction in the layer to calculate a potential. They concluded that the bubble layer thickness is not a strong function of current density but is a function of electrode orientation; the layer thins as one goes from horizontal position to vertical. They found a significant polarization caused by the bubble layer and suggested dispersing it to save energy.

Hine et al. (24) in 1956 discussed the anode shift potential caused by the actual local current density being higher than the superficial current density because the bubbles screen the electrode surface. Hine et al. (32) in 1975 recognized that bubbles may not be uniformly distributed in the interelectrode gap; they used the Bruggeman relation to predict the conductivity of these distributions.

I conclude from the work of the foregoing authors that the voltage drop in the bubble layer can be hundreds of millivolts and thus deserve attention. Theory and experiments on model systems can illuminate important effects of this layer and this is the contribution of Chapters 2 and 3.

## 2. Introduction to the Calculations

In this chapter I present several calculations which describe pertinent effects of bubbles on and off electrodes. The effect of the bubble layer, present during electrolysis, differs from that of bubbles dispersed in the bulk electrolyte because the environment of a bubble sitting on the surface is asymmetric; the electrode, an equipotential surface, is in contact with a planar array of bubbles, while electrolyte extends to a large distance on the opposite side of this array. In the following an analytical solution is presented which describes the potential field around a spherical bubble in point contact with a planar equipotential surface when the field far from the sphere is linear. The current distribution on the electrode plane and the incremental resistance caused by a dilute array of bubbles are also evaluated. I compare this resistance to the resistance presented by bubbles out in the bulk in order to contrast the tangent sphere result, the solution for a single bubble in bulk electrolyte, and Maxwell's result. In subsequent examples I show that not only does the closeness of approach of bubbles affect their resistance, but also that the orientation of bubble systems with respect to the flow of current determines the overall resistance they present. Based on the insight afforded by the foregoing calculations, a simpler analysis is presented which illustrates the dominant contribution to the resistance presented by densely occupied bubble layers on electrodes.

### 3. The Tangent-Sphere Calculation\*

#### Theoretical

We use tangent sphere coordinates to solve Laplace's equation for the potential field and current distribution on the planar electrode around the insulating sphere. The coordinate planes are spheres tangent to the plane and toroids without center openings; they are related to Cartesian coordinates by

$$z = \frac{v}{v^2 + \mu^2}, \quad x = \frac{\mu}{\mu^2 + v^2} \quad (1)$$

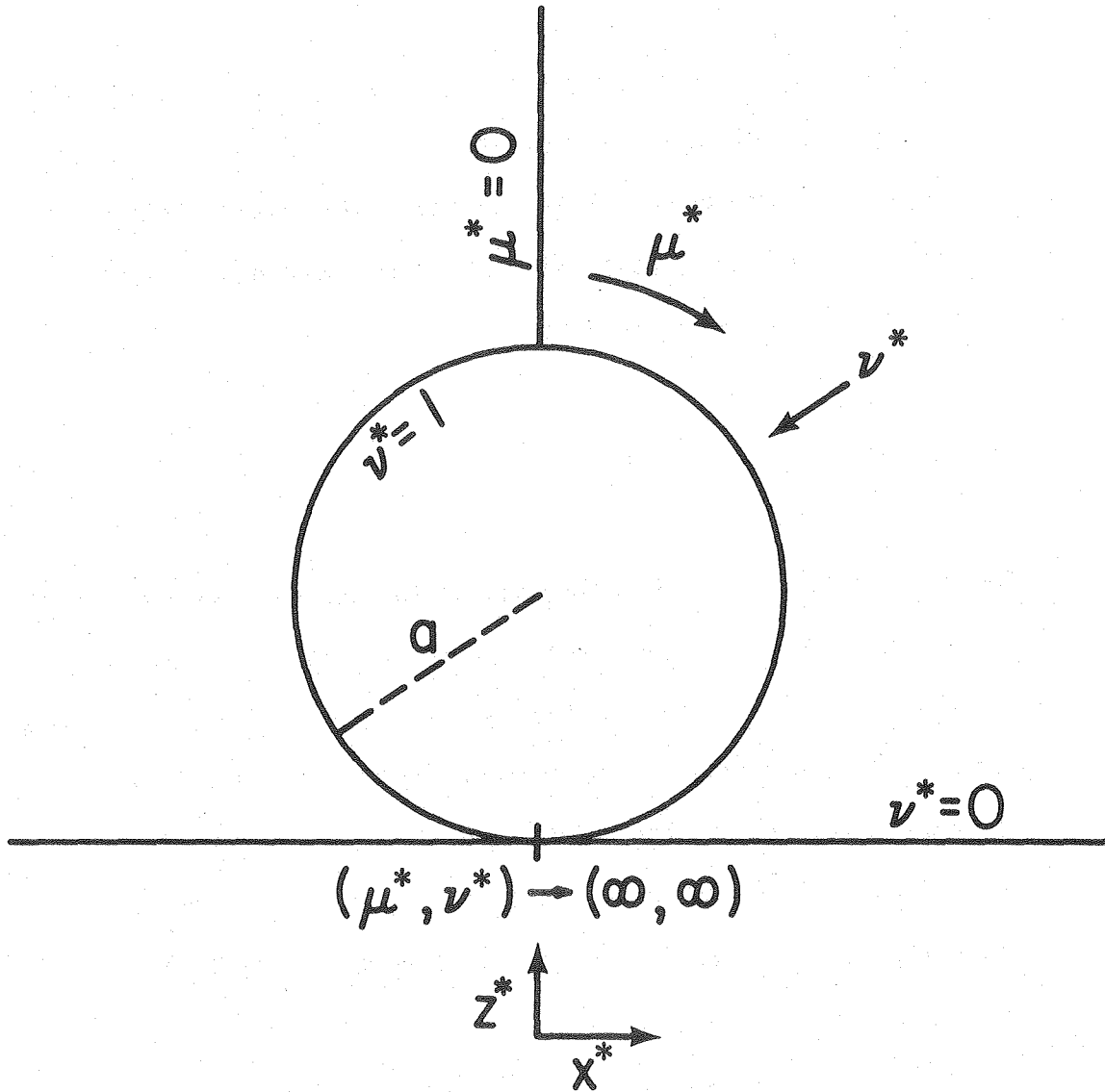
The coordinates and their relations to the geometry appear in Fig. 1.  $v$  corresponds to the inverse of radial distance from the contact point while  $\mu$  is analogous to an angular coordinate. Infinity of both coordinates specifies the contact point. Moon and Spencer (26) present a rather complete discussion of various coordinate systems, including the one above, in their Field Theory Handbook.

The variables, defined in dimensionless form, are as follows:

$$\begin{aligned} z^* &= z/2a \\ x^* &= x/2a \\ v^* &= 2av \\ \mu^* &= 2a\mu \\ \phi^* &= \phi/2a\phi_0 \\ i^* &= i/\kappa\phi_0 \end{aligned} \quad (2)$$

---

\*Section II has appeared in print in substantially the same form. P. J. Sides and C. W. Tobias, J. Electrochem. Soc. 127, 288 (1980).



XBL 793-993

Fig. 1. Tangent sphere coordinates in two dimensions.

The distance variables are normalized to the bubble diameter; therefore,  $x^* = 1$  defines a plane parallel to the  $y^*z^*$  plane and located one bubble diameter from the axis passing through the center of the bubble and the contact point.

We write the potential as the sum of a disturbance and a linear term:

$$\phi^* = \phi_d^* + z^* \quad (3)$$

The second term already satisfies Laplace's equation and all boundary conditions except the one on the bubble surface; therefore,

$$\nabla^2 \phi_d^* = 0 \quad (4)$$

The disturbance must vanish both on the electrode and far away; the potential must be asymmetric about an axis passing through the center of the bubble and the contact point; finally, no current passes through the bubble. In tangent sphere coordinates Eq. (4) and these boundary conditions are:

$$\frac{(\mu^{*2} + \nu^{*2})^3}{\mu^*} \left[ \frac{\partial}{\partial \mu^*} \left( \frac{\mu^*}{\mu^{*2} + \nu^{*2}} \frac{\partial \phi_d^*}{\partial \mu^*} \right) + \mu^* \frac{\partial}{\partial \nu^*} \left( \frac{1}{\mu^{*2} + \nu^{*2}} \frac{\partial \phi_d^*}{\partial \nu^*} \right) \right] = 0 \quad (5)$$

$$\phi_d^* \Big|_{\nu^*=0} = 0 = \phi_d^* \Big|_{\substack{\nu^*=0 \\ \mu^*=0}} \quad (6)$$

$$\left. \frac{\partial \phi_d^*}{\partial \mu^*} \right|_{\mu^*=0} = 0 \quad (7)$$

$$\left. \frac{\partial \phi_d^*}{\partial \nu^*} \right|_{\nu^*=1} = 0 \quad (8)$$

Moon and Spencer (26) give the separation criteria, the separated equations, and their general solutions. After applying conditions, Eqs. (6) and (7), we obtain

$$\phi_d^* = A \sinh(q\nu^*) J_0(q\mu^*) (\mu^{*2} + \nu^{*2})^{1/2} \quad (9)$$

Because the domain is infinite, the solution must include all values of  $q$ ; therefore, Eq. (9) passes to an integral.

$$\phi_d^* = (\mu^{*2} + \nu^{*2})^{1/2} \int_0^{\infty} A \sinh(q\nu^*) J_0(q\mu^*) dq \quad (10)$$

The insulation condition, Eq. (8), determines  $A$  as a function of  $q$ .

Upon differentiating the complete potential  $\phi^*$ , evaluating this expression at  $\nu^* = 1$ , and equating it to zero, we obtain

$$0 = \frac{1}{(\mu^{*2} + 1)^{1/2}} \int_0^{\infty} A \sinh q J_0(q\mu^*) dq + (\mu^{*2} + 1)^{1/2} \int_0^{\infty} A q \cosh q J_0(q\mu^*) dq + \frac{(\mu^{*2} - 1)}{(\mu^{*2} + 1)^2} \quad (11)$$

Following Witze, Schrock, and Chambre (27), we use the differential equation satisfied by  $J_0$  and integrate twice by parts to obtain

$$\frac{1 - \mu^{*2}}{(\mu^{*2} + 1)^{3/2}} = \int_0^{\infty} qH J_0(q\mu^*) dq \quad (12)$$

where

$$H(q) = \frac{1}{q} \left\{ -\frac{d}{dq} \left[ q \frac{d}{dq} (A \cosh q) \right] + A(q \cosh q + \sinh q) \right\} \quad (13)$$

After inverting the transform with the help of the Erdelyi Tables (10) and rearranging the equations, we obtain

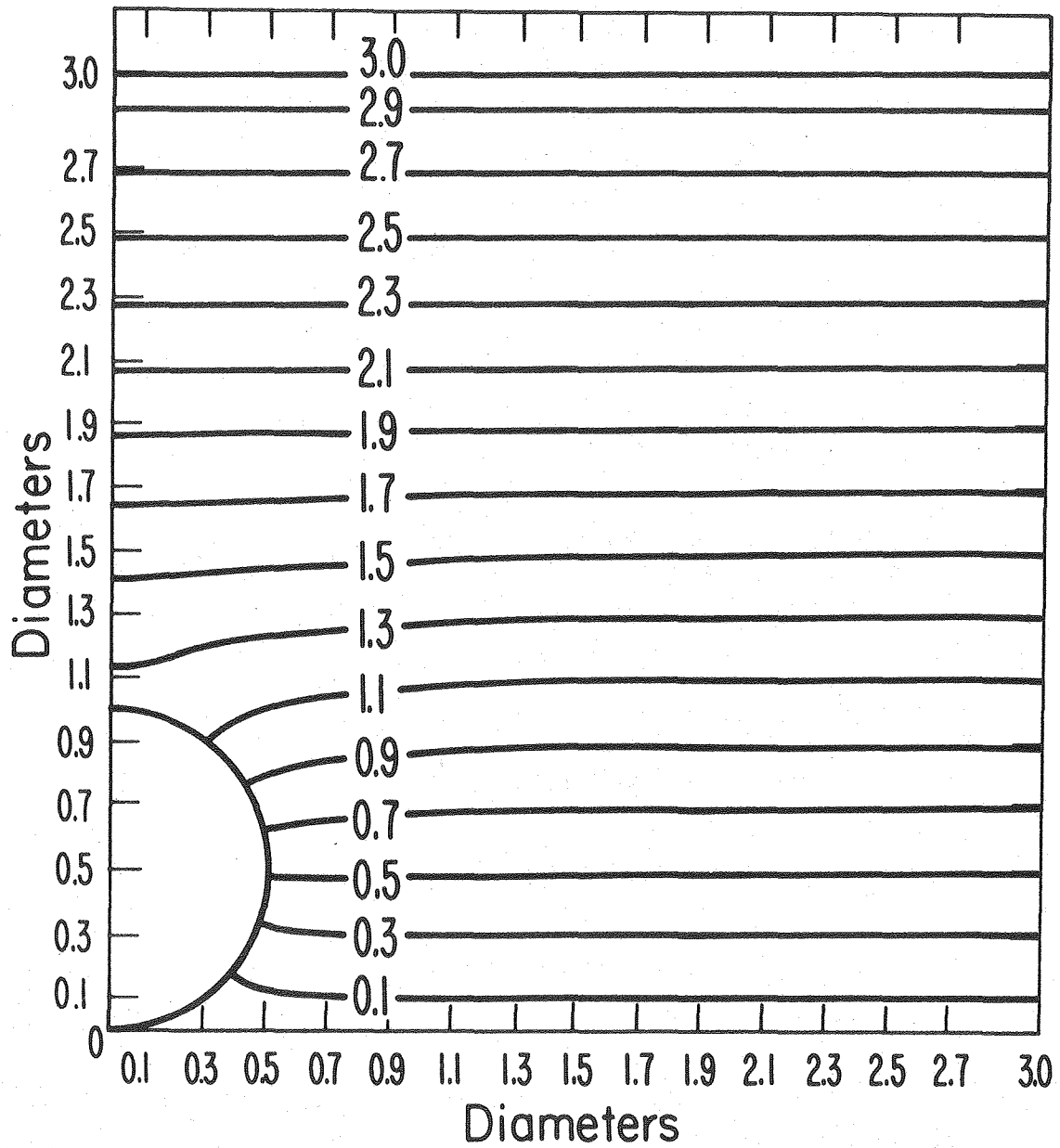
$$\frac{dA}{dq} = \frac{1 - q + e^{-2q}}{2 \cosh^2 q} + \frac{C}{2q \cosh^2 q} \quad (14)$$

C must be zero for the derivative to remain finite at  $q = 0$ .

$$A = \int_0^{\infty} \frac{1 - q + e^{-2q}}{2 \cosh^2 q} dq \quad (15)$$

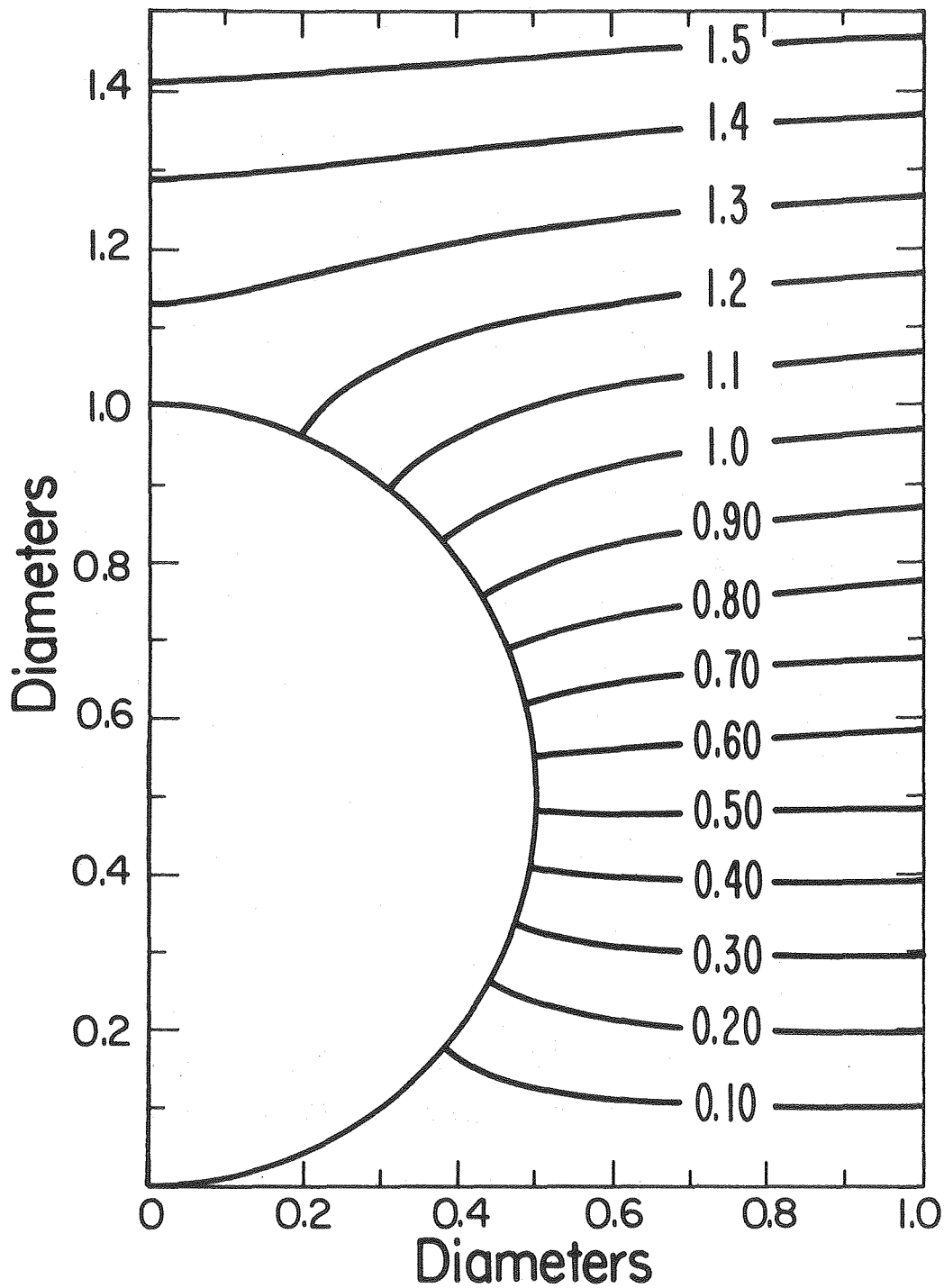
The potential is now given by

$$\phi^* = (v^{*2} + \mu^{*2})^{1/2} \int_0^{\infty} A J_0(q\mu^*) \sinh q(v^*) dq + \frac{v^*}{(\mu^{*2} + v^{*2})} \quad (16)$$



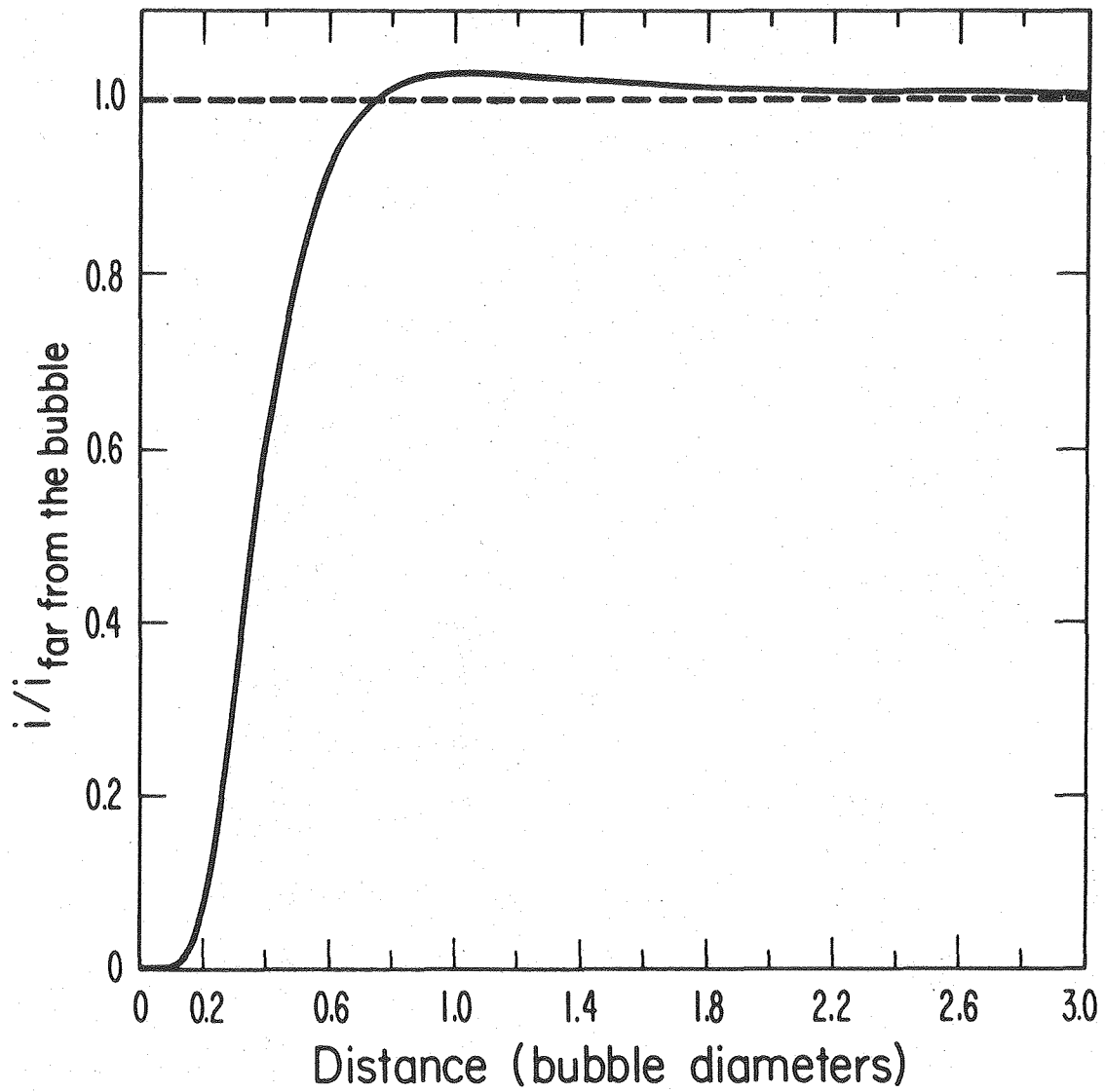
XBL 793-997

Fig. 2(a). Potential around an insulating sphere tangent to an electrode.



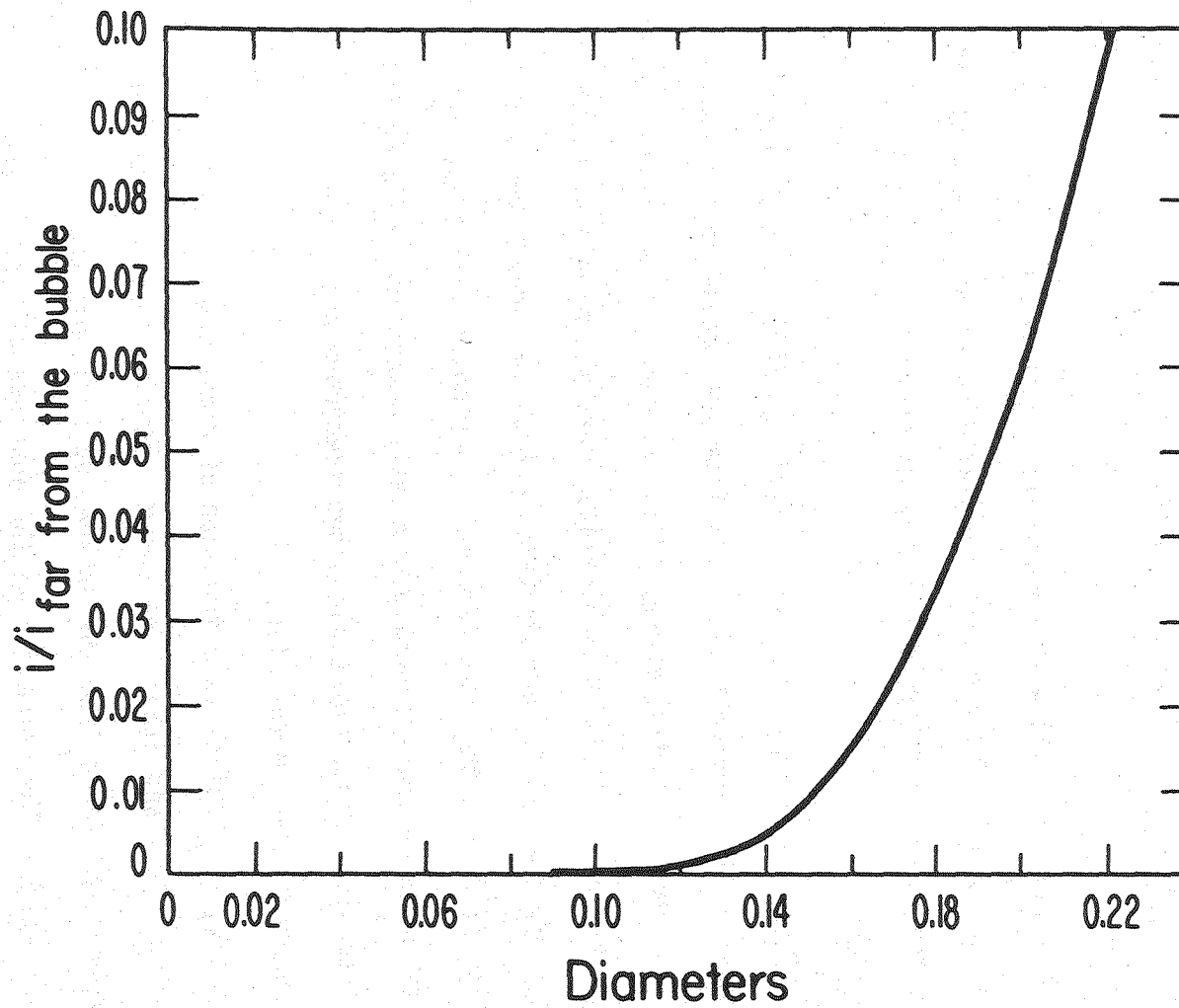
XBL 793-996

Fig. 2(b). Detail of potential close to sphere.



XBL 793-998

Fig. 3(a). Current distribution near a spherical insulator tangent to a surface.



XBL 793-999

Fig. 3(b). Detail of current distribution near the contact point.

and the primary current distribution is

$$i^* = \mu^* \left. \frac{\partial \phi^*}{\partial v^*} \right|_{v^*=0} = \mu^* \int_0^\infty q A dq J_0(q \mu^*) dq + 1 \quad (17)$$

Equations (16) and (17) were numerically evaluated by routines that calculated the Bessel functions and integrated their products with the hyperbolic functions over the appropriate domains.

#### Discussion

The electric field appears in Figs. 2(a) and 2(b). The potential is normalized so that equipotentials far from the bubble coincide with distance from the electrode (see Eq. (3)). As required by the insulation condition, Eq. (8), the equipotentials meet the bubble at right angles; they approach their undistributed values far away. One can see from Fig. 2(a) that the displacement of equipotentials caused by the insulating sphere becomes negligibly small beyond one and a half diameters from its contact point along the electrode and three diameters perpendicular to the electrode.

The current distribution as a function of dimensionless distance appears in Figs. 3(a) and 3(b). The current density is normalized to be 1.0 at a great distance from the sphere; we call this the "undisturbed" value. The value 0.5 on the abscissa of Fig. 3 marks the outermost circle on the electrode shadowed by the bubble; here, the current density is 80 percent of its undisturbed value. The current density farther from the bubble exceeds 1.0 because the upper half of the sphere deflects the flux and thereby creates a maximum

current density 2 percent greater than the undisturbed value at one diameter from the contact point. We conclude that fields around spheres separated by more than three diameters affect each other negligibly.

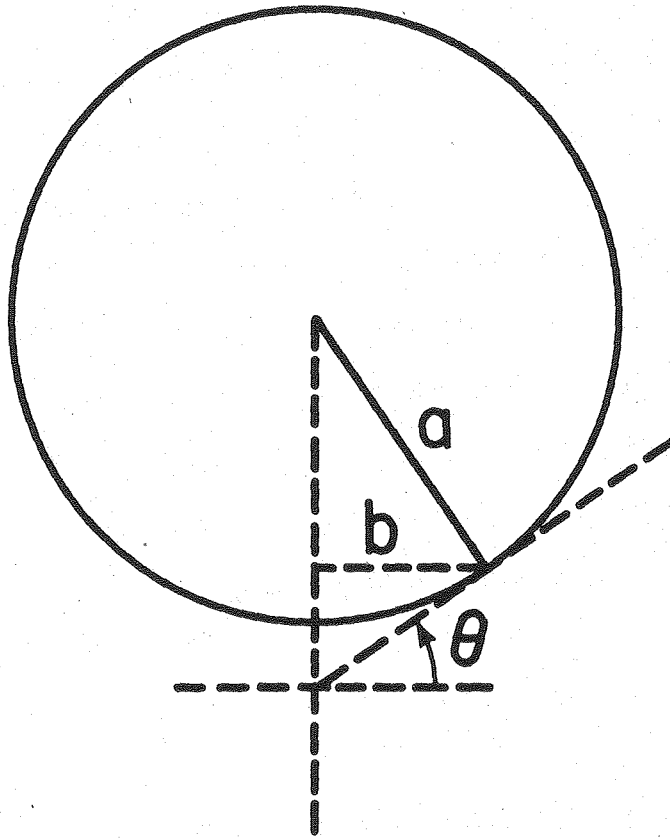
A detail of the current distribution near the contact point appears in Fig. 3(b). Zero at the axis, the current density reaches only 1 percent of its undisturbed value at 30 percent of the radius from the contact point; therefore, we can insulate the area inside this distance with a surface which coincides with a surface of flow. Thus the effect of a tangent insulating sphere on the current distribution approximates that of a bubble having a nearly spherical shape and a contact area less than  $0.09 \pi a^2$ . Calculating the contact angle for this base area according to the geometry in Fig. 4,

$$\theta = 90^\circ - \cos^{-1}(b/a) = 17.5^\circ \quad , \quad (18)$$

we conclude that the effect of a sphere on a plane approximates that of a nearly spherical bubble having a contact angle less than  $17.5^\circ$ .

The bubble increases the resistance by deforming the otherwise straight lines of current. We evaluate the effect by integrating the potential disturbance over a plane far from the electrode and parallel to it.

$$\Delta\phi = 4a^2 \int_0^\infty 2\pi x^* \phi_d^* \Big|_{z^* \rightarrow \infty} dx^* = A_0 \pi a^2 \quad (19)$$



XBL 793-994

Fig. 4. Geometry for calculation of contact angle  $\theta$ .

Bubbles whose contact points are three diameters apart in a planar hexagonal array give a number density  $0.0321/a^2$ . If the bubble diameter is a tenth of the interelectrode gap in a parallel plane cell geometry, Eq. (22) predicts a resistance increase of only 1 percent. This means that the resistance caused by a sparse collection of small bubbles is negligible. When closer than three diameters, the bubbles interact significantly and thereby disturb the potential more than predicted by Eq. (22); nevertheless, this equation establishes that when the bubble diameters are a tenth of the interelectrode spacing, the minimum added resistance caused by a close-packed array of bubbles on a surface is at least 8 percent of the cell resistance. In reality, because of the severe pinching of the field between the bubbles, the effect must be substantially larger than this, perhaps by a factor of two to three.

#### 4. Maxwell's Equation, the Single Bubble Calculation, the Tangent Sphere Result

As discussed in the first chapter, Maxwell derived a fundamental equation for the conductivity of a medium containing a dilute dispersion of spheres Eq. (1-11).

$$K_m = \left[ \frac{1 - f}{1 + \frac{f}{2}} \right] \quad (1-11)$$

There is a case simpler than his; that is, one can deduce a resistance caused by a single sphere in an infinite medium as the limiting case of Maxwell's solution for a dilute dispersion of spheres. Consider

where

$$\begin{aligned} A_0 &= 8 \int_0^{\infty} qAdq \\ &= 0.9015 \end{aligned} \quad (20)$$

$\Delta\phi$  does not depend on distance from the electrode; it is the net disturbance of potential integrated with area. "n" bubbles per unit area, distributed such that their contributions are independent, cause a net potential disturbance.

$$\Delta\phi^* = nA_0\pi a^2 \quad (21)$$

One cannot deduce a conductivity analogous to Maxwell's because the layer of bubbles is two-dimensional; the effect must be characterized as a polarization at the electrode surface. The increment of resistance caused by the bubbles on an electrode of area  $S$  is the net potential disturbance, Eq. (21), divided by the total current to the electrode,  $\kappa\phi_0 S$ .

$$\Delta R = \frac{\Delta\phi^*}{\kappa S\phi_0} = \frac{2A_0 n\pi a^3}{\kappa S} = 1.352 af/\kappa S \quad (22)$$

where  $f$  is the gas void fraction in the bubble layer.  $\Delta R$  is a resistance increment related only to the disturbance caused by the bubbles. Its sum with the cell's resistance in the absence of gas gives the net cell resistance.

the schematic in Fig. 5. There,  $r$  is the radial distance from the sphere's center,  $a$  is the sphere's radius, and  $\theta$  is the angular coordinate. The medium must be large enough for the disturbance caused by the sphere to vanish because the resistance itself is the macroscopic result of this disturbance of the flux lines.

I write an expression for the potential around a single sphere in an otherwise linear field (1).

$$\phi = \phi_0 r \cos\theta + \frac{\phi_0}{2} \frac{a^3}{r^2} \cos\theta \quad (23)$$

which was derived by solving the Laplace equation in the surrounding medium.  $\phi_0$  is the slope of the linear field prevailing at large distances; multiplied by the conductivity, it gives the current density in the sphere's absence. The first term in Eq. (23) is the linear solution specified at large distances; the second modifies the linear solution to account for the sphere; that is, the solution consists of linear and disturbance terms. The resistance related specifically to the geometrical obstruction presented by the sphere comes from the second term. Evaluating the net potential disturbance as in Eq. (19) and dividing this increment of potential by the current density far from the bubble, one obtains the resistance caused by the sphere.

$$\Delta R = \frac{2\pi a^3}{kS^2} \quad (24)$$

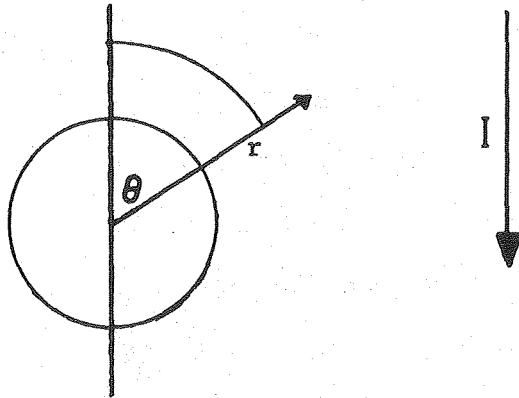
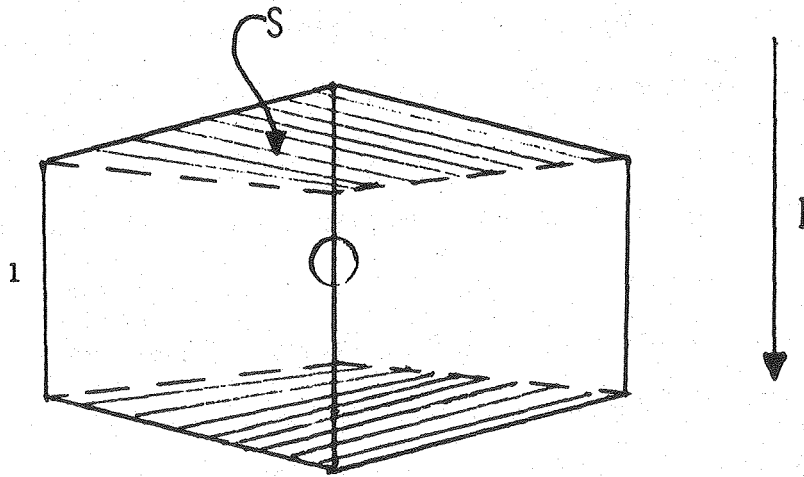


Fig. 5. Geometry for single sphere analysis.



XBL 8011-7597

Fig. 6. Single sphere in a flat plate cell.

where  $k$  is the conductivity and  $\Delta R$  is the increment of resistance related only to the sphere's presence.

To express this equation in terms comparable to Maxwell's result, I consider a two-flat-plate cell as depicted in Fig. 6. The resistance of this cell in the absence of any spheres is

$$R = \ell/KS \quad (25)$$

Combining Eq. (24) with Eq. (25) one obtains an expression for the total resistance of the cell

$$R_T = \frac{\ell}{KS} + \frac{2\pi a^3}{KS^2} \quad (26)$$

Dividing Eq. (26) by Eq. (25) and noting that the void fraction  $f$  is the sphere volume divided by the cell volume, one finds

$$\frac{1}{K_m} = 1 + \frac{3}{2} f \quad (27)$$

Equation (27) is a limiting case of Maxwell's result which can be proved by expanding the latter around zero void fraction.

$$\frac{1}{K_m} = 1 + \frac{3}{2} f + \dots \quad (28)$$

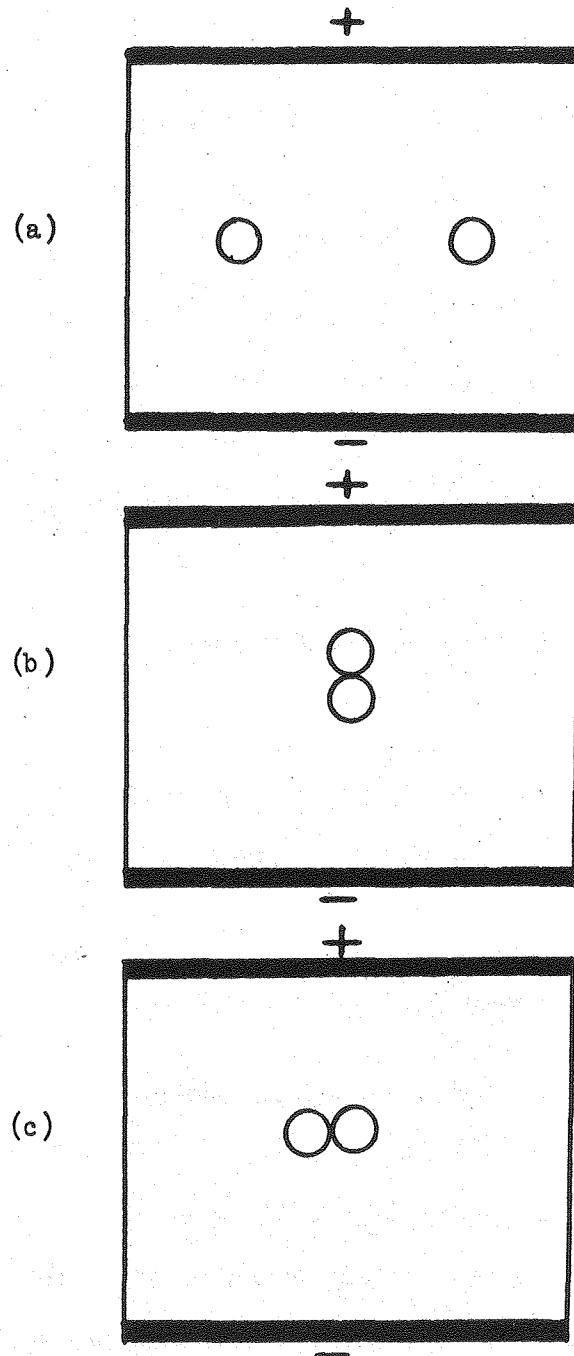
I conclude that a very dilute dispersion of spheres behaves like individual spheres having absolutely no interaction with other spheres

in the dispersion. Maxwell's solution is a correction to this case even though it itself is derived for non-interacting spheres. There is no contradiction between the ideality in the single sphere case and that in Maxwell's case; while one can evaluate the disturbance due to a single sphere over a plane and account for all the disturbance, one cannot use this method to evaluate the disturbance due to spheres which behave as a three dimensional collection. The difference between Maxwell's case and the single-sphere case is the three dimensional nature of the dispersion.

Dividing Eq. (22) by Eq. (28), one can compare the tangent sphere result with the single-sphere result; the ratio equals 0.9015. A sphere on the electrode surface presents 90 percent of the resistance of a sphere in the bulk because the electrode plane terminates the disturbance in current at the base of the sphere instead of permitting it to slowly recover to straight paths. There is no equivalent of Maxwell's result for a bubble layer because it is two dimensional.

#### 5. Effect of Orientation of Two-Sphere Combinations on the Resistance They Present

In Section III, I calculated the resistance caused by bubbles' screening the electrode from current. To contrast this screening effect to the constriction of current to flow between two bubbles side by side with respect to the overall direction of current, I compare three cases which illuminate the dependence of the resistance of bubble systems on their orientation with respect to the direction of current. Schematics of the three cases appear in Fig. 7. In case (a) the two



XBL 8011-7571

Fig. 7. Arrangements for demonstration of effect of bubble orientation.  
(a) Bubbles completely separated.  
(b) Bubbles oriented in line with the current.  
(c) Bubbles oriented side by side with respect to the current.

spheres are far enough apart from the boundaries and each other that they do not interact. In case (b) the line joining the bubbles' centers is parallel to the flow of current while in case (c) the line joining the bubbles' centers is perpendicular to the overall current. In each of the last two cases the spheres are tangent.

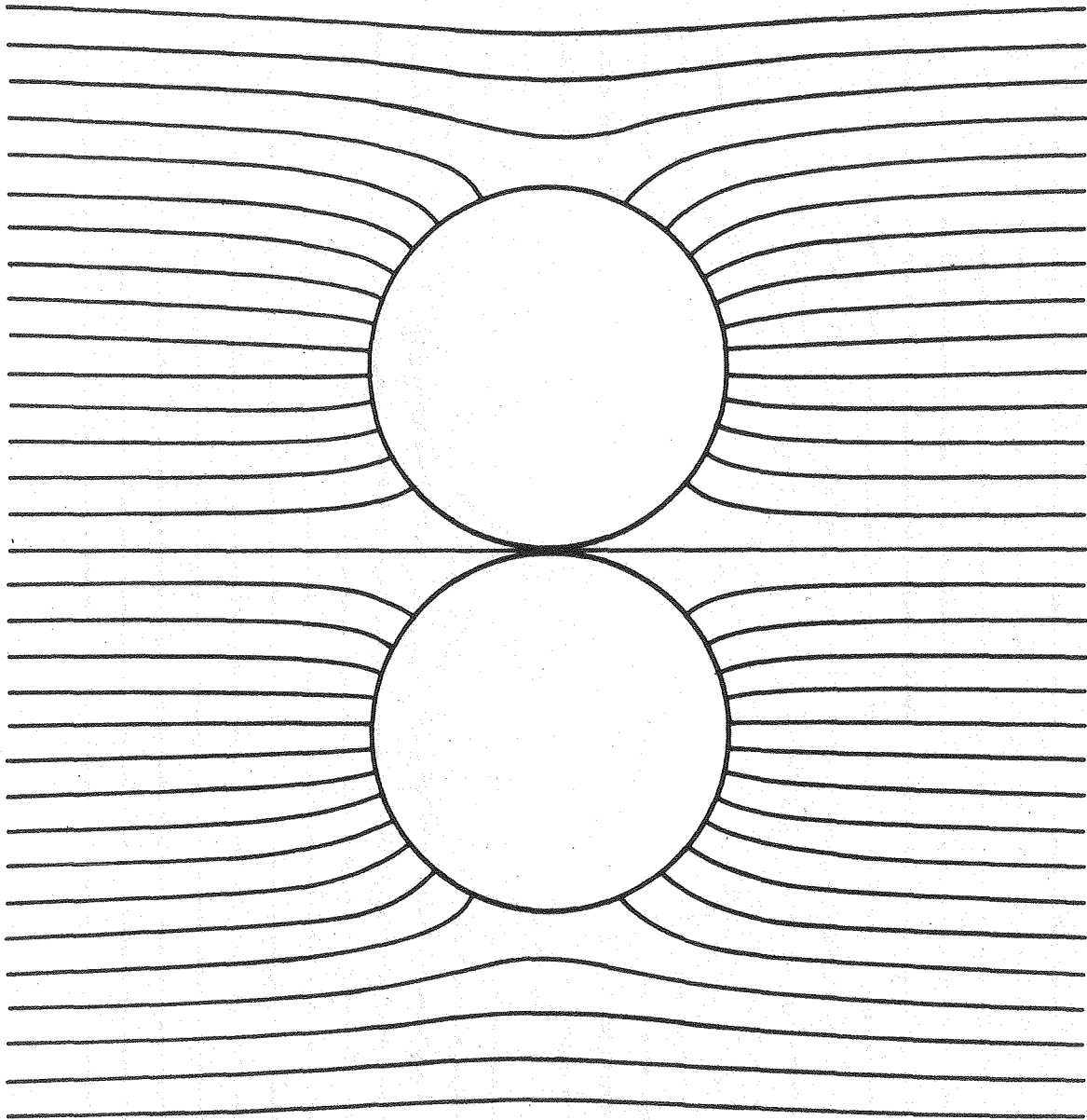
The net resistance increase for a single bubble of the type in (a) is given by Eq. (24). Multiplying by 2 to account for both bubbles,

$$\Delta R_a = \frac{4\pi a^3}{\kappa S^2} \quad (29)$$

The net increase for the system in case (b) is given by twice the amount presented in the tangent sphere calculation.

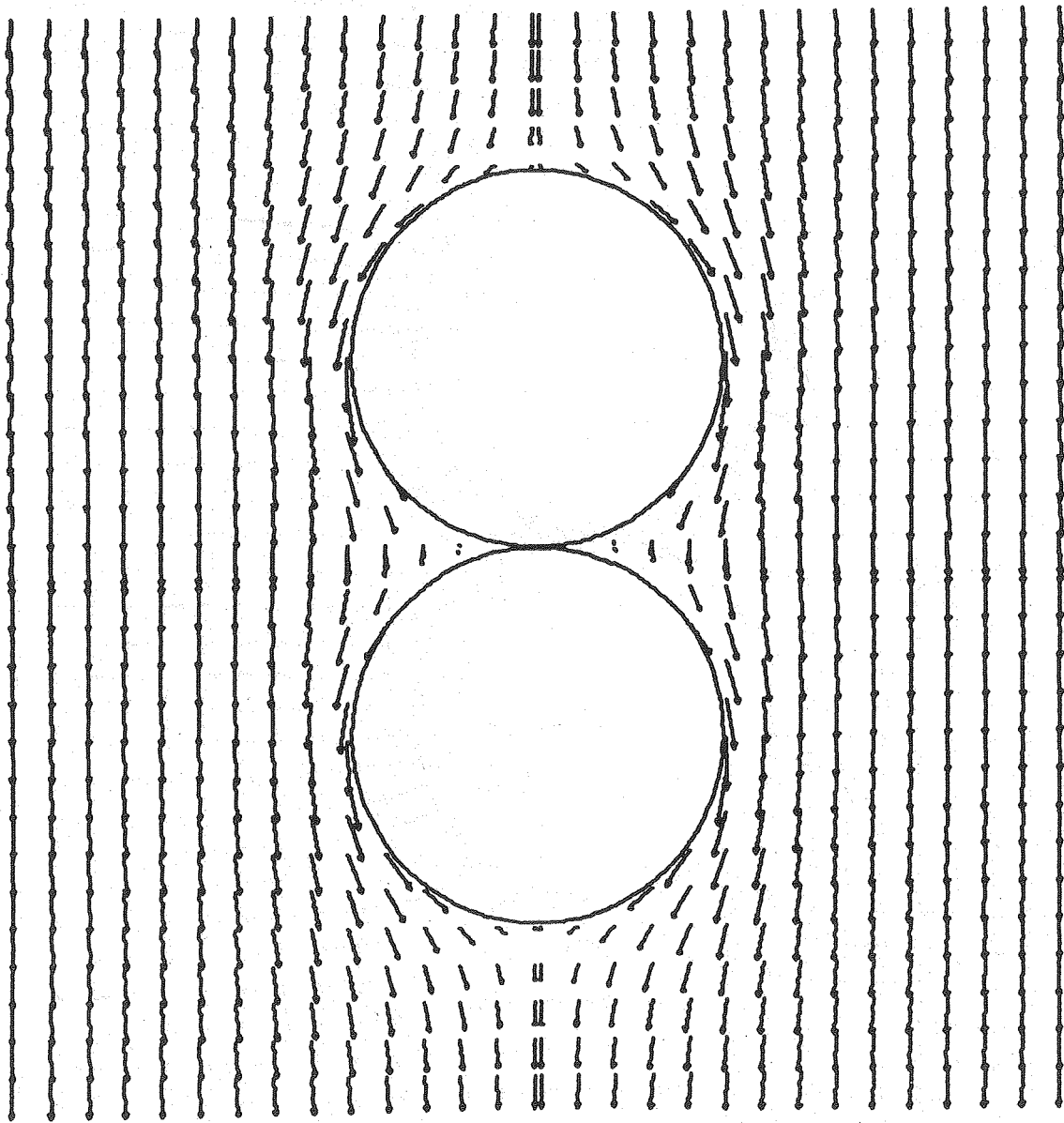
$$\Delta R_b = (0.9015) \frac{4\pi a^3}{\kappa S^2} \quad (30)$$

After dividing Eq. (30) by Eq. (29), one finds that the resistance of two tangent spheres whose line containing their centers is parallel to the direction of current is 90 percent that of two bubbles whose fields do not interact. The equipotentials around two such spheres appear in Fig. 8 and a vector graph of the current appears in Fig. 9. Note the absence of equipotential lines near the point of tangency; it means that there is little electrical activity between the spheres. In Fig. 9 the length of the arrows is proportional to the current and their orientation indicates the direction of current at the point from which



XBL 801-7737

Fig. 8. Equipotentials around bubbles oriented in line with current.



XBL 801-7743

Fig. 9. Vector graph of currents around bubbles in line with current.

they are drawn. The current changes direction to avoid the top sphere and then begins to fill the volume between the spheres before passing the plane of symmetry and avoiding the second sphere, but the currents in the volume between the spheres is small. The decrease in electrical activity between the spheres accounts for the 10 percent drop in resistance realized by moving the spheres from far apart to tangent with their line of centers parallel to the overall current.

To evaluate case (c), in which the line joining the spheres' centers is perpendicular to the current, I used the tangent sphere coordinates defined in Eq. (1) and again add linear and disturbance terms to solve Laplace's equation with boundary conditions which resemble those of the earlier solution; however, the current far from the pair of spheres now flows parallel to the x direction illustrated in Fig. 1 of the previous section; therefore the solution is written as

$$\phi^* = \phi_d^* + x^* \quad (31)$$

in contrast to Eq. (3). Also, the problem is no longer axisymmetric, but three dimensional; the angular coordinate rotates the coordinates of Figure 8 about the line containing the bubbles' centers. The solution to the problem in this case is

$$\phi^* = (\mu^{*2} + \nu^{*2})^{1/2} \int_0^{\infty} A J_1(q\mu^*) \cosh(q\nu^*) \cos\psi dq + \frac{\mu^* \cos\psi}{\mu^{*2} + \nu^{*2}} \quad (32)$$

This equation satisfies the boundary conditions

$$\begin{aligned}
 \phi_d^* \Big|_{\mu^*=0} &= 0 \\
 \mu^{*2} \frac{\partial \phi_d^*}{\partial v^*} \Big|_{v^*=0} &= 0 \qquad \phi_d^* \Big|_{\mu^*, v^*=0} = 0 \\
 \frac{\partial \phi_d^*}{\partial \psi} \Big|_{\psi=0, \pi} &= 0
 \end{aligned} \tag{33}$$

I use the condition of no current through the bubble to determine the transform coefficient A as a function of the variable q.

$$\frac{\partial \phi^*}{\partial v^*} \Big|_{v^*=1} = 0 \tag{34}$$

Applied to Eq. (32), this equation gives

$$\begin{aligned}
 \frac{2\mu^*}{(\mu^{*2} + 1)^{3/2}} &= \int_0^\infty AJ_1(q\mu^*)(\cosh q + q \sinh q) dq \\
 &+ \mu^{*2} \int_0^\infty AJ_1(q\mu^*) q \sinh q dq
 \end{aligned} \tag{35}$$

I again use the differential equation satisfied by  $J_1(q)$  and two integrations by parts to rearrange the right hand side to a form suitable for using the Erdelyi Tables (31). After some rearrangement, I

find the following ordinary differential equation for  $A$ , the transform coefficient.

$$A'' + \left(\frac{1}{q} + 2\coth q\right) A' - \frac{A}{q^2} = \frac{-2q}{e^q \sinh q} \quad (36)$$

The conditions on this equation are that  $A$  be bounded at  $q = 0$  and vanish at infinity. ( $q = 0$ ) is a regular singular point so I begin the solution by examining the behavior around that point. Near ( $q = 0$ ), the differential equation is

$$A'' + \frac{3}{q} A' - \frac{1}{q^2} A = \frac{-2}{q} \quad (37)$$

The homogeneous portion of Eq. (37) is an Euler equation which has the solution

$$A(0) = C_1 q^{\sqrt{2}-1} + C_2 q^{-\sqrt{2}-1} \quad (38)$$

where  $A(0)$  is the function  $A$  near ( $q = 0$ ). I throw away the unbounded second term. The particular integral is  $(-q)$  so the total solution near ( $q = 0$ ) is

$$A(0) = C_1 q^{\sqrt{2}-1} - q \quad (39)$$

Thus the value of A at zero is zero. I construct the overall solution to the problem by solving the general equation twice numerically, first as the homogeneous portion using starting values of  $q^{\sqrt{2}-1}$  for A and  $(\sqrt{2} - 1) q^{\sqrt{2}-1}$  for A', and second as the entire equation using starting values derived from the particular solution (-q). This gives two solutions which are combined linearly to give the correct behavior at infinity.

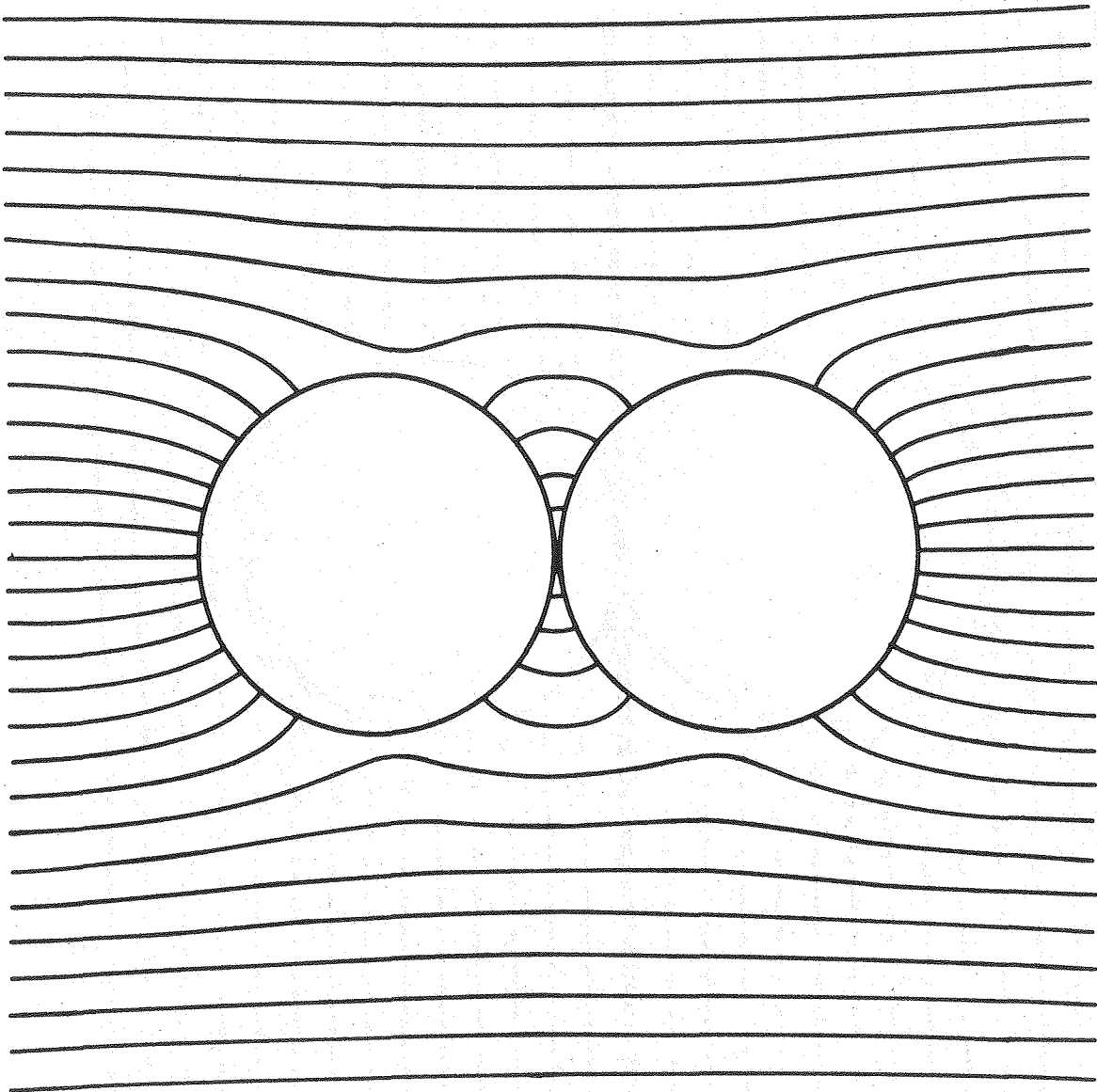
The resistance presented by this two sphere system is calculated as before Eq. (19) and the result is

$$\Delta R_c = (1.831) \frac{4\pi a^3}{KS^2} \quad (40)$$

Normalizing case (c) to (a), one obtains

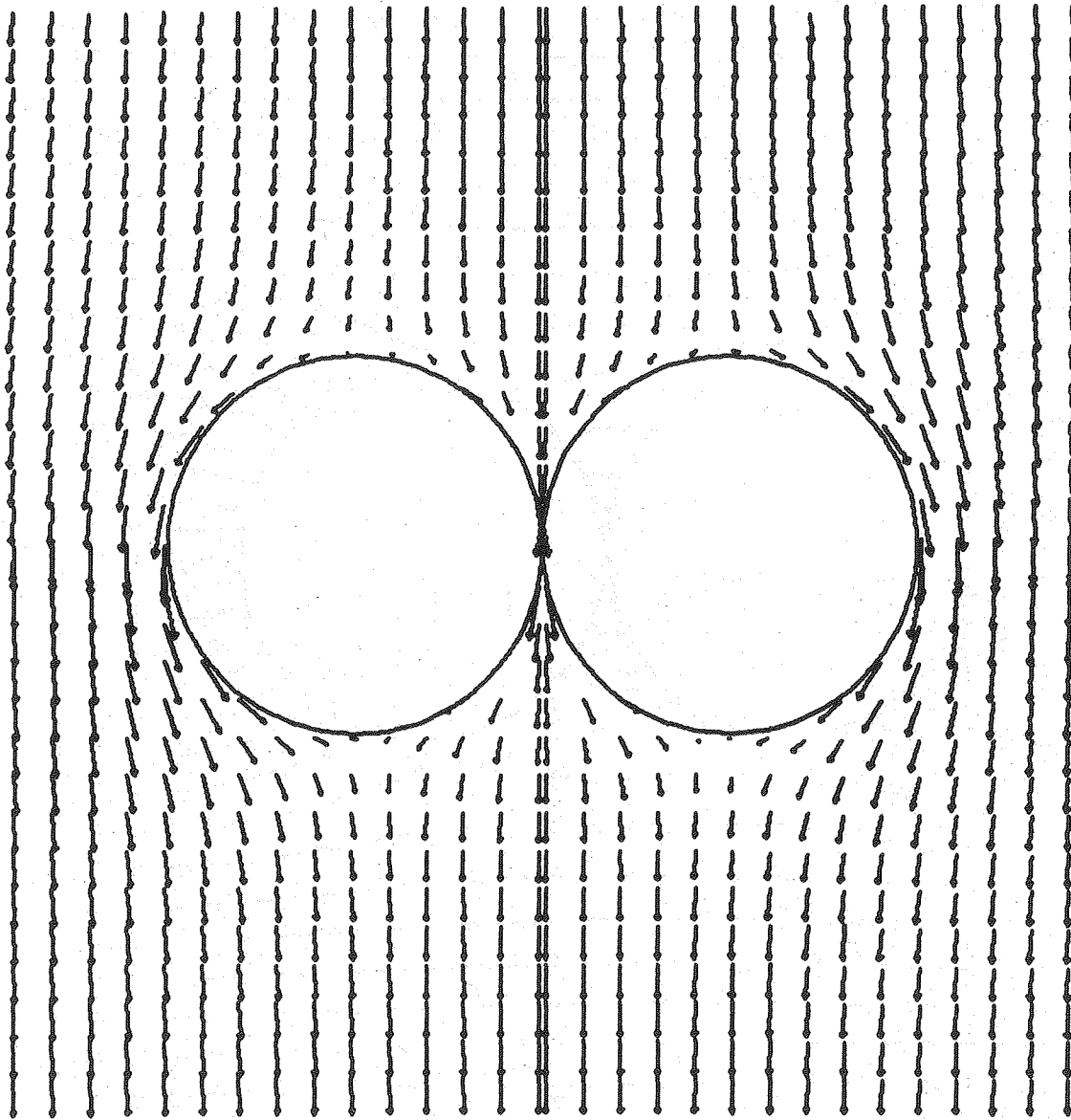
$$\frac{\Delta R_c}{\Delta R_a} = 1.831 \quad (41)$$

Thus the two spheres oriented such that the line joining their centers is perpendicular to the flow of current offer 83 percent more resistance than two separate spheres while two spheres whose line joining their centers is parallel to the current presents 10 percent less resistance than two separate spheres. I conclude that interactions between bubbles side by side with respect to the current present much more resistance than bubbles oriented top to bottom.



XBL 801-7741

Fig. 10. Equipotentials around bubbles side by side with respect to the current.



XBL 801-7744

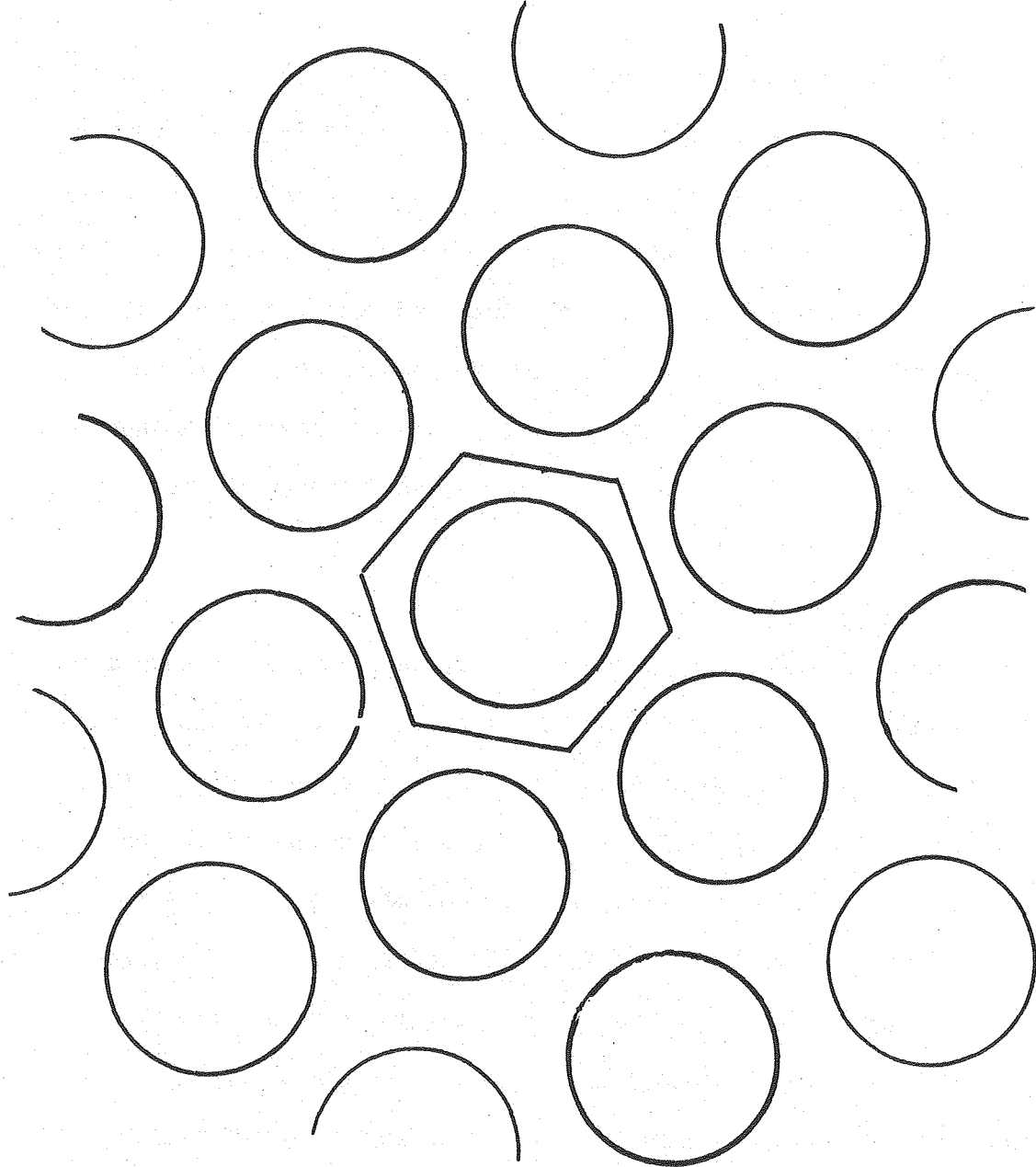
Fig. 11. Vector graph of currents around bubbles side by side with respect to the current.

There is more electric activity in the potential field around the spheres in case (c) than in case (b), illustrated in Figs. 8 and 10. One sees from Figs. 9 and 11, the vector currents, that in case (b) there is a streamline effect in which the disturbance is minimized by one sphere being placed behind the other and hence shielding it, but in case (c) the two spheres maximize the resistance by forcing the current to take long paths to get around the two-sphere combination and forcing the current to negotiate the constriction between the two spheres.

#### 6. The Constriction Calculation

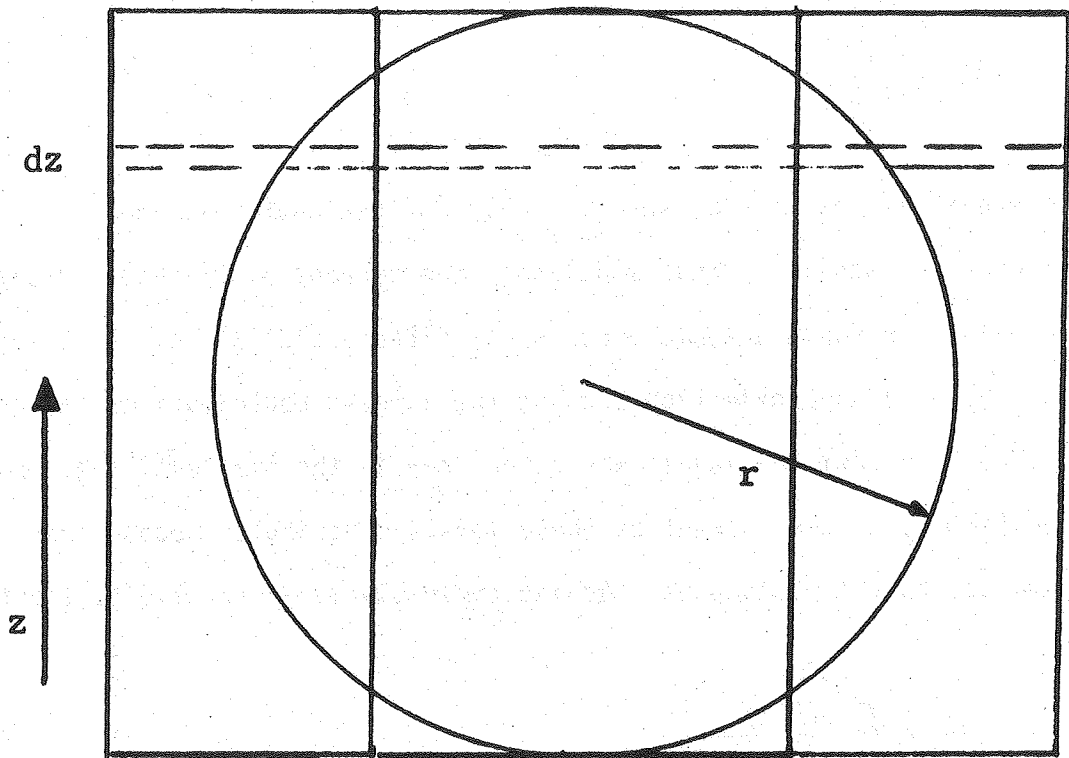
I demonstrated in the preceding section that one can double the resistance to current presented by a two-sphere combination by rotating the combination from an orientation in which the line joining the spheres' centers is parallel to the overall direction of current to an orientation in which this line is perpendicular to the current. This means that the side-to-side interactions of spheres, that is, the constriction of current between spheres, dominates the resistance presented by such heterogeneous systems. In order to explore this conclusion farther, I calculate a pure "constriction resistance" for a bubble layer and compare it to the results from the tangent sphere calculation.

The layer is modeled as a sphere contained in a unit cell of a planar hexagonal array, as shown in Fig. 12(a). The layer is one bubble thick, as shown in (b). The dotted lines define a differential



XBL 8011-7592

Fig. 12(a). Unit cell of a planar hexagonal array of spheres.



XBL 8011-7593

Fig. 12(b). Side view of a differential slice at position  $z$  in a unit cell of a planar hexagonal array.

slice of the cell parallel to the electrode. The differential resistance of such a slice is

$$dR_T = \frac{dz}{kS_C} \quad (42)$$

where  $S_C$  is the area between the walls of the unit cell and the sphere. I assume in this model that the current distributes itself evenly over the available area in any differential slice. This may not be a bad approximation because the largest contributions to resistance come from the levels where the area is the smallest; the non-uniformity of the current at these levels contributes second order amounts to the resistance. Adding these slices in the limit, I obtain

$$R_T = 2 \int_0^r \frac{dz}{k(A_h - \pi r_c^2)} \quad (43)$$

in which  $A_h$  is the area of the hexagonal unit cell,  $r_c$  is the radius of the circular slice in the sphere at position  $y$ , and  $r$  is the sphere radius. After algebraic rearrangement, integration and substitution of

$$f = \frac{2\pi r^2}{A_h}, \quad R = \frac{2r}{kA_h} \quad (44)$$

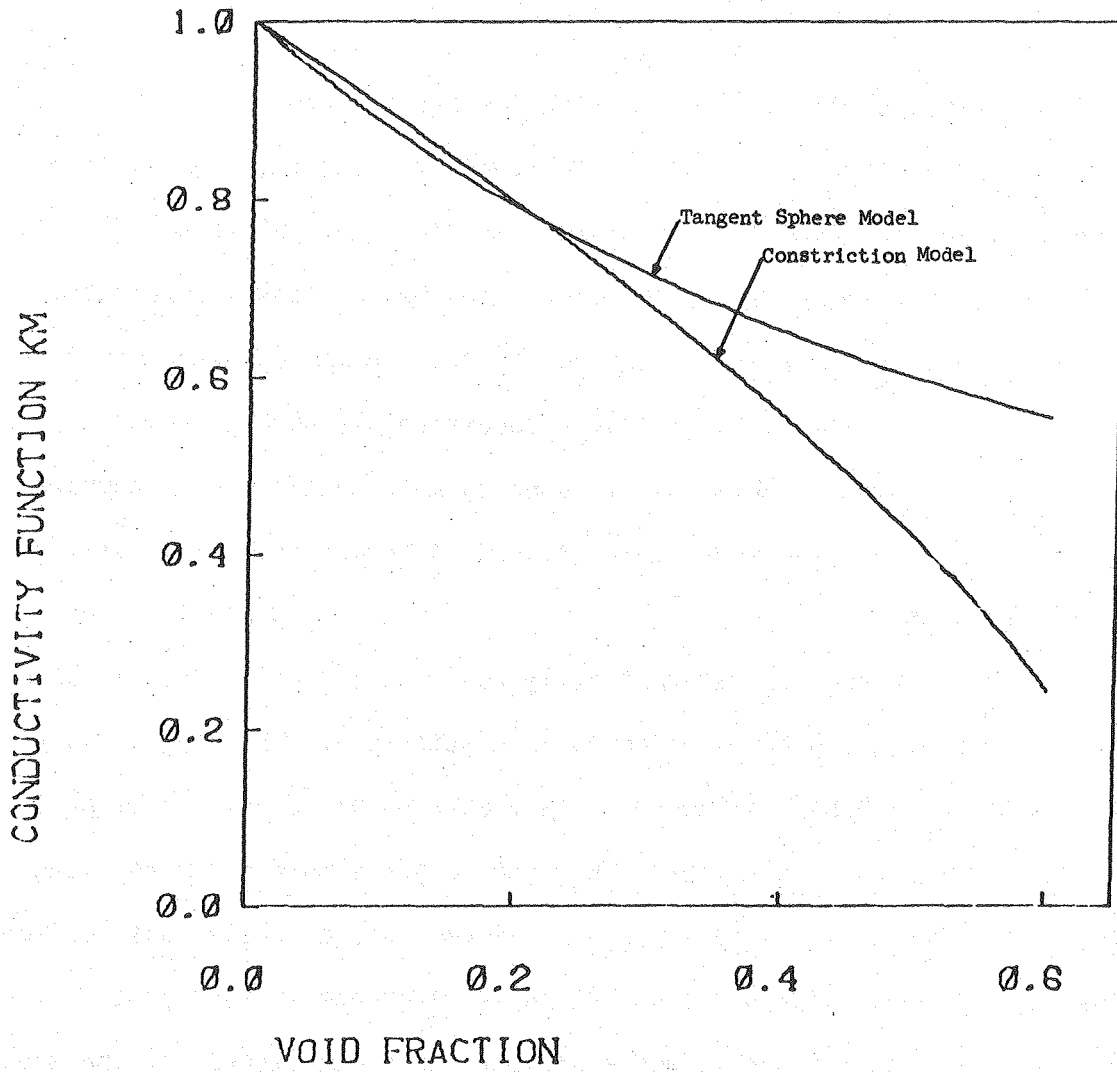
I obtain

$$\frac{1}{K_m} = 2 \left( \frac{1}{3f} \right)^{1/2} \left( \frac{1}{2-3f} \right)^{1/2} \text{TAN}^{-1} \left( \frac{3f}{2-3f} \right)^{1/2} \quad (45)$$

Equation (45) appears in Fig. 13 with the result from the tangent sphere calculation. At low void fractions, the constriction model overestimates the conductivity because it does not contain any allowance for deformation of the flux lines by the sphere's surface. The constriction calculation, however, shows a dramatic decrease of conductivity relative to the tangent sphere result at high void fractions. I discuss this result later in more detail when I compare the results of all the model calculations to the experimental data.

## 7. Conclusions

In this chapter, we mathematically analyzed several models to study the effects of gas bubbles immersed in electrolyte. The tangent sphere is a model of a bubble attached to an electrode and an idealization of a bubble layer on an electrode. An exact expression for the resistance presented by such a dilute layer of uniformly sized bubbles was derived. The current density around a bubble on an electrode is zero at the contact point of the bubble and electrode; it rises steeply in the area on the electrode shadowed by the bubble; and it goes through a maximum one bubble diameter from the contact point before declining to the current density which would exist were the bubble not there. The two-sphere calculations illustrated the importance of orientation of bubbles with respect to the current in determining the electrical resistance they present. The constriction of current between bubbles side by side with respect to the current contributes substantially to



XBL 8011-7594

Fig. 13. The results of the tangent sphere and constriction effect calculations.

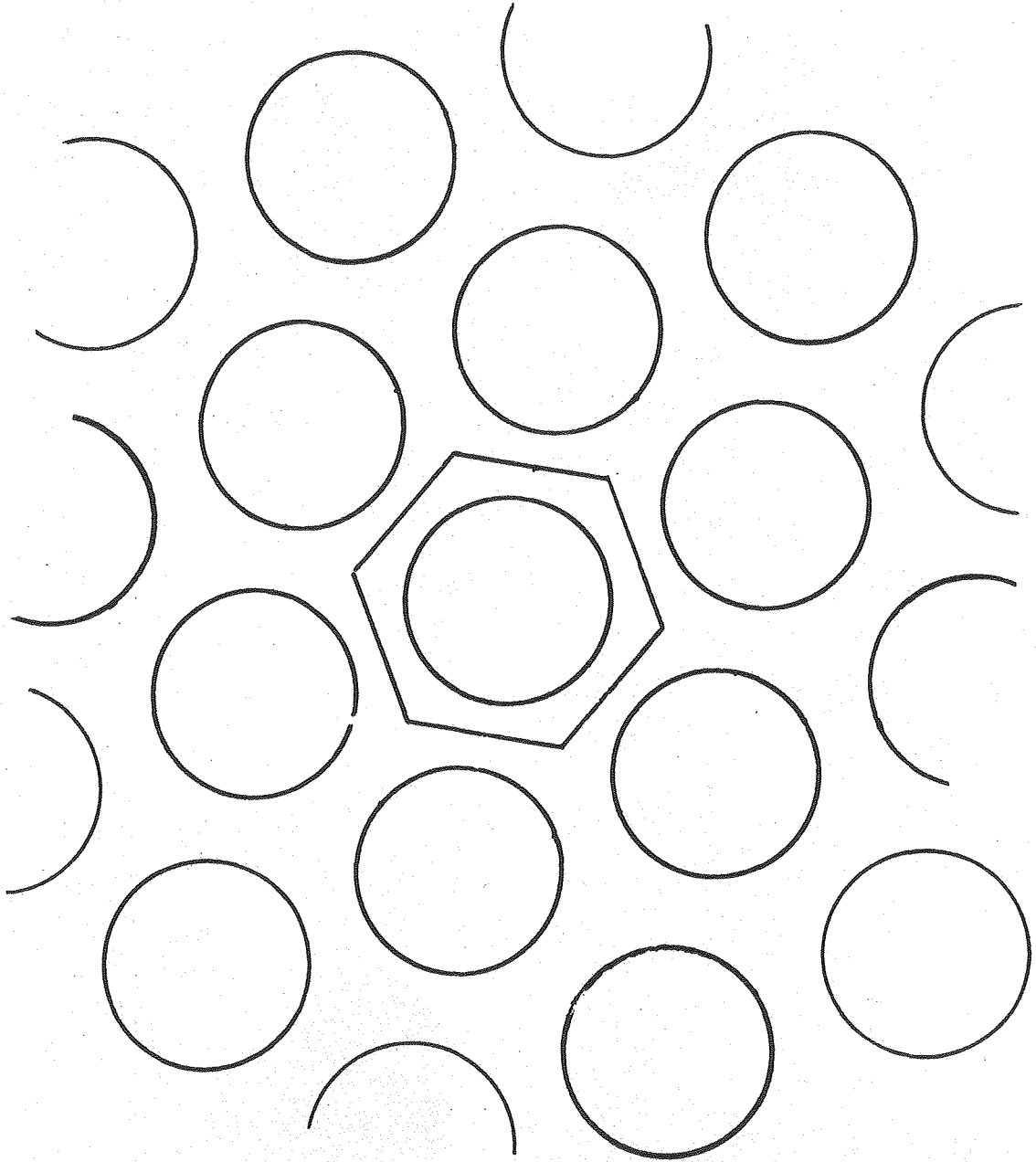
the resistance. Where an infinitely sparse coverage was assumed in the tangent sphere model, meaning no constriction, this calculation was based entirely on the constriction of current to flow in small areas between bubbles. It overestimates the conductivity at low layer packing densities, as shown by values higher than the tangent-sphere calculation, but predicts conductivities lower than the tangent-sphere model at high void fractions. In the next chapter, an experimental inquiry into the conductivity of closely packed spheres is presented and compared to the models discussed in this chapter.

#### IV. EXPERIMENTS ON A MODEL OF A BUBBLE LAYER

##### 1. The Hexagonal Cell Experiments

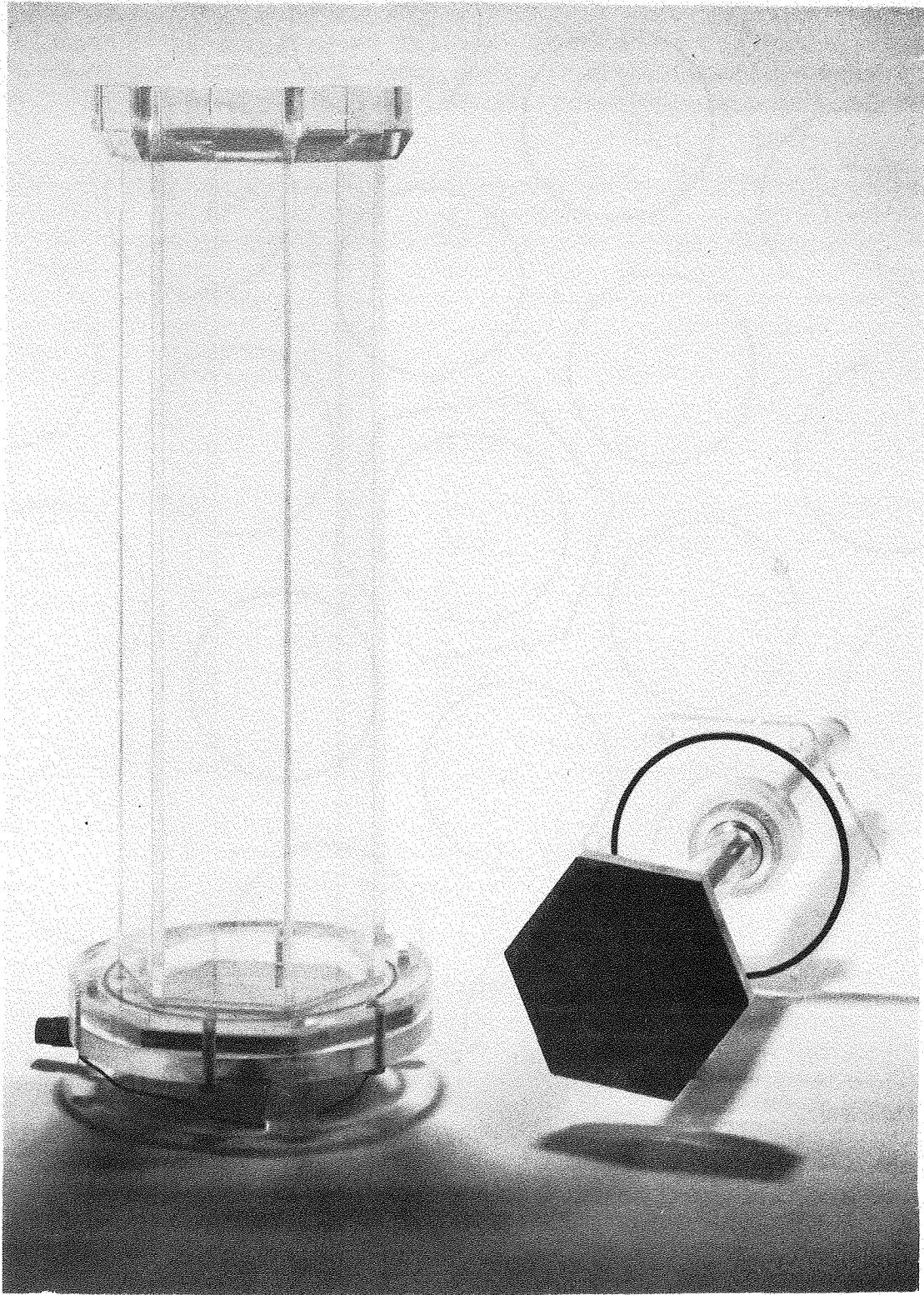
I have demonstrated that the constriction between spheres side by side with respect to the overall current resists current flow and may account for much of the resistance in heterogeneous systems. I wish to calculate analytically the resistance of a populous bubble layer, but solving Laplace's equation for multi-bubble systems would require extensive computer calculations; therefore, I experimented with planar arrays of spheres which simulate bubble layers on electrodes.

A planar hexagonal array was chosen because it gives the highest packing density for equal sized spheres. One can section out a cell representative of the entire array as shown in Fig. 1. A Lucite tube 40 cm long, having a hexagonal crosssection, and stopped at either end by flat gold-plated copper electrodes, was built as a model for this unit cell around a bubble on an electrode. This device appears in Fig. 2. The cell and sphere dimensions are tabulated in Appendix B where error in the system is discussed. The cell accommodates a 10.16 cm diameter sphere, at the maximum, which represents close packing. The spheres rest on the bottom electrode while the upper electrode is attached to a piston so that the distance between the two electrodes can be changed. The cell, containing the largest sphere and surrounded by others 9.65, 9.14, 8.64, 7.11, and 5.84 cm in diameter, appears in Fig. 3. The different-sized spheres, simulating a range of void fractions in the bubble layer, were placed one at a time in the cell and the resistance was measured.



XBL 8011-7592

Fig. 1. Unit cell of a planar hexagonal array of spheres.



CBB 796-8252

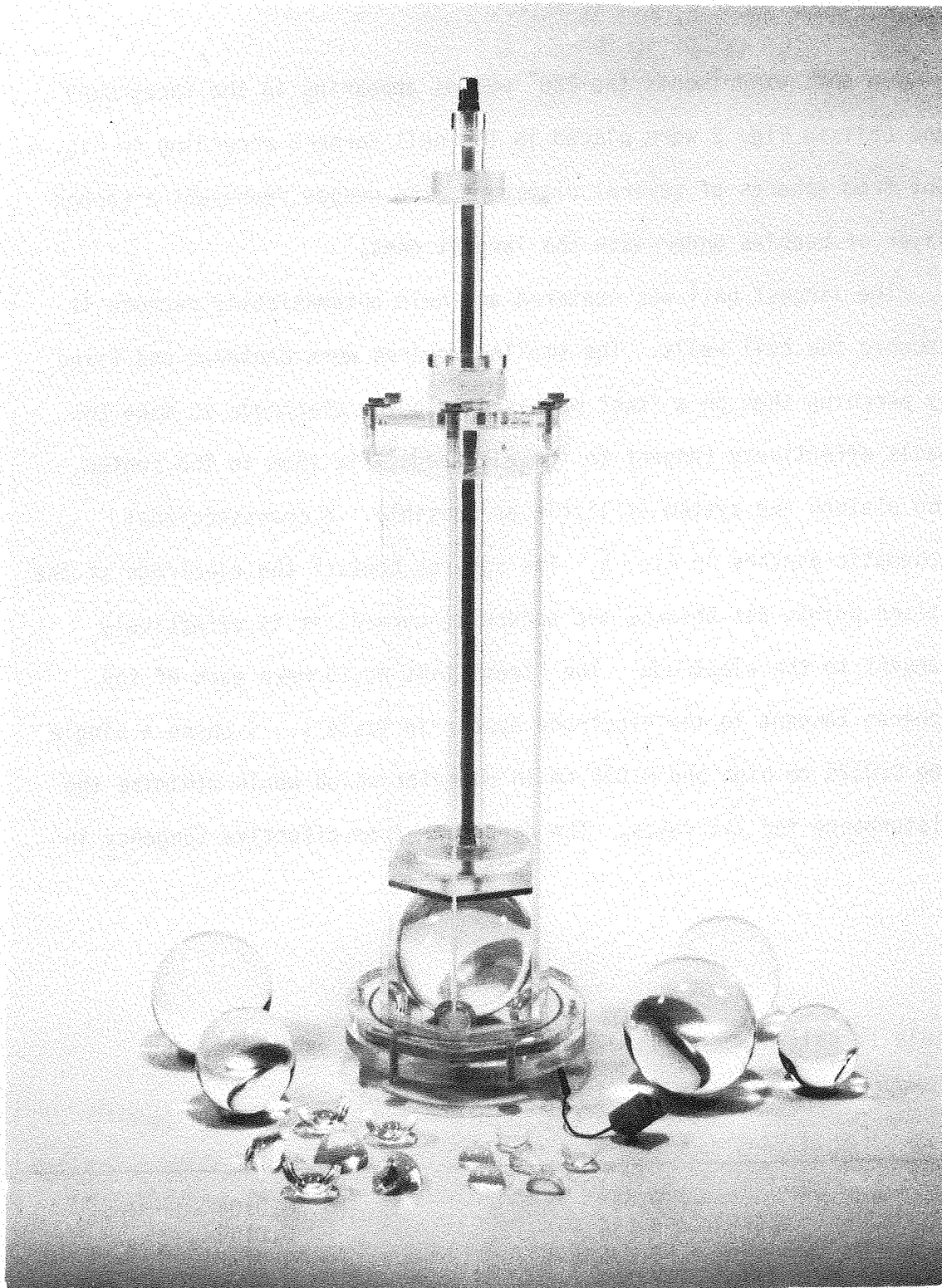
Fig. 2. Hexagonal cell disassembled, hexagonal tube and piston electrode.

In some experiments the  $120^\circ$  wedges appearing in the foreground and cell in Fig. 3 were placed in the cell corners according to Fig. 4. Cut from spheres of several diameters, the wedges represent a second layer of bubbles underneath the largest ones.

The largest ball was centered and held automatically because it touched the cell walls. The smaller spheres were centered and fixed by perching them on a "tee" machined into the electrode to make the balls effectively tangent to the electrode, fix them in the center, and disturb the system as little as possible. A crosssectional schematic appears in Fig. 5. The spheres contact the electrode at the raised points but because the sphere is curved, it is effectively tangent to the electrode. The "tees" that would make each of the spheres tangent to the electrode appear in Table 1. I chose a single tee 0.0125 cm high and 0.635 cm in diameter which would minimize the disturbance for all cases. The departure from effective tangency in

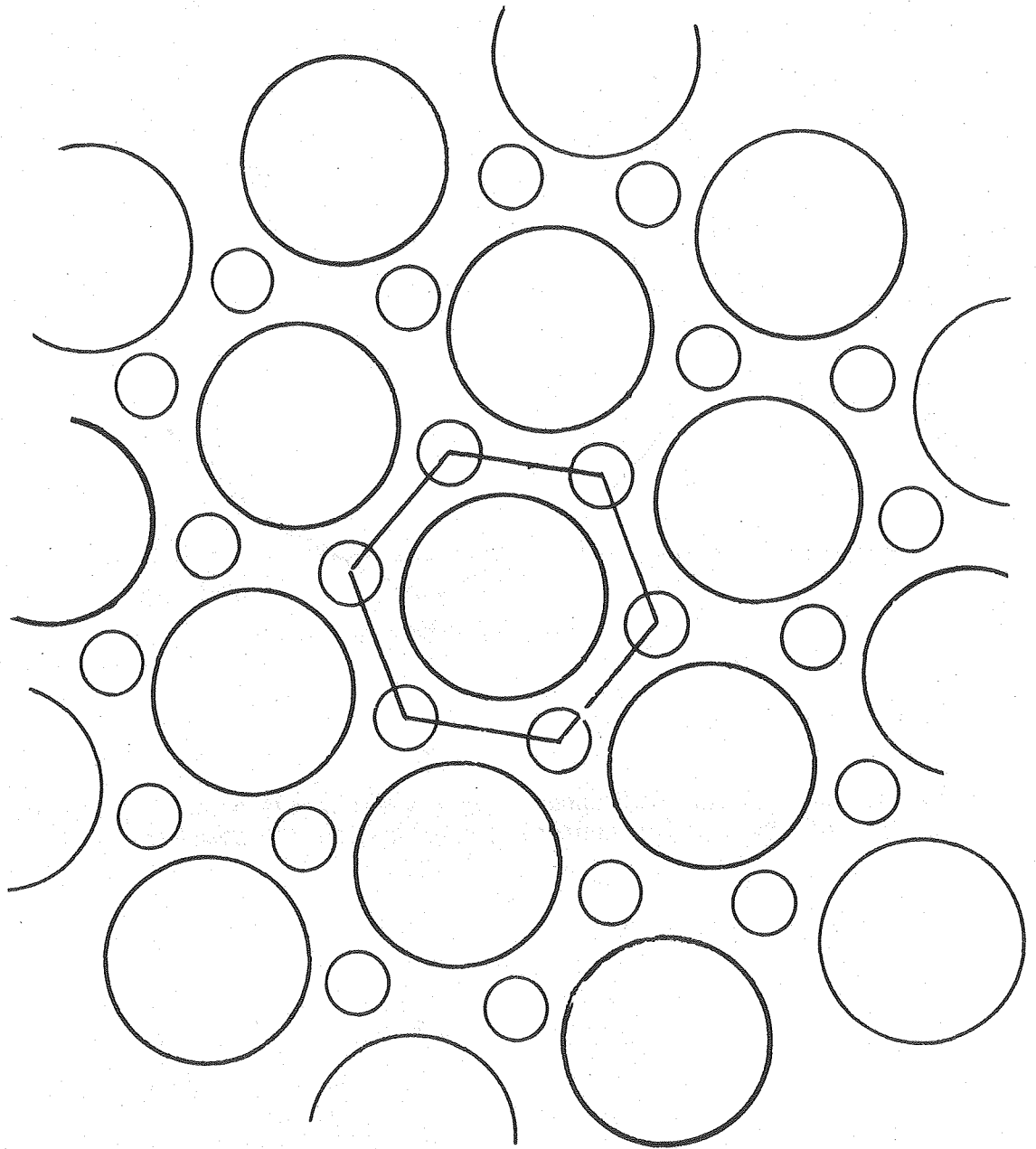
Table 1. Ball diameter (cm) amount by which the sphere must be lowered (cm).

9.652	0.0104
9.144	0.0109
8.636	0.0117
7.112	0.0142
5.842	0.0173



CBB 801-242

Fig. 3. Hexagonal cell with lucite spheres and wedges in the foreground. Note assembly with large sphere in cell and wedges placed in the corners.



XBL 8011-7595

Fig. 4. Unit cell of a hexagonal planar array showing symmetrical placement of second layer underneath the first.

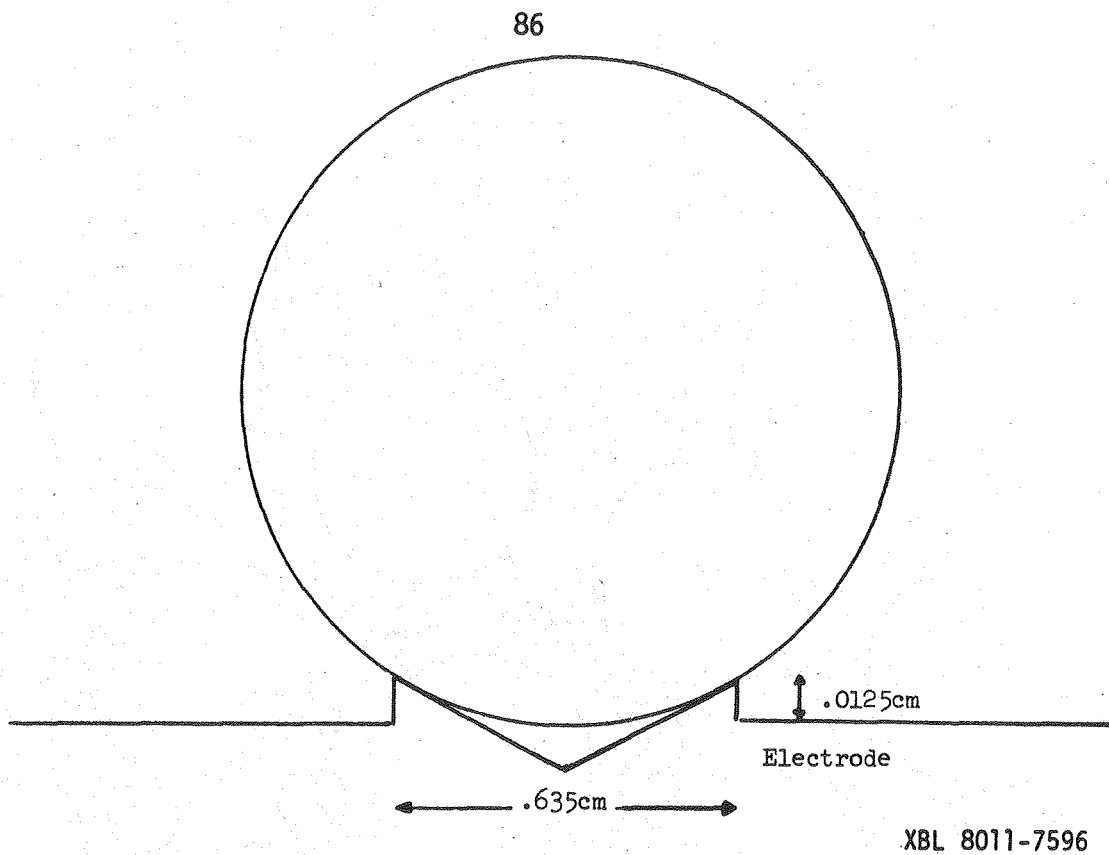


Fig. 5. Crosssection of spheres on the electrode showing geometry of the tee for centering and holding the small spheres.

the worst case was less than 0.1 percent of the sphere diameter. This deviation was on the order of the accuracy of the spheres themselves. As discussed in Chapter 2 with respect to a tangent sphere, little or no current reaches the area just around the contact point so the disturbance due to the tee was considered small. To check this assumption, I employed the largest ball with and without the tee and found no measurable difference.

The system resistance was measured with an Electro-Scientific Industries Model 861A Generator/Detector and Model 290 Conductivity Bridge which gave readings to five significant figures. The generator signal was set at a frequency high enough to eliminate capacitance and polarizations in our system (2000 Hz). Test measurements at higher frequencies showed no change in the measured resistance.

The conductivity solutions were 0.1 Demal aqueous KCl prepared according to the prescriptions of Jones and Bradshaw (28). One tenth of a gram equivalent weight was added to deionized water to make a solution whose total weight was 1000 g. Bremner and Thompson (29) give an equation for the conductivity of this solution in the range 0° to 25°C:

$$10^6 \times K(0.1N KCl) = 7137.6 + 208.312T + 0.99077 T^2 - 0.006964 T \quad (1)$$

Assuming that the electrodes and solution were at thermal equilibrium, I inserted a chromel-alumel thermocouple into the base electrode to measure the cell temperature. An ice bath provided the reference

temperature and a digital multimeter having  $10^4$  megohms input impedance and a 1 mv scale recorded the thermocouple potential. Values of the resistance measured at cell temperature were first corrected to  $25^\circ$ . Dividing the resistance with a sphere present by a resistance calculated from the known cell area, solution conductivity at  $25^\circ\text{C}$ , and electrode separation, one can find  $K_m$  for the bubble layer from the following operational definition.

I introduce a modification of the equation used by other investigators to present results of studies on the conductivity of heterogeneous media. One usually defines a quantity which is a ratio between the conductivity with gas present and the conductivity with no gas present and then calculates the resistance of such systems according to

$$R_T = \frac{R}{K_m} \quad (2)$$

in which  $R$  is the gas-absent cell resistance and  $R_T$  is the gas-present resistance. Assuming that the gas is confined to a layer of thickness  $xl$  close to the electrode where  $x$  is the fraction of the interelectrode gap  $l$  occupied by a bubble layer, I use the following form for a parallel plate configuration,

$$R_T = (1 - x) \frac{l}{kS} + \frac{xl}{kSK_m} \quad (3)$$

in which  $k$  is the homogeneous electrolyte conductivity and  $S$  is the electrode area. The two quantities  $x$  and  $K_m$  must be determined in addition to the cell dimensions and homogeneous electrolyte conductivity. All theoretical and experimental results will be presented in terms of the function  $K_m$  for convenient comparison of the various models and data.

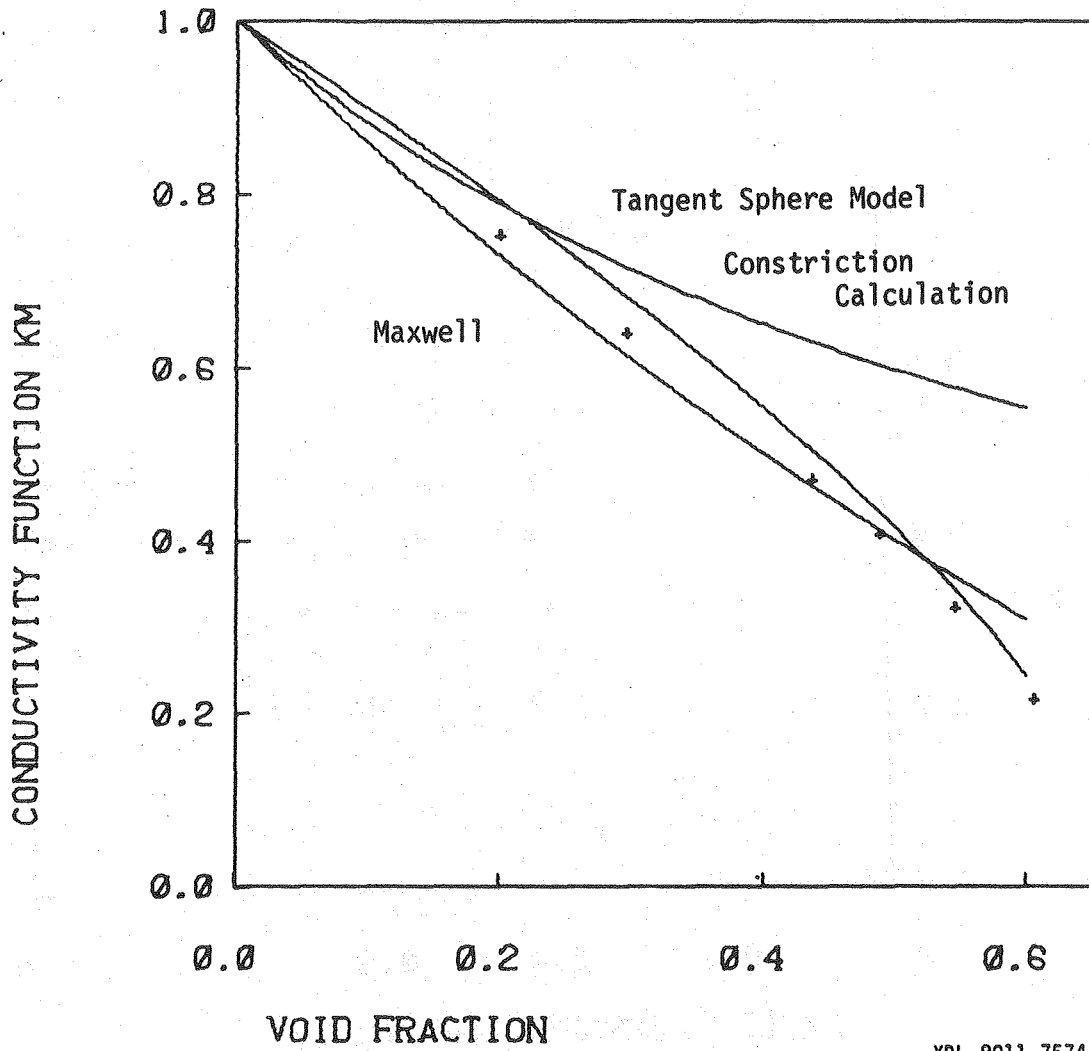
## 2. Results of the Hexagonal Cell Experiments

The results of the hexagonal cell experiments on monosized spheres, the tangent sphere prediction, the constriction calculation, and Maxwell's result for reference appear in Fig. 6. As predicted by the tangent sphere calculation, the experimental resistance values are greater than those predicted by the Maxwell relation at small void fractions; the electrode plane on one side of the bubble terminates the electrical activity and hence limits the resistance presented by a tangent sphere to 90 percent that of a similar sphere in the bulk electrolyte. At close packing, the conductivity of the bubble layer is reduced by a factor of nearly 5. This means that a close-packed bubble layer occupying 5 percent of the interelectrode gap causes a 20 percent increase of the overall cell resistance according to Eq. (2).

The tangent sphere calculation grossly overestimates the conductivity except at the low bubble layer occupancies for which it was derived. The opposite is true of the constriction calculation. It does not agree with the data at dilute bubble occupancies because the sphere's curved surfaces force the current to take net longer

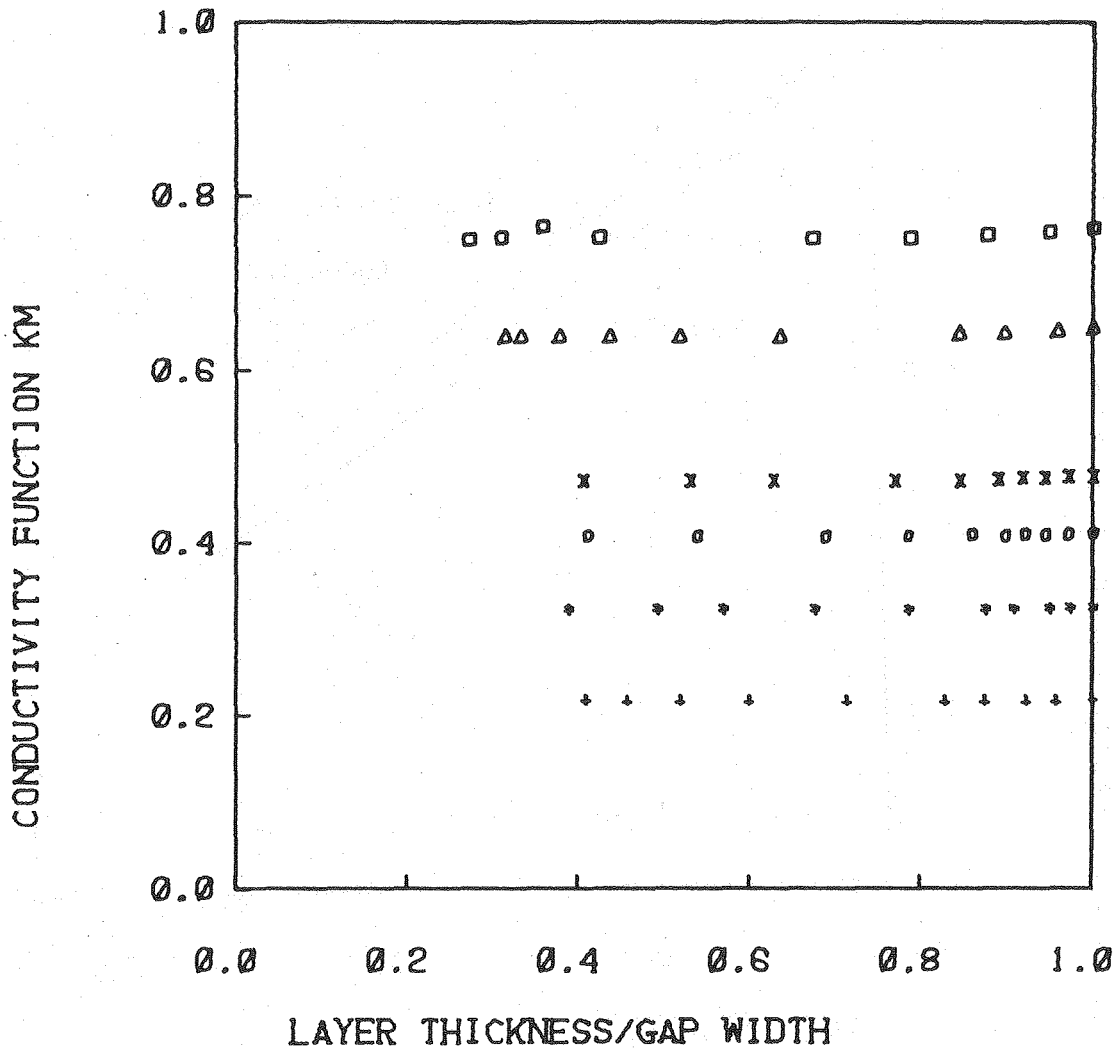
Table 2. The hexagonal cell results.

Diameter of sphere, cm	Diameter of wedges, cm	Bubble layer void fraction	K m
10.160	none	0.6046	0.2155
10.160	2.54	0.6239	0.2076
10.160	3.175	0.6415	0.1932
9.652	none	0.5457	0.3196
9.652	2.54	0.5661	0.3070
9.652	3.175	0.5845	0.2844
9.144	none	0.4897	0.4076
9.144	2.54	0.5089	0.3820
9.144	3.175	0.5307	0.3583
8.636	none	0.4368	0.4707
8.636	2.54	0.4591	0.4498
8.636	3.175	0.4802	0.4188
8.636	3.810	0.5118	0.3564
7.112	none	0.2963	0.6388
7.112	2.54	0.3239	0.6024
7.112	3.175	0.3490	0.5685
7.112	3.810	0.3877	0.5074
5.842	none	0.1999	0.7503
5.842	2.54	0.2328	0.7027
5.842	3.175	0.2641	0.6601
5.842	3.810	0.3108	0.5970



XBL 8011-7574

Fig. 6. Data of hexagonal cell for single spheres compared to calculated values.



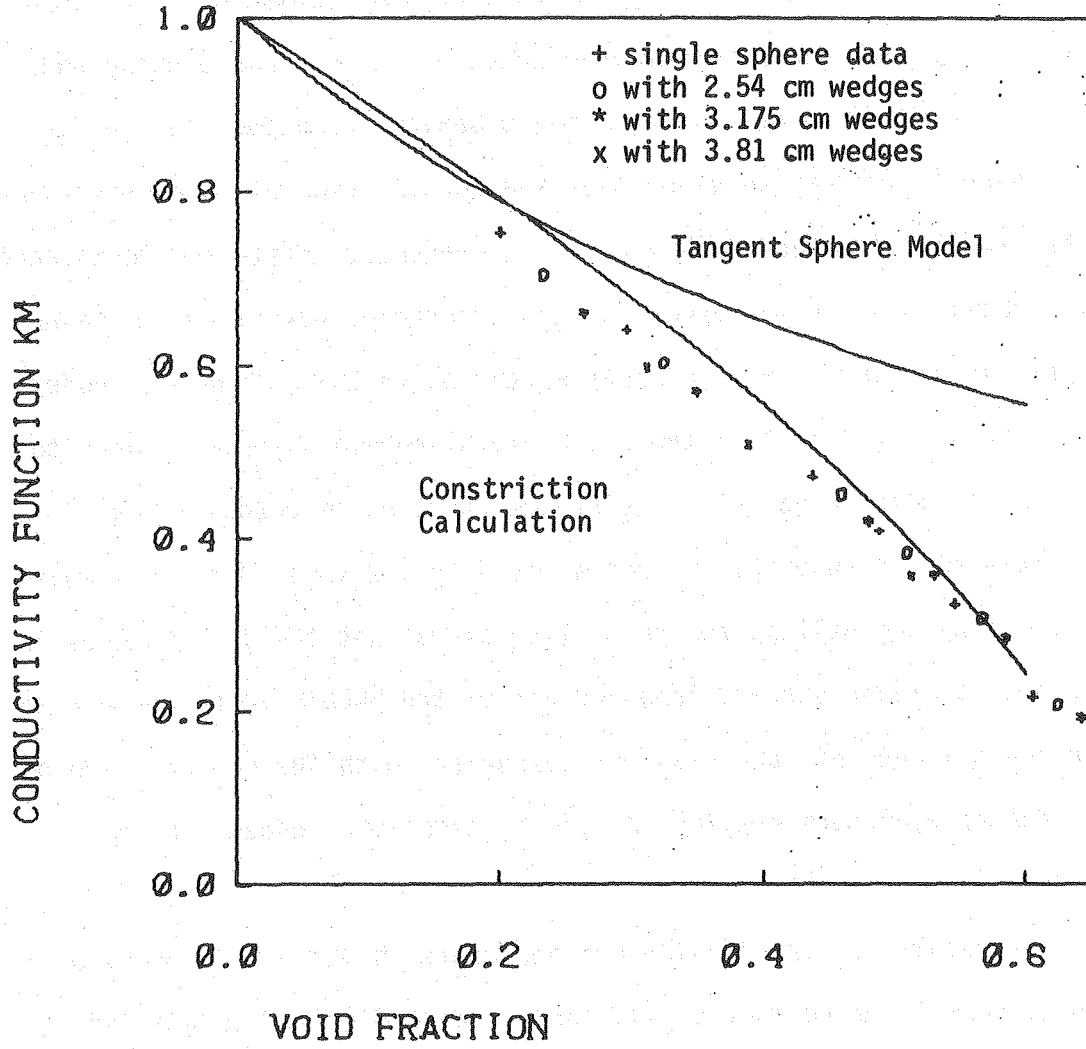
XBL 8011-7572

Fig. 7. Variation of resistance presented by the spheres with the interelectrode gap.

paths through the electrolyte to get around them and hence resist the current more than the constriction calculation allows for. The constriction effect dominates at void fractions near close packing and the constriction calculation becomes a better approximation there.

There is further evidence that the constriction of current between bubbles dominates the resistance in heterogeneous systems. Resistances were measured while the upper "piston" electrode was placed at several different distances from the sphere resting on the bottom electrode. Plotted in Fig. 7 against the ratio of the bubble layer thickness to the interelectrode gap, the resistance function  $K_m$  changes only slightly as the upper electrode is moved from several diameters away to touching the ball at the top. I conclude that the disturbances in the potential and current fore and aft of the bubble (with respect to the overall current) are small by comparison with the constriction of current between bubbles sitting side by side with respect to the current.

The results of the two-layer experiments in which the wedges of Fig. 3 were inserted in the cell corners according to the plan of Fig. 1, appear in Fig. 8. Note that at the lowest void fractions, the new conductivities are lower than just the single sphere line would predict while at the high bubble occupancies the new conductivities are higher than the single-sphere data alone would predict. The transition from one tendency to the other occurs near a bubble coverage of 0.4. This trend indicates that as the small spheres are added, the



XBL 8011-7573

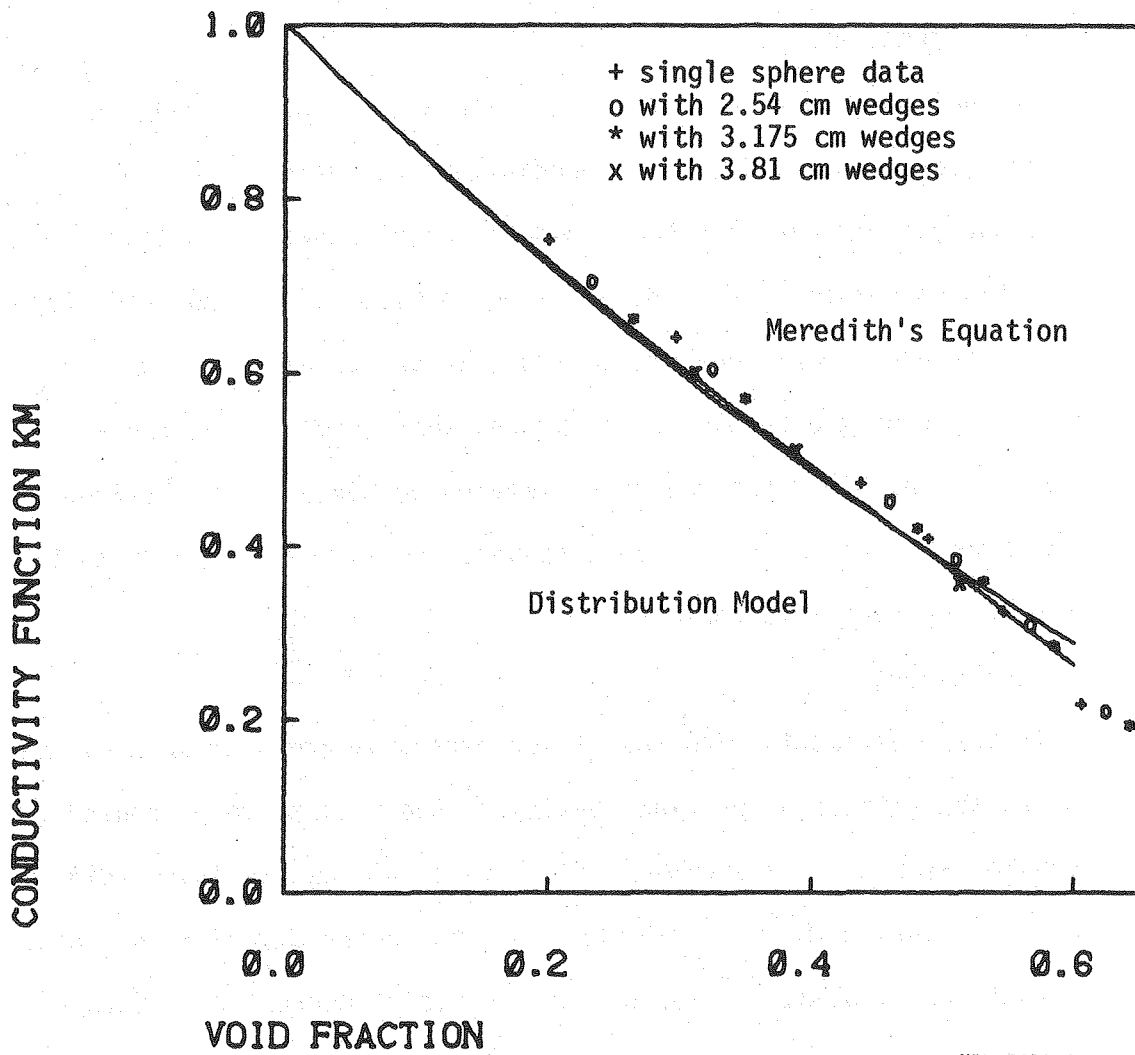
Fig. 8. Two layer results for hexagonal cell.

system becomes a bulk-like three dimensional dispersion rather than a two-dimensional array.

If many spheres were added, the Distribution Model (II-45) or Prager's equation (II-40) would predict the conductivity of the layer. Graphs of the Distribution Model and Meredith's equation (II-42) compared to the hexagonal cell data appear in Fig. 9. At low void fractions, the experiment confirms the theoretical prediction that the conductivity of the bubble layer exceeds that predicted by these equations. At high void fractions, where the constriction between bubbles dominates whether in bulk solution or on the electrode surface, the data and equations agree.

### 3. Conclusions

In the experiments with the planar hexagonal array of spheres, we studied the effects of packing density on the resistance presented by a bubble layer on an electrode. The results at low gas layer void fractions confirm the result of the tangent sphere calculation, that is, that sparse planar arrays of spheres resist current less than Maxwell's equation predicts because it is a two dimensional rather than a three dimensional array and the electrode terminates the disturbance caused by the sphere in the electric field. The hexagonal cell results also show how the constriction model, while it severely overestimates the conductivity at low void fractions, estimates better the conductivity at high void fractions where we expected that it should be more appropriate. Comparison of the results to Meredith's equation and the Distribution Model (see Chapter II) revealed that these



XBL 8011-7585

Fig. 9. The hexagonal cell results compared to the Distribution Model and Meredith's equation.

equations, derived for homogeneously dispersed or ordered spheres, are not grossly in error when applied to a bubble layer. Finally, when closely packed, a bubble layer resists current five times as much as the same layer of electrolyte without bubbles.

## V. A CLOSE VIEW OF GAS EVOLUTION FROM THE BACKSIDE OF A TRANSPARENT ELECTRODE

### 1. A Review of Literature on the Observation of Bubble Behavior

Gas evolution begins with nucleation of bubbles from highly supersaturated solutions near the electrode surface. The bubbles grow by diffusion of dissolved gas to the bubble surface and by coalescence with other bubbles. They ultimately depart from the electrode when the forces pulling the bubbles away overcome the surface forces which bind them to the electrode. There is a body of theory behind each one of the stages in gas evolution. For example, nucleation is described by the probability for survival of a critical nucleus (33). Scriven (34) and others (35,36) discussed growth by diffusion of dissolved gas to the gas/liquid interface. Frumkin and Kabanov (37) presented experimental and theoretical evidence concerning the detachment of bubbles. Other writers have investigated the phenomena of gas evolution by photographing them and in some cases comparing their findings to theory. In this chapter, I concentrate on these physical observations in preparation for the description of our own work in the chapter following.

Using a microelectrode and a high speed camera, Westerheide and Westwater (38) quantitatively studied the growth of single electrolytic hydrogen bubbles and compared the result to the theoretical work of Scriven (34) who analyzed the diffusion limited growth of a spherical cavity. Scriven's square root of time growth dependence agreed with

their data for a single bubble but multiple bubbles interfered with each others' growth. In some cases, bubble growth was accelerated by the appearance of another bubble; the writers suggested that the second bubble's growth could enhance the mass transfer of dissolved gas to the bubble already there. The opposite also occurred; two bubbles grew with exponents less than 0.5 which the writers explained by the competition for dissolved gas which starved both bubbles. Understanding that the enhancement and the competition were contradictory, they suggested that bubbles a sufficient distance apart competed for gas while close bubbles enhanced the mass transfer sufficiently to compensate. When two bubbles of equal size coalesced, the resulting bubble jumped off the electrode and sometimes returned. The writers speculated that the expanding boundaries of the new bubble mechanically forced it off the electrode; to explain the bubbles' return, they left the possibility open that there could be electrostatic forces operating on a moving bubble, and they also mentioned that surface forces varying with concentration could be important. Nucleation occurred at preferred sites such as pits and scratches on the electrode. Growing bubbles were not necessarily attached to their nucleation site but moved around on the electrode.

Glas and Westwater (39) extended the work of Westerheid et al. (38) to include different gases and different electrode materials. There were two stages in the growth of the bubbles: an early growth period

which was a function of the electrode metal and its nucleation site, and an asymptotic stage which obeyed the square root of time functionality deduced by Scriven (34). The writers proposed two equations to describe the growth of electrolytic bubbles as a function of current density; in the first, they assumed that the bubble volume is directly proportional to the current; in the second, they assumed that the growth obeys a fractional power as per Scriven and also included a waiting period for the birth of a bubble. They concluded that each model is appropriate for different gases. Their data depended on the bubble nucleation site; hence the electrode metal and surface preparation must have influenced the results. The electrode potential did not affect the bubble growth, but the contact angle changed through the course of the growth; the writers noted that any theory which did not allow for this was flawed. Bubbles were ejected from the electrode in what the writers termed "rapid fire emission." They did not obtain this mode consistently but mentioned that if one could, electrolytic gas could be removed quickly from the electrode with resulting benefits.

Janssen and Hoogland (40) measured the mass transfer due to—and observed the growth of—electrolytic hydrogen, oxygen, and chlorine on a rotating Pt wire in  $\text{H}_2\text{SO}_4$  and  $\text{HCl}$ . Bubbles formed at fixed spots which acted as nucleation sites and depended on pretreatment as well as current density. The size distribution of bubbles also depend on current density; while randomly sized at low current, hydrogen bubbles assumed discrete sizes as the current was increased. The writers

attributed this trend to bubbles coalescing at higher current densities. The new bubble formed from two coalescing bubbles vibrated very strongly. Some bubbles jumped away from the surface but others slipped along it.

In their second article on the enhancement of mass transfer by gas evolution, Janssen and Hoogland (41) evolved gas on horizontal and vertical platinum discs and determined the size of bubbles as a function of current density and electrolyte. At low current densities, where bubbles rarely coalesced, the order of increasing sizes was: oxygen in acid, hydrogen in alkaline, hydrogen in acid and oxygen in alkaline solutions.

From the viewpoint of Kabanov and Frumkin (37), who related the ultimate size achieved by slowly grown bubbles to the electrode potential, one might conclude that the potential of oxygen evolution in acid was past the electrocapillary maximum for the Pt electrode in this experiment because the oxygen bubbles evolved in acid were smaller than those evolved in base. As the current density was increased past  $10 \text{ ma/cm}^2$ , all bubbles but hydrogen evolved in alkali increased in size; the writers attributed this to increased coalescence. Surpassing both the hydrogen evolved in acid and base, the oxygen bubbles evolved in acid became much larger at high current densities. The oxygen in base remained the largest followed by the oxygen in acid, the hydrogen in acid, and the hydrogen in base.

Venczel photographed bubbles (42) from the front of graphite, iron, copper, and Pt electrodes and from the backside of glass plates on which thin layers of Pt, Cr, Ni, and Au were vacuum deposited. He also used additives to change the properties of the electrode/electrolyte interface.

The electrode material affected the size of the bubbles; in his experiments, large bubbles formed on Pt and C, but small ones formed on Fe and Cu. There was even a difference between the bubble sizes produced on two different grades of graphite.

Venczel added gelatin, glycerine, and beta-naphthochinolin to his electrolyte; in most cases the bubble size decreased and in some cases a frothy mixture would result. The additives reduced the bubble diameter to contact diameter ratio by half in some cases. Venczel claimed that the increased wettability of the electrode in the presence of inhibitors leads to a thick film of electrolyte between the gas and the electrode; he asserted that this film is less adhesive than thin films and therefore bubbles apart sooner from wetted electrodes than from unwetted electrodes. Other explanations could be advanced. The reduced perimeter of contact area noted by Venczel means that the force holding the bubble to the electrode is reduced; furthermore, the inhibitors might be stabilizing the bubble interfaces and preventing coalescence on the electrode. This would also account for the smaller bubbles. As everyone else has observed, bubbles grew by diffusion and coalescence. On Pt and graphite, the bubbles grew uniformly and coalesced. On copper and iron, the bubbles never reached a size for

coalescence, but departed from the electrode after growing by diffusion. The size distribution was nonuniform. The bubbles' size on Pt and graphite did not depend on current density. Large bubbles consumed small bubbles when they touched. New gas-evolving sites become active in the vicinity of a larger bubble, and they cease when it detaches. This is probably due to a combination of effects. As calculated in the previous chapter (p. 49) there is a maximum in the current density one diameter from the bubble; this might account for the increased activity around an attached bubble. Subsequently, when a large bubble leaves, electrolyte from the bulk solution, which does not contain as much dissolved gas, rushes in to fill the space. The supersaturation close to the surface decreases; hence the sites around the bubble would become inactive. Venczel estimated an absolute surface coverage by determining the number of bubbles, the diameter, and knowing the rough ratio between the bubble diameter and the surface contact area. He found that the surface coverage was 25 percent near  $250 \text{ ma/cm}^2$  and was constant thereafter on graphite, platinum, and copper for currents up to  $50 \text{ ma/cm}^2$ . Venczel then determined a bubble growth time; he showed that as the current density increases, the bubble grew faster, as one might expect. His interpretation on this point is weak because he did not correlate it with the variation in bubble size that occurs with current density. At higher current density, hydrogen is formed more rapidly; if the departure size remains the same, the growth time will naturally be shorter. If the departure

size is also a function of current density, the departure time must be modified.

As did Venczel (42), Ibl and Venczel (43) observed that the size of bubbles depended on the electrode material; for example, they found that bubbles evolved on Pt were much larger than those evolved on Cu. They observed that adding inhibitors caused the bubbles to become smaller and also that as the current density increased, the bubble size decreased.

Ibl (44) reviewed the physical phenomena associated with gas evolution: the ideas of nucleation, growth by diffusion, coalescence, and departure. He described in detail the theoretical work related to growth by diffusion and to detachment. He mentioned coalescence only in passing as responsible for determining bubble size. Ibl pointed out the discrepancy between the work of Venczel, who said that bubble size decreases with current density, and the work of Janssen and Hoogland, who found that bubbles increased in size with current density.

Landolt, Acosta, Muller, and Tobias (45) photographed hydrogen evolution from the side of a transparent cell which simulated the high electrolyte flow rates characteristic of electrochemical machining. The size of bubble was a function of current density and flow rate. In agreement with Janssen and Hoogland (40), but contrary to Venczel (42), and contrary to the theory of Frumkin and Kabanov (32), bubbles increased in size with current density; they did not mention increased coalescence as a possible explanation. The bubble size decreased with

flow rate; at high flow rates (1000 cm/sec) nearly all the bubbles were blown away from the interelectrode area; hence there was no influence on cell behavior. As long as sufficient flow was applied, current densities were achieved that were much higher than those which in stagnant electrolyte would lead to anode effect. The writers noted that the thickness of the two phase region next to the electrode could not be explained simply by the rise of bubbles under the influence of gravity; they suggested that a bubble ejection mechanism such as that noted by Glas and Westwater (39) may account for this. Perhaps gas was evolving at such a high rate that old bubbles were pushed away from the electrode by new bubbles.

Ron Putt (46) used a still camera and microscope to photograph the growth of hydrogen and oxygen bubbles evolved electrolytically in base and acid on nickel electrodes. He documented the incipient bubble growth period by evolving gas for a fixed short amount of time and then triggering his camera. He reported both sequences of photographs and graphs showing the growth of bubbles as a function of time. The hydrogen bubbles in KOH grew to an asymptotic limit of approximately 150 microns through a combined mechanism of growth by diffusion and by coalescence. The hydrogen produced in acid grew large by a scavenging mechanism in which the bubbles slid along the electrode and consumed other smaller bubbles. Putt noted a bimodal distribution of large bubbles (700 microns) and small bubbles (125 microns). The size distribution for oxygen bubbles evolved in KOH was narrow and centered around 250 microns. Although the bubbles slid along the electrode,

they did not scavenge as much as the hydrogen bubbles in acid. The oxygen bubbles grew faster at equal gas generation rates than hydrogen. Putt attributed the difference in size between the oxygen and hydrogen bubbles evolved in KOH to the Frumkin/Kabanov theory of electrode potential and interfacial tension. Oxygen bubbles, evolved at a higher potential than hydrogen, are bound by a higher interfacial tension and hence should grow to a higher diameter at departure. The writer discussed adhesion of bubbles to a solid surface in a semi-quantitative manner. He determined that the bubbles evolved at a finite rate were five times smaller than one expects under conditions of equilibrium growth. He pointed out that a new bubble formed by coalescence leaves the surface and returns until the hydrodynamic forces in the vicinity tear it off and do not permit it to return.

The size of hydrogen bubbles in KOH increased with current density in the range 15-500 ma/cm<sup>2</sup>. This result agrees with Janssen and Hoogland, but disagrees with the result of Venczel and the theory of Frumkin and Kabanov. Putt concluded that bubbles grow by diffusion of dissolved gas and by coalescence and that these modes operate to some extent in series as well as in parallel. Bubble growth is governed by the effect of the electrode potential in physical properties at the electrode surface. He speculated that bubble departure at industrial gas evolution rates is controlled by "dynamics of the bubble interactions" which presumably means collisions, coalescences, and the resulting hydrodynamic environment near the bubbles.

Darby and Haque (47) photographed hydrogen evolution on a microelectrode from the side and found that the radius was proportional to the cube root of time at current densities near  $10 \text{ a/cm}^2$  rather than the 0.5 found by other investigators at lower current densities. Since this rate law can be derived by assuming that all the gas produced at the electrode goes into forming the bubble, they concluded that at high current density the rate-limiting step is not mass transfer of dissolved gas. They theorized that recombination of atomic hydrogen to molecules limited the rate.

Electrolytic gas evolution is complicated because it is a nonequilibrium process affected by interactions among all the variables. For example, the fundamental force binding the bubble to the electrode depends on the electrolyte's surface tension and the bubble's contact angle which in turn depends on the interaction of the electrode and electrolyte to determine the potential and rate at which gas is evolved. Since the process occurs at a surface, small quantities of impurities may have a large effect as noted by Venczel (42) who reported differences between gas evolution on two different grades of graphite. It is important to observe and catalog the various phenomena of gas evolution that must be the result of such complexities.

We expect to see some of the phenomena already reported in the foregoing discussion.

1. Growth of bubbles by diffusion and coalescence.
2. Various modes of bubble departure such as detachment after a coalescence and the "rapid fire emission" discussed by Westwater (39).
3. Bubbles sliding along the surface or remaining stationary.
4. Preference of bubbles for certain nucleation sites.
5. Vibration of bubbles newly formed by coalescence.

Furthermore, the dynamics of bubble evolution should depend on current density, electrode morphology, composition, and pretreatment. It should also depend on the electrolyte composition and the presence or absence of surface active agents which affect either or both the electrode potential and the mobility of the gas/electrolyte interface.

## 2. The Transparent Electrode Experiment

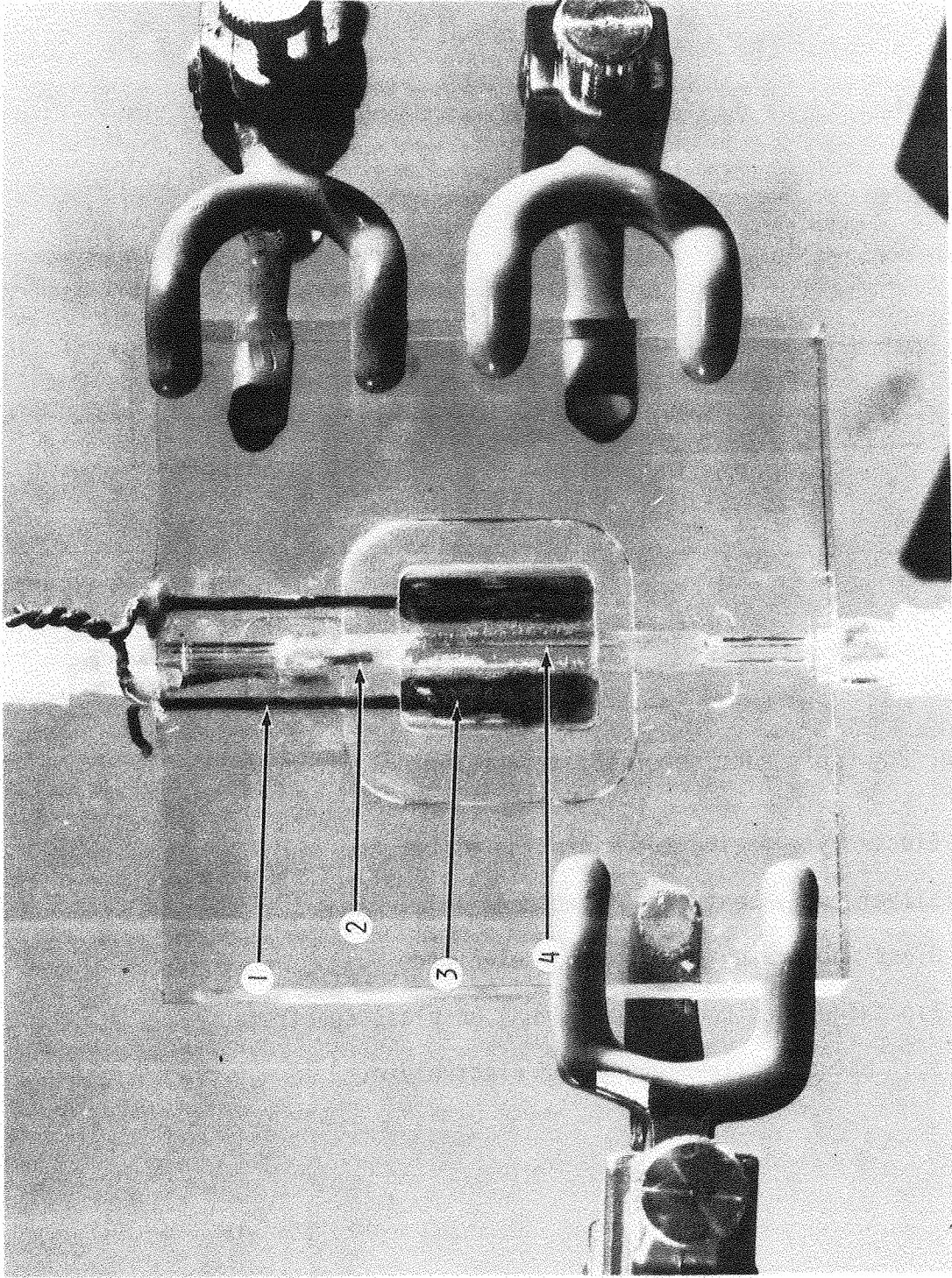
Experimenting in the lab with metal gas-evolving electrodes, one concludes that the events on gas-evolving electrodes are microscopic, they occur quickly, and that some events may be obscured from the camera by the outer bubbles on the electrode; that is, one cannot see clearly what is happening very close to the electrode surface. Magnification and a high speed camera can overcome the first two difficulties, but one must use a transparent electrode to view the phenomena close to the surface. Not only does a transparent electrode allow close observation of gas evolution, but the microscope objective can approach the electrode without shielding it from current or affecting the dynamics at the surface. Furthermore, light can be

transmitted directly into the camera; one is not forced to reflect it from the metal surface.

We used a 0.2 micron thick antimony-doped film of  $\text{SnO}_2$  chemically vapor deposited on a 2 mm thick glass substrate as a transparent electrode. The samples were made by Dr. Werner Kern at RCA Laboratories who donated them for this research. The film conductivity was 100 ohms per square. The electrode was incorporated into a cell which allowed electrical contact to some part of the surface while sealing off the contacts from electrolyte. Figure 1 is a picture of the cell which shows how the 2 cm square piece of the  $\text{SnO}_2$  electrode fits into a shallow opening in the lucite body. Illustrated in Fig. 2 is a cross section through the window electrode which shows the two basins and the channel opening in this shallow area where the electrode sits. The basins are filled with silver epoxy to make contact to the electrode. The strips of lucite between the silver epoxy basins and the channel opening were coated with insulating epoxy when the cell was assembled in order to seal the electrolyte from the silver contacts. The clear area in the center is where the electrode faces the electrolyte. The wires leading out are copper electrical contacts. The channel of electrolyte facing the  $\text{SnO}_2$  was 0.3 cm wide, 0.5 cm deep, and 1.9 cm long. Since there was significant resistance in the  $\text{SnO}_2$  film, we made the distance between the two contacts (of same polarity) on either side of the electrolyte channel as small as practical for lowest resistance, easy departure of the bubbles, and avoidance of wall effects. There were holes leading out through the top

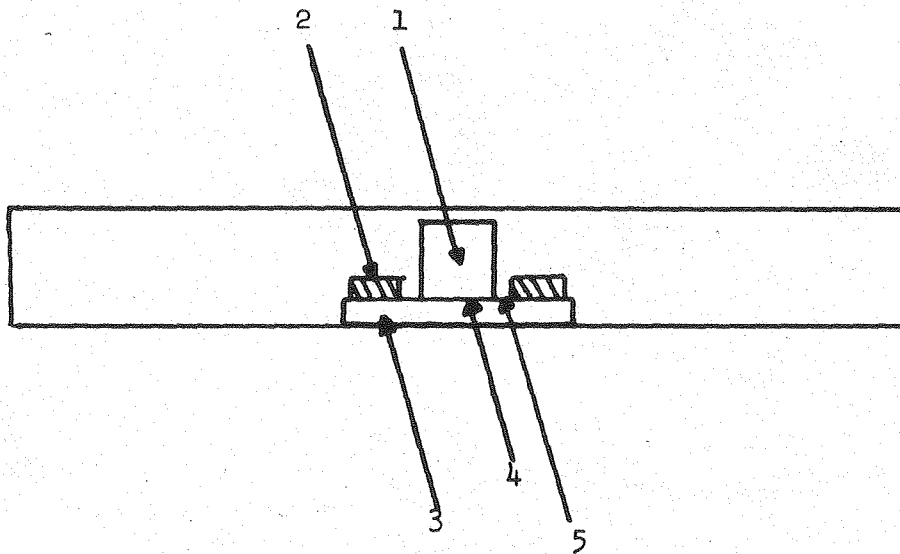
Key to Fig. 1. The transparent electrode cell.

1. Copper current collector.
2. Pt wire counter electrode.
3. Silver epoxy making contact to  $\text{SnO}_2$  surface.
4. Transparent  $\text{SnO}_2$  electrode facing electrolyte.



XBB 804-4910A

Fig. 1.



XBL 8011-7591

Fig. 2. Cross section of the transparent electrode cell.

1. Electrolyte facing the tin oxide electrode.
2. Silver epoxy contact to electrode film.
3. Glass substrate for tin oxide electrode.
4. Tin oxide electrode film (2000A) on glass substrate.
5. Seal between silver epoxy and electrolyte.

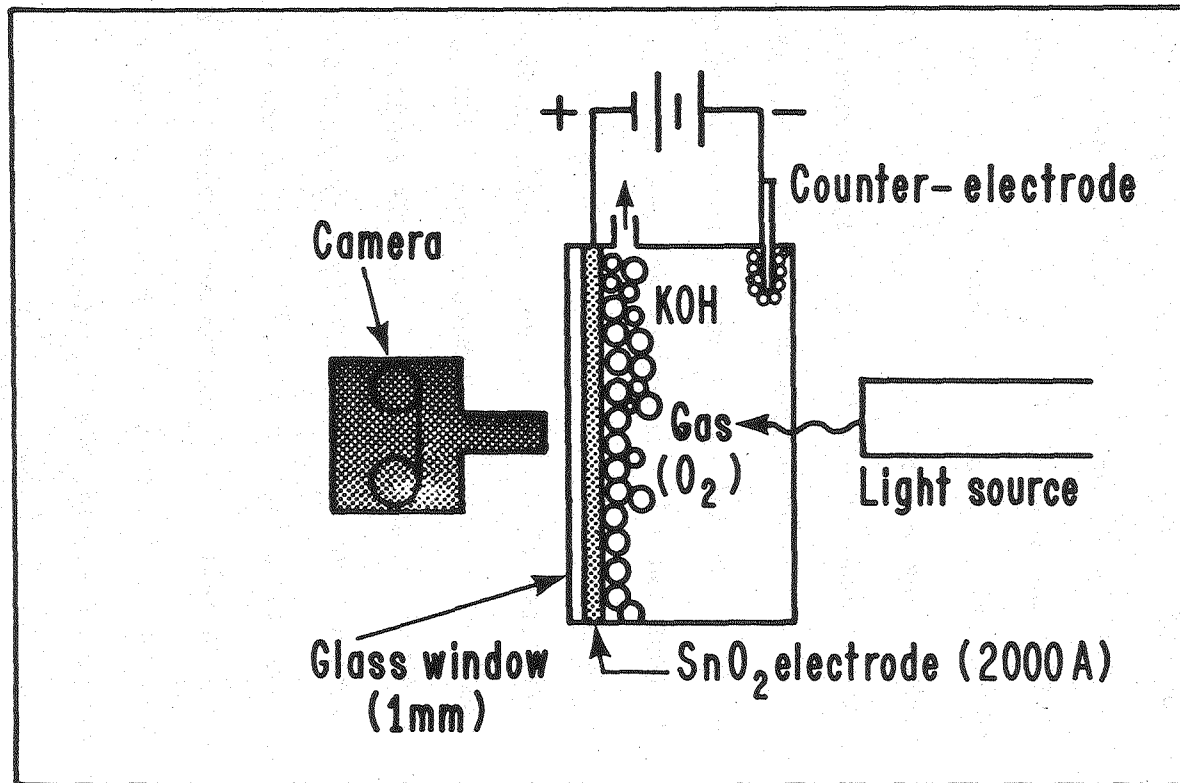
and bottom of the cell for adding electrolyte and directing gas out of the cell. The counterelectrode was a Pt wire placed above the vertically positioned electrode so that gas evolving on it would not interfere with observation of the working electrode gas.

The arrangement of the apparatus is shown in Figs. 3 and 4. Intense light from an Ealing Corporation Model 22-0004 fiber optic light source passed through a clear lucite plate which faced the window electrode across the channel of electrolyte. Passing through the electrolyte and cell, the light became an image which was magnified by a Bausch and Lomb microscope and passed to a Redlakes HYCAM high speed camera. The microscope had a 10x objective and 15x eyepiece. The 16 mm movie frame bounded an area 0.6 mm on a side as determined by photographing a calibrated microscope slide. Capable of framing rates from 10 to  $10^4$  frames per second, the camera accepted 100 to 400 ft rolls of KODAK TXR 430 high speed camera film. The exposure was determined by trial and error. Illuminated by a 250 watt slide projector lamp, the fiber optic tip was placed 3 cm from the cell back and the power turned on full. This transmitted enough light to produce clear images at film rates of around  $10^4$  frames per second after traveling through 1 cm of lucite, electrolyte, and glass.

#### Procedure

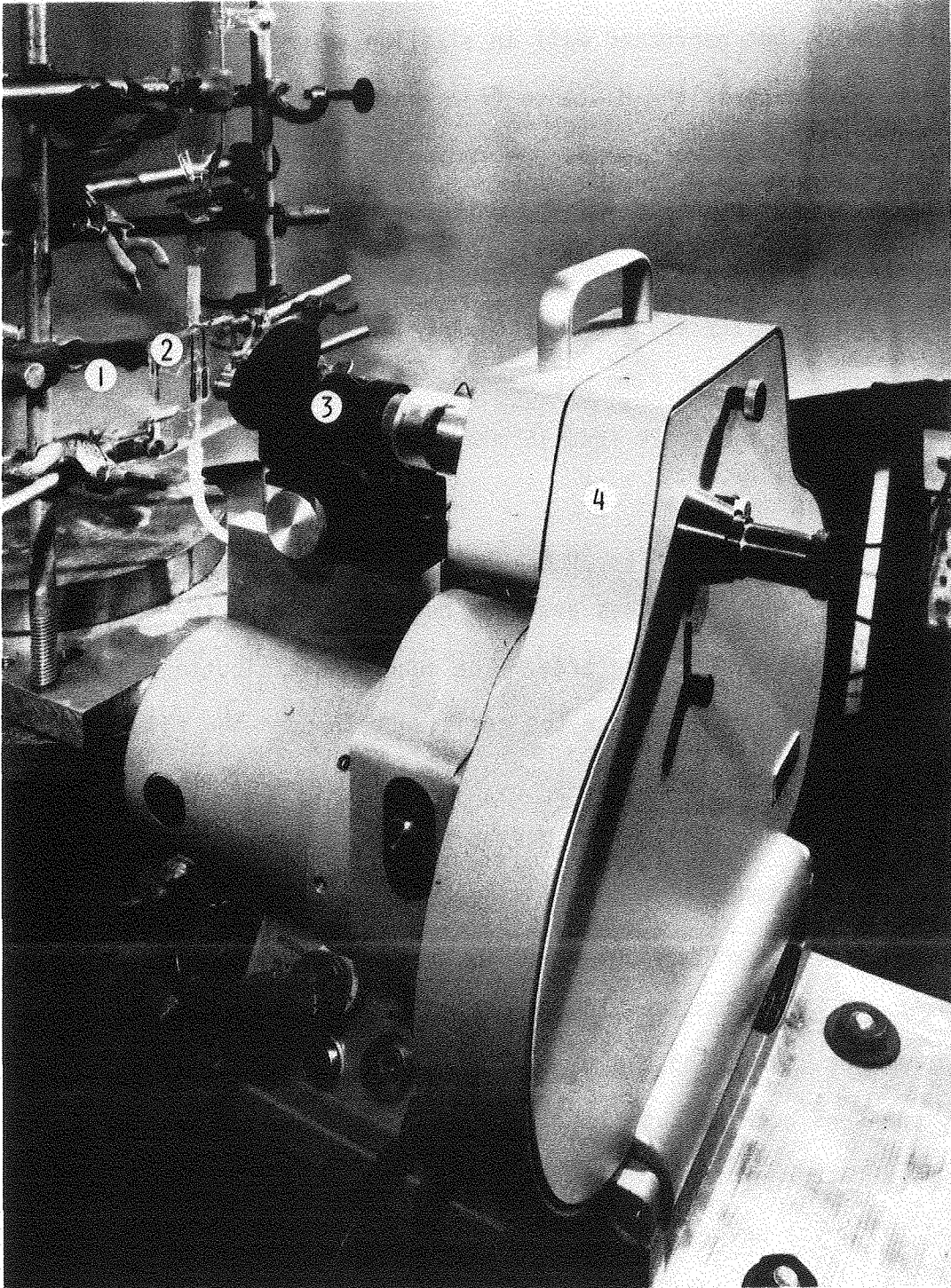
The cell was filled from a reservoir above it and drained to a flask below. The electrolyte in most experiments was KOH, but sodium sulfate was used instead in a few runs. We polarized the electrode positively to produce oxygen. The oxide electrode did not last long

# Schematic of observation apparatus



XBL 796-1708

Fig. 3. The observation apparatus.



XBB 804-4914A

Fig. 4. Key to Fig. 4.  
1. Fiber optic light guide. 2. Transparent electrode cell. 3. Microscope. 4. Red Lakes HYCAM high speed camera.

in acid or NaCl, but performed well in alkaline solution. When the microscope was focused, the distance from the camera to the eyepiece was set every time to the same length for optimum exposure of the film. An Amel Model 551 potentiostat operated in galvanostatic mode provided the power for the reaction. Upon turning on the power to the cell, the camera was manually actuated. The experiments required only a few seconds to run; 400 ft of film was exposed in around 5 sec. At standard projection rate, 24 fps, 16 min are required to view the events of 5 sec.

A catalog of films appears in Appendix C. The current density listed for each film is a gross average found by dividing the total current by the total electrode area. The current distribution on the electrode was nonuniform because the resistance through the film from the edges to the center was high.

The intense fiber optic light passes through the bubbles' spherical caps but is deflected by the curved sides. The bubbles' image is a two dimensional dark annulus as shown in Fig. 5. An additional light pointed at the cell from the side gave the bubble a highlight and the third dimension. Watching the movies taken at the standard speed, 24 fps, one sees nothing but much blurred motion. After slowing the action by a factor of ten, one already sees many of the phenomena referred to in the review of observation of gas evolution. Like other investigators, we observed nucleation, growth by diffusion, coalescence and detachment. Occurring on a scale of  $10^{-7}$  cm, nucleation could not be resolved by our optics, but the preference for nucleation at

surface imperfections such as scratches was noted. We inferred growth by diffusion when the bubble became enlarged with no apparent coalescences. The most interesting behavior was the frequent coalescence between bubbles of various sizes. It is difficult to convey the impact of the films in words and still pictures; in fact, we made the motion pictures because the process is best viewed continuously; therefore, a 30 min motion picture which summarizes the transparent electrode studies has been made and may be obtained for private viewing by contacting

Charles W. Tobias  
Department of Chemical Engineering  
University of California  
Berkeley, CA 94720

or

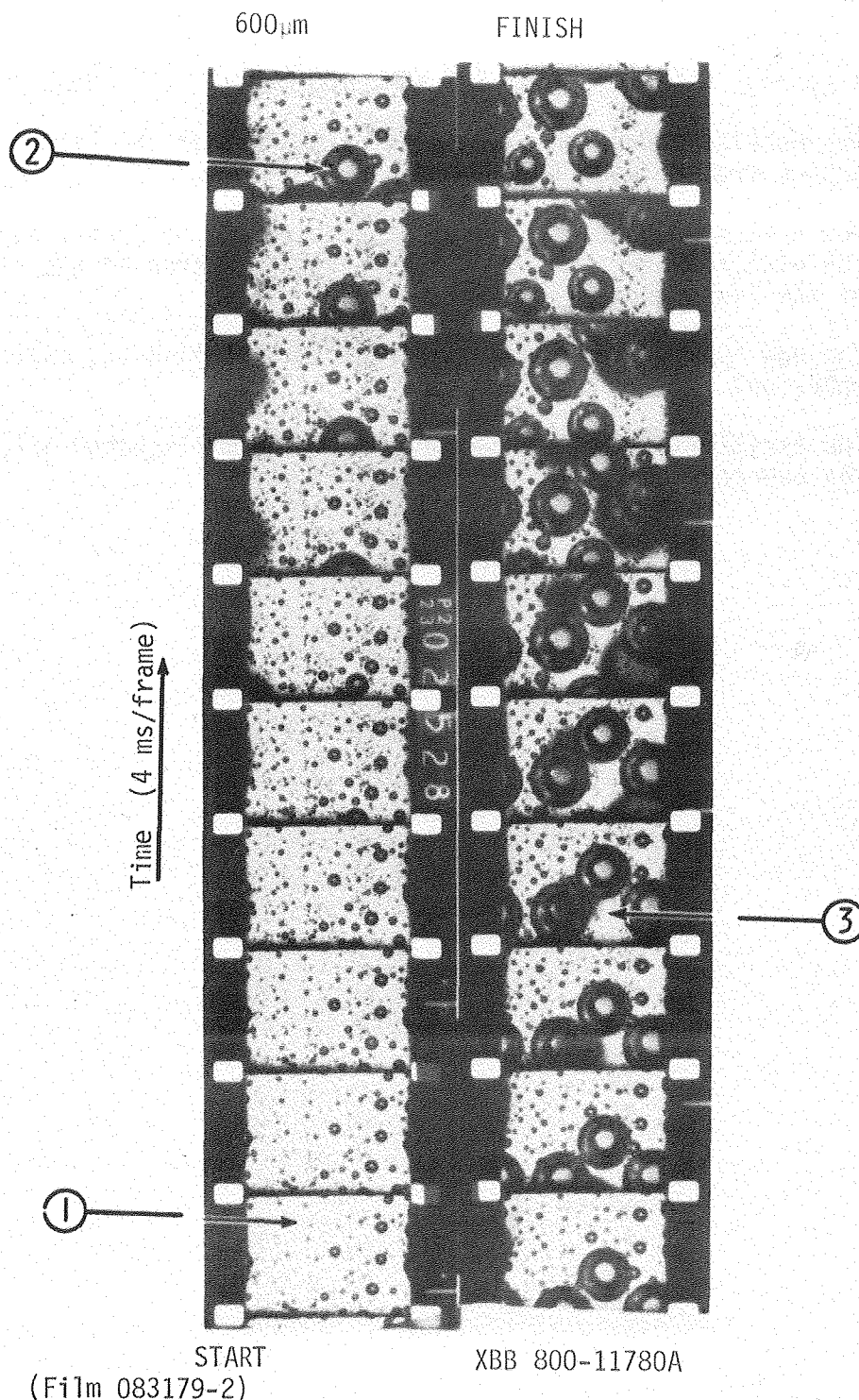
Paul J. Sides  
Department of Chemical Engineering  
Carnegie-Mellon University  
Schenley Park, Pittsburgh, PA 15213

In the following, five movie sequences which show a cyclical mechanism of bubble growth, the hydrodynamics close to the electrode, the departure and return of a bubble, the effect of different electrolytes, and bubbles being drawn toward other bubbles and coalescing with them are discussed.

There is a cyclical mechanism of bubble growth that was present in all of the films. Bubbles nucleated, grew to a small size (<10 microns) rapidly by diffusion, coalesced with other small and medium size bubbles to form medium size bubbles (<100 microns), and then were scavenged from the electrode surface by large bubbles

(200 microns) traveling upward along the surface under the influence of buoyancy. A film clip showing this appears in Fig. 5. A group of large bubbles has just passed through and a new group of bubbles has nucleated and grown to a size of 10 to 15 microns in diameter. A new group of large bubbles (200 microns) moves through and scavenges the smaller bubbles in their path. The large bubbles are attached to the surface and move along it or are very close to it. In some cases, as discussed later, one can see a darkened area in the light center which is the flattened area of attachment.

These films show that coalescence causes fluid motions close to the electrode surface which may be important in the mass transport enhancement due to gas evolution reported by Ibl (44), Venczel (42), and Janssen and Hoogland (40). This mode joins the flow due to gas lift and fluid replacement due to bubble departure as a contributor to mass transfer enhancement. A coalescence sequence between two large bubbles near the electrode and moving along it appears in Fig. 6. The two bubbles appear to be touching for many frames as the film between them thins and finally ruptures. The bubbles coalesce so quickly that the film rupture and the change from two bubbles to one occurs between two frames, that is, in much less than 100 microseconds. The new bubble is compressed along the axis of coalescence by the fluid rushing into the space behind the coalescing bubbles. The bubble vibrates like this for several frames before becoming spherical again. This is an example of coalescence of two relatively large bubbles, both traveling along the electrode surface.



Time proceeds from the lower left frame up and from the lower right up. 1. Dispersion of small bubbles which grew on the electrode surface after a group of large bubbles swept through. 2. Several large bubbles travel along the surface and scavenge the small and medium size bubbles before them. 3. One can see the empty area behind a large bubble in its path.

Fig. 5. Gas evolution slowed by a factor of 10.

Notes to Fig. 6 (early film, 10% KOH, 100 ma/cm<sup>2</sup>, 10<sup>4</sup> frames/s)

1. Two bubbles touch for a number of frames while the film drains from between them.
2. New coalesced bubbles: Note compression of the bubble against the electrode as shown by the enlarged dark area in the middle of the light center.
3. The new bubble vibrates as it tries to establish its equilibrium spherical form.
4. The oscillations have ended one half of a millisecond after the bubbles coalesced.

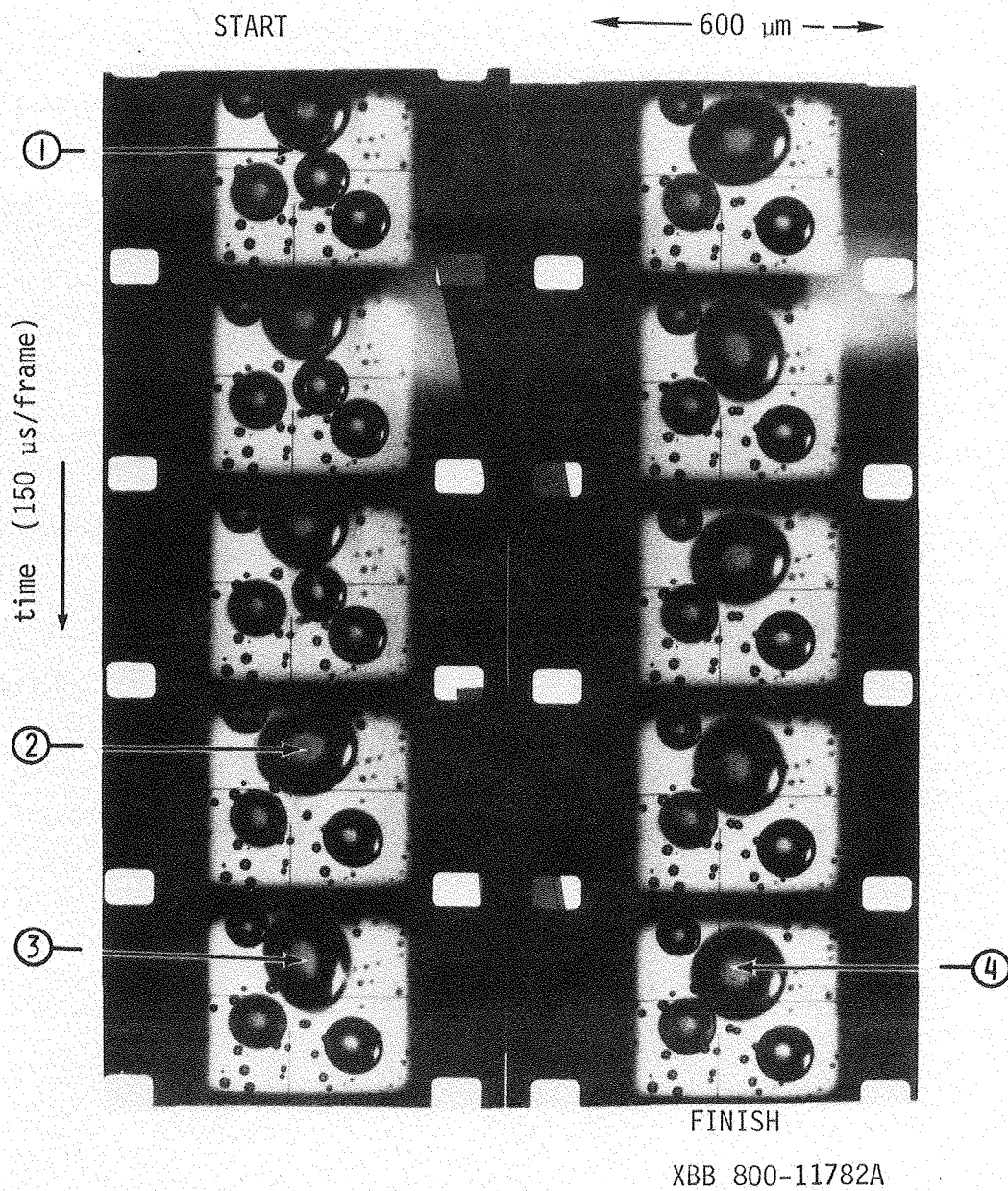


Fig. 6. Coalescence of two bubbles and subsequent vibration of the new bubble (100 microsec per frame).



We observed coalescence between large bubbles moving along the electrode, between small bubbles still on the electrode, and between large bubbles moving along the electrode with small bubbles still on it. The last, a scavenging coalescence, was mentioned before in connection with the cyclical nature of bubble growth.

Mentioned by other investigators, especially by Glas and Westwater (39), the return of a bubble to the electrode after departing appears in Fig. 7. One can see the contact area under the bubbles as a dark spot in the light central area. When the bubbles coalesce, the contact spot disappears in the next frame and subsequently reappears. Coehn and Newman (48) would argue that the return to the electrode was caused by the attraction of the charged bubble to the electrode surface. Glas and Westwater speculated that a surface tension gradient caused the bubbles' return. A third possibility is that the bubble is still oscillating after the coalescence and reattaches when one part of it touches the electrode. Furthermore, local fluid motions could also push the bubble back to the surface.

Characterizing the detachment of a bubble from a vertical electrode is difficult because the buoyancy force does not act perpendicularly to the electrode. The only force pushing the bubble away from the surface is that exerted by the bubbles' internal pressure against the flattened bubble base. The sequence shown in Fig. 7 indicates that coalescence of two bubbles to form a new bubble which, being compressed against the electrode, pushes away from it, may be an important mechanism by which bubbles depart from vertical electrodes.

## Notes to Fig. 7.

1. A bubble on the electrode touches another off the frame to the left. Note the circular dark area within the light center of the bubble. This is the bubble's contact with the electrode.
2. The bubbles coalesce.
3. The new bubble vibrates violently as it establishes its spherical boundary.
4. The new bubble is off the surface. One can see small bubbles on the surface between the large bubble and the surface.
5. The dark area in the light center shows that the bubble has re-established contact with the electrode.

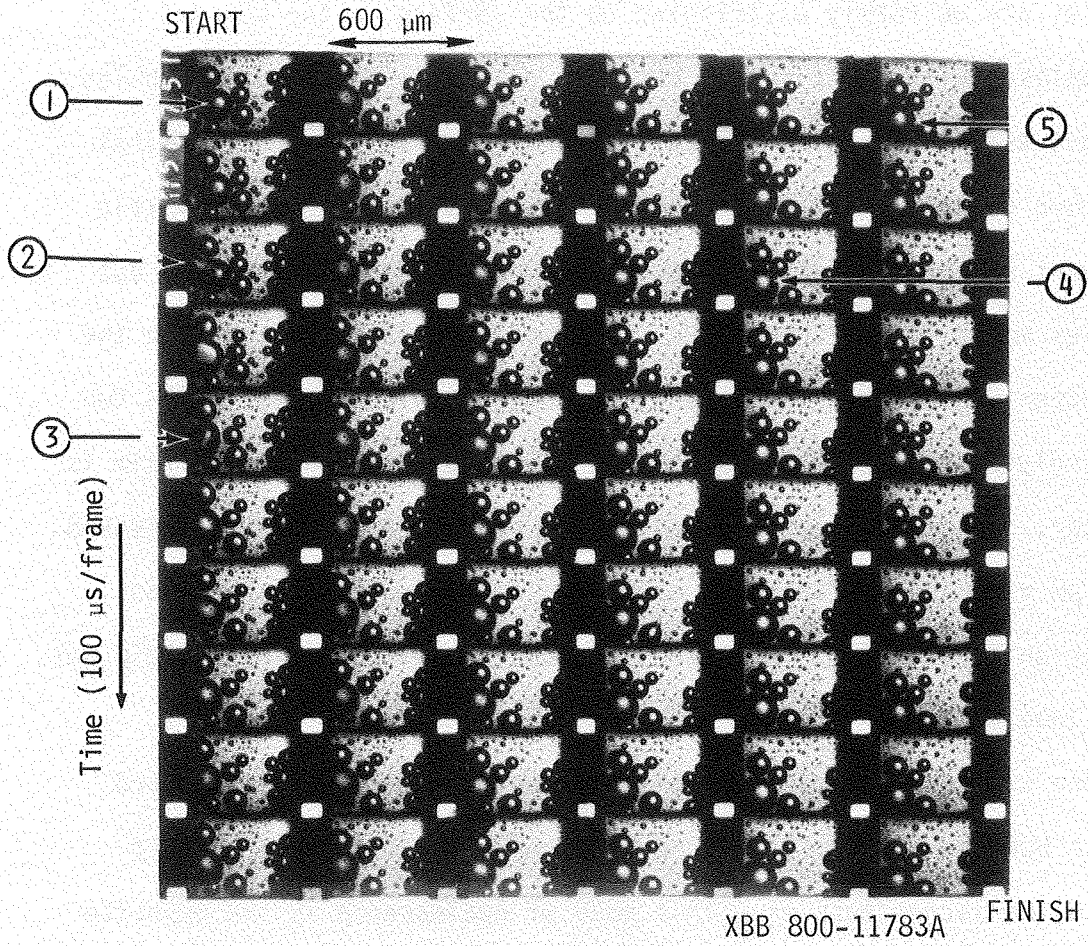


Fig. 7. Sequence showing the departure and return of a bubble.

An effect of using different electrolyte is shown in Fig. 8 in which oxygen is evolved in aqueous KOH and  $\text{Na}_2\text{SO}_4$  solutions. Nucleated bubbles are uniformly distributed on the surface in the KOH and move to coalesce with fewer large, but also uniformly distributed bubbles. By contrast, the bubbles nucleate in  $\text{Na}_2\text{SO}_4$  at a few specific sites and then coalesce with large bubbles at the site. There was little movement of bubbles away from a nucleation site in the sulfate, but bubbles moved freely in the KOH. Whether the differences between the two experiments are related to differing gas solubilities in the two electrolytes or to the effect of the electrolyte on the oxide film is unclear. Water was electrolyzed in the neutral solution; the electrolyte pH near the surface must have been lowered with the resultant effect on the surface. We noted previously that the electrode did not last long in acid.

One can see more clearly this movement of small bubbles toward larger bubbles in Fig. 9. The bubbles move as if drawn or sucked toward the larger bubbles. This mode of coalescence is the opposite of the scavenging of small bubbles by large ones. The movement may be a result of fluid motions since the coalescence of one bubble with another draws electrolyte toward the new bubble. Continual coalescence could establish a flow pattern which would suck other small bubbles toward the central large bubble.

Large bubbles touched for many frames before coalescing but small ones coalesced almost immediately with each other or with large bubbles. Perhaps the small newly formed bubbles do not have film

Notes to Fig. 8 (film 061880-2 and 061880-5).

1. There is a uniform distribution of nucleation sites on the electrode.
2. The small bubbles move toward these medium size bubbles and are consumed by them.
3. Large bubbles moving along the surface scavenge the small and medium size bubbles.
4. Bubbles are grouped at a nucleation site and coalesce with each other.

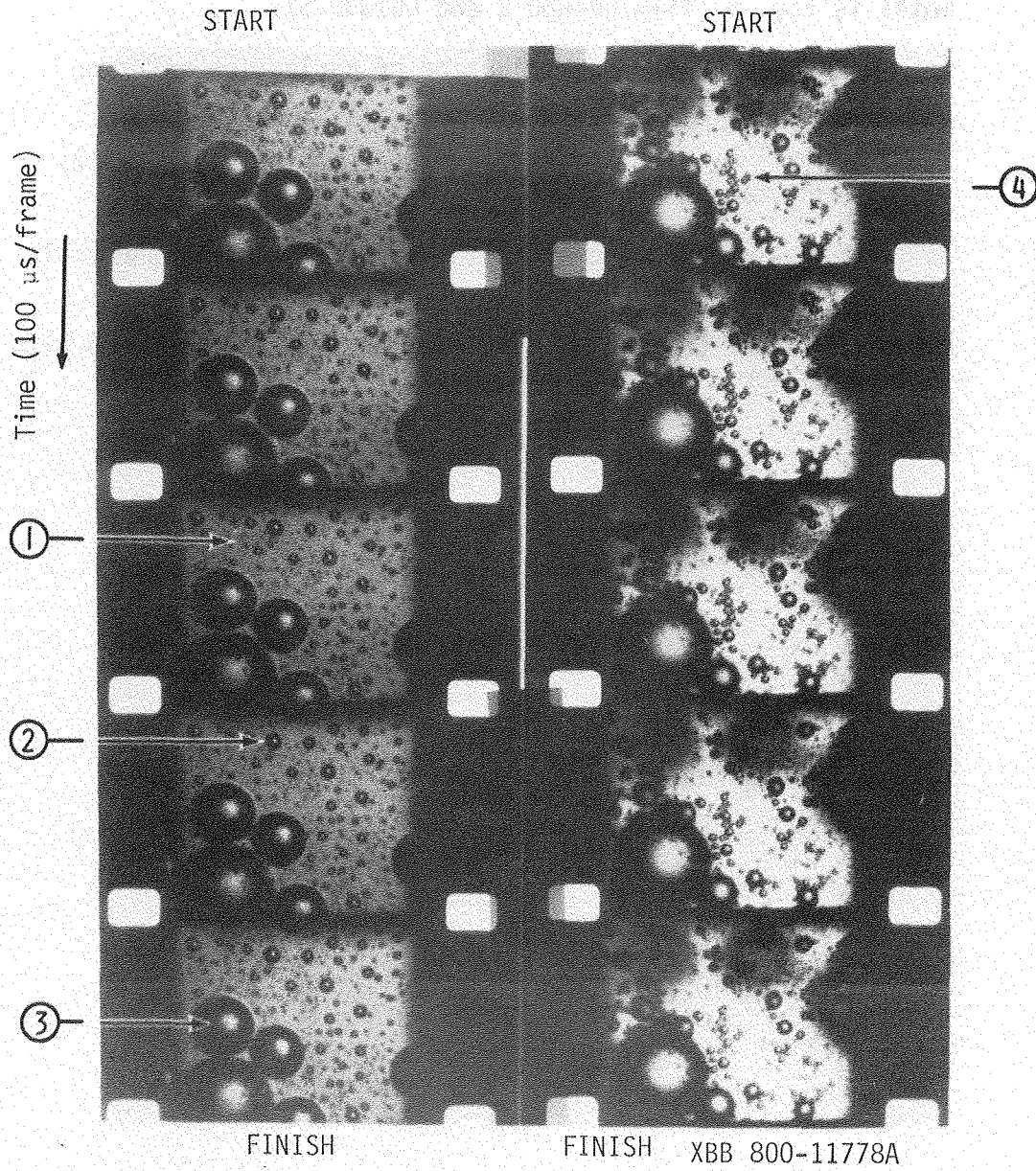
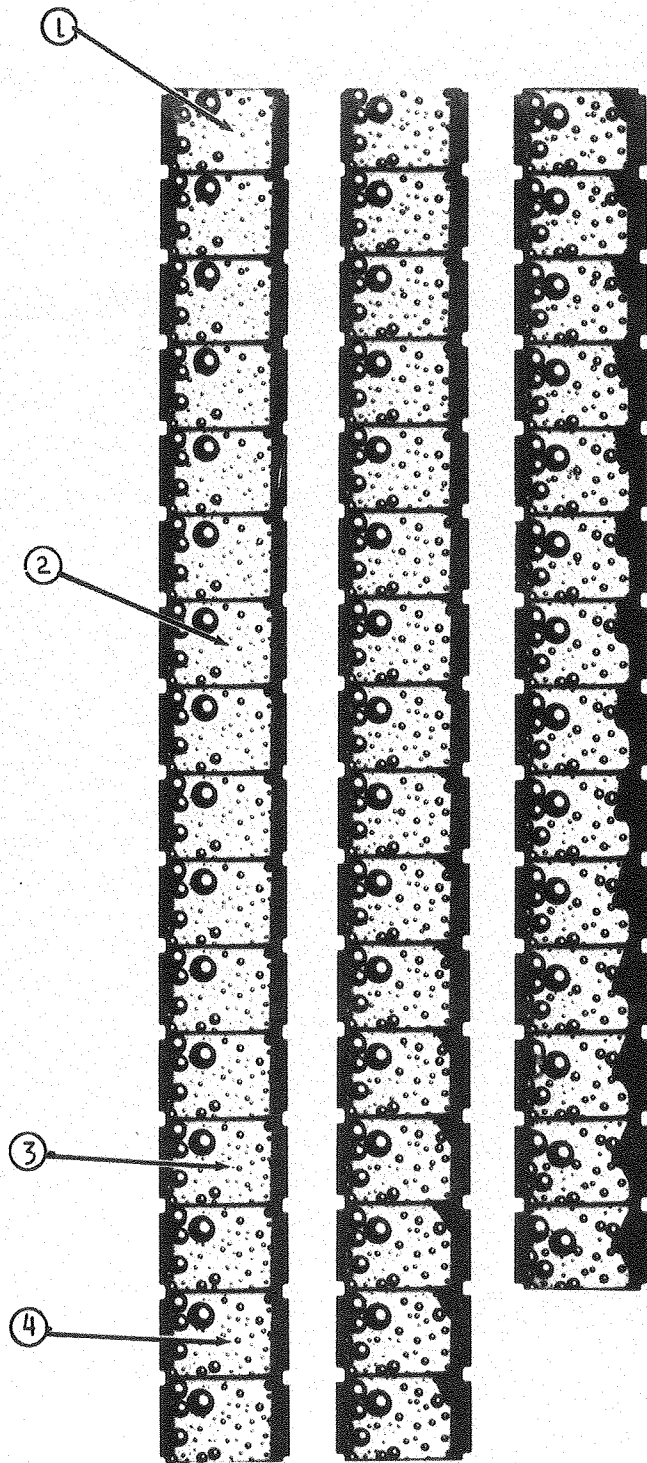


Fig. 8. Comparison of gas evolution in two different electrolytes: on the left, KOH; on the right,  $\text{Na}_2\text{SO}_4$ .

**Key to Fig. 9.**

1. A very small bubble at the tip of the arrow will coalesce with the large.
2. The same bubble, but larger.
3. The same bubble, but larger and closer.
4. The small bubble has coalesced with the larger.



XBB 800-14619

Fig. 9. A movie sequence showing the radial movement of small bubbles to coalesce with larger bubbles.

stabilizing compounds adsorbed at their surfaces as the large ones, which have been in the electrolyte for a while do.

At high camera speeds, the bubbles do not noticeably grow without coalescing. Using the theoretical results of Scriven (34) and the experimental confirmation of Westerheide and Westwater (38), we show that growth by diffusion is slow in the time frame of the movie for all but very small bubbles. Scriven's formula for bubble growth is

$$d = 4\beta\sqrt{Dt} \quad (1)$$

where  $d$  is the bubble diameter,  $\beta$  is a growth constant depending on the gas supersaturation level,  $D$  is the gas diffusivity through the electrolyte, and  $t$  is time in seconds. Differentiating (Eq. (1)) with respect to time, dividing this result by Eq. (1) and by a factor of 400 to account for the slowing of events obtained by projecting the movies at 24 frames per second after filming them at 10,000 frames per second, we obtain

$$d^* = 1/800 t \quad (2)$$

where  $d^*$  is the rate of growth of a bubble at any time relative to its diameter. To find the dependence of  $d^*$  on the bubble radius, we resubstitute Eq. (1) for  $t$ .

$$d^* = \frac{D\beta^2}{50} \left( \frac{1}{d^2} \right) \quad (3)$$

The growth coefficient for Run 1 of Westerheide et al. was 0.56. A graph of Eq. (3) appears in Fig. 10. One can see that, under the conditions of the experiment, which was hydrogen evolution at around

100 ma/cm<sup>2</sup>, the relative growth rate in the slow time frame of the movie falls rapidly to a few percent per second; this makes the bubbles appear not to grow by diffusion in the movies.

The bubble size depended on the number of coalescences. This means that one can control the bubble size by controlling coalescence. One must remove the bubbles before they coalesce or somehow stabilize the liquid film between the two touching bubbles, perhaps by surfactant, so it cannot rupture. We also observed the "rapid fire mechanism" of Glas and Westwater (39) at some nucleation sites. The bubbles nucleate quickly one after the other and do not stay on the electrode but are ejected either into the electrolyte or into other bubbles. This mechanism may occur generally on the electrode, but the resulting bubbles coalesce with the large bubbles sitting on the surface or moving along it so that the small ejected bubbles never reach the bulk electrolyte.

The bubble layer on this electrode consists of three sizes of bubbles. There are many small bubbles on the order of ten microns on the surface. These are coalescing with medium size bubbles (<100 microns). Both the small and medium size bubbles are scavenged on the surface by large bubbles (250 microns) moving along it.

### 3. Conclusions

The tin oxide transparent electrode allowed observation of oxygen evolution in KOH and Na<sub>2</sub>SO<sub>4</sub> from the backside, a unique vantage from which to view the rapid and microscopic phenomena of gas evolution. The phenomena observed in this study are the same as reported

in the review of literature with three exceptions. First, coalescence seemed more important to the overall process of gas evolution than was indicated in many of the earlier studies. Second, the cycle of growth by diffusion and coalescence followed by scavenging coalescence has not been reported before. Third, small bubbles moved radially in toward a medium size central bubble and coalesced with it before it in turn was scavenged by large bubbles moving along the surface.

There are several problems associated with using the transparent electrode. To study gas evolution quantitatively, one must know the current density to know the maximum gas volume production rate, but the current distribution on the tin oxide transparent electrode is nonuniform because of the large surface resistance to current flow in the oxide film. In a cell like the one used in these experiments, one would have to solve Laplace's equation in the electrolyte and on the semiconductor strip bounding it with a nonlinear boundary condition on the potential at their interface in order to determine the current distribution and hence the current density at any point on the electrode. Other problems include the fact that the electrode cannot be polarized negatively and hence one cannot study hydrogen evolution with the tin oxide electrode. Neither was the electrode stable during chlorine evolution.

Some subjects for further qualitative investigation of gas evolution based on the use of the tin oxide electrode include the study of coalescence and hence bubble size. If one could stabilize the film between two touching bubbles, perhaps with surfactants, the bubbles

probably would not coalesce. The electrode could also be used to investigate the mechanisms of detachment of bubbles from vertical surfaces. One could further study coalescence by going to higher framing rates in the hope of observing the process of film rupture more closely. The very transparency of the electrode makes observation of nucleation sites difficult, but some effects such as that noted when two different electrolytes were used could be studied further.

## NOMENCLATURE

a	radius, cm
$a_1$	radius of inner sphere, cm
$a_2$	radius of outer sphere, cm
A	(Chapter 1) coefficient in expansion of potential in spherical harmonics, volts/cm
A	(Chapter 2) Fourier constant, dimensionless
$A_0$	0.9015, dimensionless
b	radius of bubble base, cm
B	coefficient in expansion of potential in spherical harmonics
C	constant of integration, dimensionless
$C_0$	constant in Rayleigh's equation for potential in spherical harmonics, volts
$C_1$	constant coefficient of solution to ordinary differential equation, dimensionless
$C_2$	constant coefficient of solution to ordinary differential equation, dimensionless
$D_0$	constant in Rayleigh's expansion of potential in spherical harmonics, volts
$E_0$	intensity of average electric field in an array of spheres, volts/cm
E	volume averaged electric field, volts/cm
f	void fraction of gas in electrolyte, dimensionless
i	current density, a/cm <sup>2</sup>
k	conductivity (ohm-cm) <sup>-1</sup>

$K_m$	conductivity of electrolyte with gas present compared to that with gas absent (dimensionless)
$l$	electrode separation, cm
$n$	number density of bubbles, $(\text{cm})^{-2}$
$N$	number of bubbles, dimensionless
$q$	separation parameter, dimensionless
$r$	radius, cm
$R$	resistance, ohms
$\Delta R$	net resistance increase caused by the layer of bubbles, ohms
$S$	area of electrode, $\text{cm}^2$
$S_1$	the first angular harmonic, $\cos \theta$ , dimensionless
$S_c$	area between hexagonal walls and sphere surface, $\text{cm}^2$
$x, y, z$	distance, cm
$V$	potential, volts
$\phi$	potential, volts
$\phi_0$	slope of linear potential far from the bubble, volts/cm
$\Delta\phi$	net potential disturbance far from the electrode integrated with area, $\text{volt-cm}^2$
$\nu$	tangent sphere coordinate, $\text{cm}^{-1}$
$\mu$	tangent sphere coordinate, $\text{cm}^{-1}$
$\kappa$	conductivity $(\text{ohm-cm})^{-1}$
$\theta$	angle, radians
$\psi$	angular tangent sphere coordinate, radians
$\rho$	resistivity, $\text{ohm-cm}$
$\alpha$	length of a side of Rayleigh's array, cm

- $\epsilon, n, \zeta$  constants of coordinate translation, cm  
 $\beta$  quantity in Slawinski's equation, dimensionless

#### Subscripts and Superscripts

- c continuous medium  
d (Chapter 1) dispersed medium  
d (Chapter 2) disturbance  
\* dimensionless quantity  
T total

## APPENDIX A. SOURCES FOR THE DATA

In Chapter I, I compared various equations for the conductivity of heterogeneous media to experimental data. The following articles are sources of the data on ordered arrangements and random dispersions of dielectric spheres.

Meredith (12)

Published graphs in 1960 (13) and tabulations of data in his Ph. D. Thesis (12) on the conductivities of cubically ordered arrays and non-ordered dispersions are the results of Meredith's experiments with large precisely machined hemispheres and with dispersions of small glass spheres. Careful attention to experimental technique with alternating current and a Wheatstone bridge indicates the high quality of these results. Using tap water as his electrolyte, he explored the variation of his experimental results with frequency and showed that high frequencies were necessary to obtain accurate results.

DeLaRue (10,18)

DeLaRue experimented with uniform and multisized dispersions of glass spheres which he suspended by gyrating his cell during the measurements until he obtained a steady state value for the conductance. He used alternating current techniques and a near saturated solution of aqueous zinc bromide as the continuous phase to match the density of the glass spheres. Conductance across an identical size cell compartment not containing spheres provided directly conductance ratios which did not have to be corrected for temperature.

Mashovets (14)

Mashovets investigated ordered arrays of spheres in face centered cubic, hexagonal, and simple cubic arrays. He used a solution of copper sulfate, sulfuric acid, and alcohol and an otherwise undefined "usual potentiometric method" with a current of 50 ma through his cell.

Slawinski (11)

Slawinski measured the conductance of a tube 10.5 cm in diameter and 21.5 cm long which contained 0.56 and 0.64 cm enameled spheres. The electrolyte was KCl, he used alternating current techniques, and the spheres were arranged in various manners. He also measured the conductivity of dispersions of castor oil in a mixture of gum arabic and 0.05 N KCl. I grouped the former data with the random, monosized spheres category and the latter data with the random multisized spheres.

Clark (25)

Clark experimented with foams and thus obtained data at very high void fractions. He used alternating current at 1 kHz in the experiments. I plotted Clark's data with the randomly ordered multisized spheres because his foam was undefined.

Neale and Nader (8)

Neale and Nader, using a tubular plastic cell, copper electrodes, copper sulfate, and alternating current, investigated conduction through packed glass spheres at void fractions of 60 to 70 percent. The spheres were 25 times smaller than the tube diameter to eliminate wall effects. The spheres of their experiments were probably of

unequal sizes so their data are also grouped into the random multisized class.

Other works describing experimental investigations (Turner (19), Sigrist (17), Fricke (20) did not provide numerical data so their results could not be included. Wyllie and Gregory (21) illuminated some experimental problems other than those associated with polarization of the electrodes. In order to explore the effect of dispersed particle and cell size, they plotted the conductivity ratio against the ratio of the cell diameter to particle diameter; they found that the conductivity ratio decreased with the tube diameter to particle diameter ratio until the latter reached 35; thereafter the conductivity ratio was constant; hence, they conclude that this was a criterion for experimental accuracy.

## APPENDIX B. ESTIMATES OF ERROR IN THE HEXAGONAL CELL MEASUREMENTS

Two equations were used to calculate the conductivity function.

The first is

$$R_C = l/ks \quad (1)$$

where  $R_C$  is the cell resistance with no gas present. The second is

$$K_m = \frac{x}{(R_m/R_C) - 1 + x} \quad (2)$$

where  $R_m$  is the resistance measured with the spheres present.  $R_C$  from Eq. (1) is substituted into Eq. (2) to determine  $K_m$ . In the following, each of the variables,  $l$ ,  $k$ ,  $S$ ,  $R_m$ ,  $x$ , and  $R_C$  is discussed for error and the ultimate percentage error is calculated.

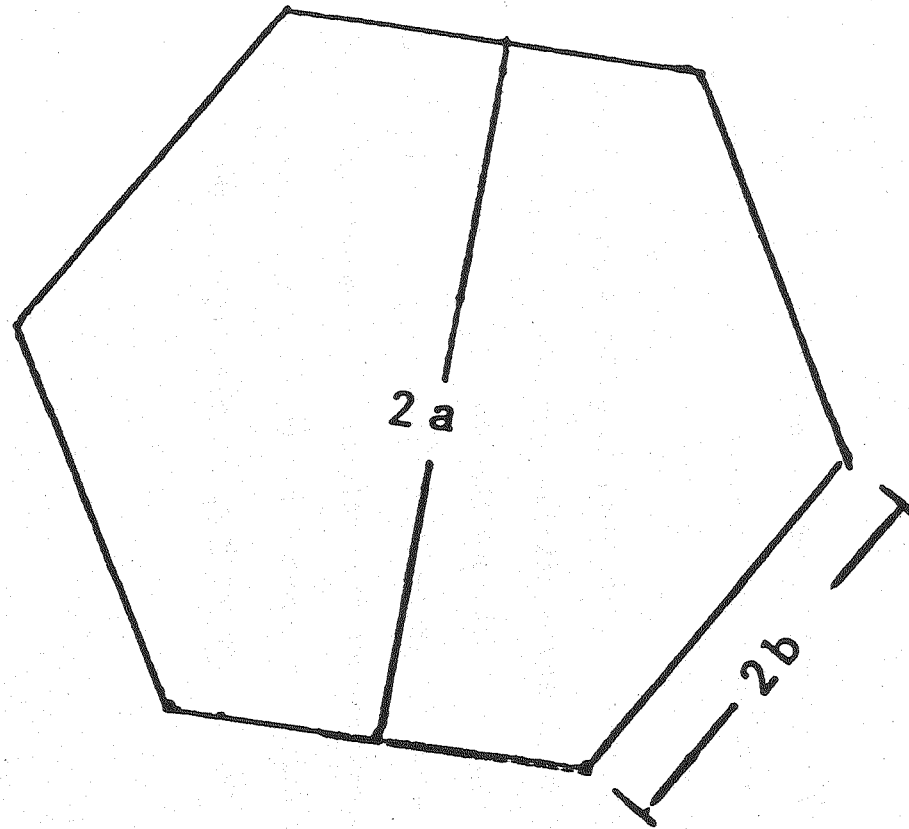
I measured the interelectrode gap,  $l$ , externally with a micrometer; the possible error in this measurement was 0.0051 cm. The error in  $x$ , the fraction of interelectrode gap occupied by the bubble layer, depends on the error in  $l$  and  $d$ , the sphere diameter. The deviation from perfect sphericity averaged 0.0076 cm; the resulting error in  $x$  as a function of  $d$  and  $l$  is given in Table 1.

Calculated from Eq. (1) of Chapter III, the conductivity could be in error by  $2.45(10^{-5}) \text{ (ohm-cm)}^{-1}$  as determined by differentiating the above equation with respect to  $T$ , and inserting  $25^\circ$  and a possible temperature measurement error of  $0.1^\circ\text{C}$ .

Table 1. The results of the error analysis of the hexagonal experiments.

d cm	l cm	R <sub>m</sub> ohms	ΔR <sub>m</sub> ohms	R <sub>c</sub> ohms	ΔR <sub>c</sub> ohms	x	$\Delta x(10^4)$	ΔK <sub>m</sub>	Δ Error
10.160	24.792	53.683	0.0166	21.546	0.038	0.4098	2.90	0.0007	0.327
10.160	22.200	51.436	0.0122	19.296	0.034	0.4577	3.35	0.0007	0.309
10.160	19.576	49.157	0.0087	17.017	0.031	0.5190	3.96	0.0007	0.321
9.652*	26.342	40.381	0.3307	22.891	0.040	0.3664	2.65	0.0052	1.60
9.652	24.792	39.208	0.0642	21.546	0.038	0.3893	2.86	0.0018	0.562
9.652	22.200	36.924	0.0337	19.296	0.034	0.4348	3.30	0.0014	0.438
9.144	24.792	33.042	0.0621	21.546	0.038	0.3681	2.82	0.0027	0.665
9.144	22.200	30.794	0.0663	19.296	0.034	0.4111	3.24	0.0027	0.665
9.144	19.576	28.581	0.0406	17.017	0.031	0.4662	3.82	0.0021	0.524
8.636*	23.929	29.616	0.4600	20.796	0.037	0.3609	2.90	0.0146	3.18
8.636	21.389	27.060	0.0731	18.592	0.033	0.4057	3.35	0.0377	0.800
8.636	18.489	24.858	0.0657	16.386	0.030	0.4582	3.95	0.0348	0.742
7.112	22.659	23.192	0.0556	19.694	0.035	0.3141	26.9	0.0066	1.03
7.112	21.389	22.079	0.0535	18.592	0.033	0.3327	3.17	0.0064	0.994
7.112	18.849	19.878	0.0492	16.386	0.030	0.3776	3.73	0.0059	0.920
5.842	21.389	20.286	0.0249	18.592	0.033	0.2731	3.04	0.0070	0.927
5.842	18.849	18.079	0.0200	16.386	0.030	0.3099	3.54	0.0061	0.812
5.842*	16.309	15.743	0.185	14.180	0.027	0.3582	4.25	0.025	3.26

Asterisk (\*) denotes a set of three experiments at a distance l for which the standard deviation showed an inconsistency.



XBL 8011-12720

Figure 1. Calculation of the area of a hexagon

The error in the calculated cross sectional area depends on the geometry of a hexagon, as shown in Fig. 1. The area is

$$S = 3 ab \quad (3)$$

I measured a and b again with a micrometer and allowed an error of 0.0051 cm in each. After differentiation Eq. (3), I calculated an error in the area of 0.122 cm<sup>2</sup>.

I measured the resistance  $R_m$  three times with different solutions at each of three different interelectrode gaps large enough not to affect the result. The final data are thus the result of nine measurements in all cases but three where the standard deviation showed one of the data sets was bad and then only six measurements were used.

The standard deviation was used as the average possible error at each interelectrode gap. The error in  $K_m$  was estimated by the following formulas:

$$\Delta R_c = \frac{\partial R_c}{\partial l} \Delta l + \frac{\partial R_c}{\partial K} \Delta K + \frac{\partial R_c}{\partial S} \Delta S \quad (4)$$

$$\Delta K_m = \frac{\partial K_m}{\partial x} \Delta x + \frac{\partial K_m}{\partial R_m} \Delta R_m + \frac{\partial K_m}{\partial R_c} \Delta R_c \quad (5)$$

The values of the variables and the estimated errors appear in Table 1. In all but three cases the error in  $K_m$  is 1 percent or less. The two cases, for which the standard deviation was large, were discarded. Since the error analysis techniques give a maximum error for the data used, I conclude that the measurements are accurate to  $\pm 1$  percent.

## APPENDIX C

1. #083179-3, 28% KOH, 2400 pps\*, 100 ma/cm<sup>2</sup>

This 100 ft movie illustrates the slowing of time by a factor of 100; that is, the film was exposed at 2400 pictures per second and projected at 24 pps. There is high contrast and the bubbles are in clear focus. The current density is relatively low so the phenomena occur slowly. The cyclinical growth processes were small bubbles coalesce with each other and are then scavenged by large bubbles, is apparent. The bubbles do not seem to grow much by diffusion for reasons discussed in the text. Bubbles nucleate uniformly over the surface.

2. #083179-3, 28% KOH, 240 pps, 100 ma/cm<sup>2</sup>

This is a high quality 100 ft movie which shows gas evolution slowed by a factor of 100. There is high contrast and the focus is sharp. At this slow speed, one sees clearly the cyclinical growth process several times. At this relatively low speed, one can distinguish events and phenomena, but one also feels the rapidity and complexity of the process which is lost when the events are slowed to a standstill. Nucleation and growth by diffusion are more apparent in this movie than in others.

---

\* Pictures per second.

3. #082579, 28% KOH, 10,000 pps, 500 ma/cm<sup>2</sup>

This is a fair quality film which shows gas evolution at a high current density. The image is somewhat overexposed, so the smallest bubbles are barely perceptible but the focus is sharp. Raising the current makes the events of lower current densities occur faster, but does not seem to change their kind. One can see movement of small bubbles along the surface to coalesce with medium size bubbles. Small bubbles detached from the surface rise in the wakes of large bubbles so there is a less uniform size distribution in the bulk electrolyte.

4. #082279-4, 28% KOH, 10,000 pps, 100 ma/cm<sup>2</sup>

This is a good quality film showing gas evolution at a relatively low current density and high framing rate. The film was shot to compare to other films taken at the same current density but lower framing rates. The nucleation density seems high in the opening frames because the current has just been turned on and a close-packed layer of bubbles has formed. As the bubble layer reaches quasi-steady state, the number density of small bubbles decreases. At this combination of high speed and low current density, events seem very slow.

5. #091379-1, 28% KOH, 1000 pps, 500 ma/cm<sup>2</sup>

This is a high-contrast sharp-focus film which shows gas evolution at a high current density and medium framing rate. All the phenomena are visible--the cyclical growth process, the motion of small bubbles to coalesce with large bubbles, the scavenging of small bubbles by large ones moving under the influence of gravity. The nucleation density is very uniform. Large bubbles sometimes are stuck between

the light and the camera and obscure the field, but they ultimately break away. This is one of the most important films from the standpoint of intensity of activity and clarity.

6. #091379-2, 28% KOH, 100 pps, 100 ma/cm<sup>2</sup>

This is also a high quality film which starts soon after the current has been turned on. The first group of bubbles, called the incipient growth, appears in the first frames. The film was taken to compare with the previous high current density movie. In this movie, one can distinguish paths cleared by large bubbles as they scavenge small ones off the surface. This indicates that they move very close to—or are still attached to the surface. New bubbles then nucleate in their path or trail on the surface. The nucleation density is uniform.

7. #060280-1, 25% KOH, 24 pps, 100 ma/cm<sup>2</sup>

This movie was taken at 24 frames per second which is also a standard projection rate. This means that there is no speed reduction. One sees much blurred action even though the focus and lighting were good. It demonstrates the need for high speed cinematography.

8. #060280-3, 25% KOH, 10,000 pps, 50 ma/cm<sup>2</sup>

This film was taken as an example of a low current density. The contrast and focus are good but there is little activity. Since the nucleation density is lower and bubbles do not apparently touch as often, one sees growth by diffusion in the early part of the movie.

9. #060980-1, 25% KOH, 10,000 pps, 250 ma/cm<sup>2</sup>

This is a very high quality movie which shows the entire electrode surface from contact to contact; one can see the bubble distribution on the tin oxide electrode. The current density is higher near the edges because the thin film electrode is very resistive. Furthermore, the bubbles are firmly attached in the sides. There are particularly good coalescences showing the vibration of the new bubble after two bubbles join.

10. #061880-01, 3% KOH, 10,000 pps, 500 ma/cm<sup>2</sup>

This is an outstanding movie which shows gas evolution at a high current density and high framing rate. The movie was taken in 3% KOH so that the conductivity would be the same as that of 22% sodium sulfate for comparison. This movie more than most others shows the movement of small bubbles toward medium size bubbles which is discussed in the text. The bubble bases, the flattened spots where the bubbles adhere to the electrode, are visible as darkened areas within the high center of the bubbles. Several times during this movie one bubble coalesces with another and the new bubble detaches from the electrode as determined by the disappearance of the base. This is discussed in the text as the detachment and return of bubbles to the electrode.

11. #061880-3, 22% Na<sub>2</sub>SO<sub>4</sub>, 10,000 pps, 367 ma/cm<sup>2</sup>

This is a high quality movie which shows gas evolution in sodium sulfate which is different from the KOH ordinarily used. Where the nucleation in KOH is uniformly distributed on the surface, bubbles in sodium sulfate nucleate rapidly at only a few sites. The bubbles do

not move from those sites, but coalesce with large bubbles at the sites until they are scavenged by large bubbles moving along the electrode.

## REFERENCES

- (1) R. E. Meredith and C. W. Tobias, Advances in Electrochemistry and Electrochemical Engineering 2, Interscience Publishers, New York, p. 15 (1962).
- (2) J. C. Maxwell, A Treatise on Electricity and Magnetism, 2nd Ed., V. 1, Clarendon Press, Oxford, p. 435 (1881).
- (3) Yu. A. Buyevich, Chemical Engineering Science 29, 37 (1974).
- (4) D. J. Jeffery, Proceedings of the Royal Society of London A 335, 355 (1973).
- (5) W. I. Higuchi, Journal of Physical Chemistry 62, 649 (1958).
- (6) Lord Rayleigh, Philosophical Magazine 34, 481 (1892).
- (7) Z. Hashin, Journal of Composite Materials 2, 284 (1963).
- (8) G. H. Neale and W. K. Nader, Journal of the American Institute of Chemical Engineers 19, 112 (1973).
- (9) S. Prager, Physica 29, 129 (1963).
- (10) R. E. DeLaRue, Electric Conductivity of Dispersed Systems, Master's Thesis, University of California (1955).
- (11) A. Slawinski, Journal de Chimie Physique 23, 710 (1926).
- (12) R. E. Meredith, Studies on the Conductivities of Dispersions, Doctoral Thesis, University of California, Berkeley (1959).
- (13) R. E. Meredith and C. W. Tobias, Journal of Applied Physics 31, 1270 (1960).
- (14) V. P. Mashovets, Journal of Applied Chemistry of the USSR 24, 391 (1951).
- (15) D. A. G. Bruggeman, Ann. Physik. 24, 636 (1935).

- (16) R. E. Meredith and C. W. Tobias, Journal of the Electrochemical Society 108, 286 (1961).
- (17) L. Sigrist, O. Dossenbach, and N. Ibl, Journal of Applied Electrochemistry 10, 223 (1980).
- (18) R. E. DeLaRue and C. W. Tobias, Journal of the Electrochemical Society 106, 827 (1959).
- (19) J. C. R. Turner, Chemical Engineering Science 31, 487 (1976).
- (20) H. Fricke and S. Morse, Physical Review 25, 361 (1925).
- (21) M. R. J. Wyllie and A. R. Gregory, Transactions of the AIME 198, 103 (1953).
- (22) V. L. Kubasov and G. I. Volkov, Soviet Electrochemistry 2, 665 (1966).
- (23) K. Takata and H. Morishita, Electrochemistry 32, 378 (1964).
- (24) F. Hine, S. Yoshizawa, and S. Okada, Journal of the Electrochemical Soc. of Japan 24, 370 (1956).
- (25) N. O. Clark, Transactions of the Faraday Society 44, 13 (1948).
- (26) P. Moon and D. E. Spencer, Field Theory Handbook, Springer-Verlag, Berlin, 104 (1961).
- (27) C. P. Witze, V. E. Schrock, and P. L. Chambre, International Journal of Heat and Mass Transfer 11, 1637 (1968).
- (28) G. Jones and B. C. Bradshaw, Journal of the American Chemical Society 55, 1781 (1933).
- (29) R. W. Bremner and T. G. Thompson, Journal of the American Chemical Society 59, 2373 (1937).
- (30) C. A. R. Pearce, British Journal of Applied Physics 6, 113 (1955).

- (31) A. Erdelyi, W. Magnus, F. Oberhettinger, and F. G. Tricomi, Tables of Integral Transforms Vol. 2, McGraw-Hill (1954).
- (32) F. Hine, M. Yasuda, R. Nakamura, Journal of the Electrochemical Society 122, 1185 (1975).
- (33) M. Blander and J. L. Katz, A. I. Ch. E. Journal 21, 833 (1975).
- (34) L. E. Scriven, Chemical Engineering Science 27, 1753 (1959).
- (35) H. Y. Cheh, On the Mechanism of Electrolytic Gas Evolution, Ph. D. Thesis, University of California, Feb. 1967.
- (36) M. S. Plesset and S. A. Zwick, Journal of Applied Physics 25, 493 (1954).
- (37) B. Kabanov and A. Frumkin, Zeitschrift fur Physikalische Chemie 165A, 433 (1933).
- (38) D. E. Westerheide and J. W. Westwater, A. I. Ch. E. Journal 7, 357 (1961).
- (39) J. P. Glass and J. W. Westwater, International Journal of Heat and Mass Transfer 7, 1427 (1964).
- (40) L. J. J. Janssen and J. G. Hoogland, Electrochimica Acta 15, 1013 (1970).
- (41) L. J. J. Janssen and J. G. Hoogland, Electrochimica Acta 18, 543 (1973).
- (42) J. Venczel, Electrochimica Acta 15, 1909 (1970).
- (43) N. Ibl and J. Venczel, Metalloberflache 24, 365 (1970).
- (44) N. Ibl, Chimie. Ing. Techn. 43, 202 (1971).
- (45) D. Landolt, R. Acosta, R. N. Muller, and C. W. Tobias, Journal of the Electrochemical Society 117, 839 (1970).

- (46) R. A. Putt, M. S. Thesis, University of California, October 1975.
- (47) R. Darby and M. Haque, Chemical Engineering Science 28, 1129 (1973).
- (48) A. Coehn, Z. Electrochem. 29, 1 (1923).
- A. Coehn and Neumann, Z. Physik 20, 54 (1923).

